Lucassen, F., Franz, G., Romer, R. L., Pudlo, D., Dulski, P. (2008): Nd, Pb, and Sr isotope composition of Late Mesozoic to Quaternary intra-plate magmatism in NE-Africa (Sudan, Egypt): high-μ, signatures from the mantle lithosphere. - Contributions to Mineralogy and Petrology, 156, 6, 765-784

DOI: 10.1007/s00410-008-0314-0

Nd, Pb, and Sr isotope composition of Late Mesozoic to Quaternary intra-plate magmatism in NE-Africa (Sudan, Egypt): high-μ signatures from the mantle lithosphere

Friedrich Lucassen[1, 2], Gerhard Franz[2], Rolf L. Romer[1], Dieter Pudlo[2,3], Peter Dulski[1]

[1] GeoForschungsZentrum Potsdam, Telegrafenberg, 14473 Potsdam, Germany
lucassen@gfz-potsdam.de
[2] Fachgebiet Mineralogie-Petrologie, Technische Universität Berlin, Sekr. ACK 9, Ackerstr. 71-76, 13355 Berlin, Germany
[3] Friedrich-Schiller-Universität Jena, Faculty of Chemistry and Earth Sciences, Institute of Earth Sciences, Burgweg 11, 07749 Jena, Germany

ABSTRACT

The isotopic composition of mafic small-volume intra-plate magmatism constrains the compositions of the sub-continental mantle sources. The Nd, Pb, and Sr isotope signatures of widespread late Mesozoic to Quaternary intra-plate magmatism in NE Africa (Sudan, South Egypt) are surprisingly uniform and indicate the presence of a high-μ (μ=$^{238}U/^{204}Pb$) source in the mantle. The rocks are characterized by small ranges in the initial isotopic composition of Nd, Pb, and Sr and most samples fall within εNd ca 3 to 6, $^{206}Pb/^{204}Pb$ ca. 19.5 to 20.5, $^{207}Pb/^{204}Pb$ ca. 15.63 to15.73, $^{208}Pb/^{204}Pb$ ca. 39 to 40 and $^{87}Sr/^{86}Sr$ ca. 0.7028 to 0.7034. We interpret this reservoir as lithospheric mantle that formed beneath the Pan-African orogens and magmatic arcs from asthenospheric mantle, which was enriched in trace elements (U, Th, and light REE). Combining our new data set with published data of intra-plate magmatic rocks from the Arabian plate indicates two compositionally different domains of lithospheric mantle in NE-Africa - Arabia. The two domains are spatially related to the subdivision of the Pan-African orogen into a western section dominated by reworked cratonic basement (NE-Africa; high-μ lithospheric mantle) and an eastern section dominated by juvenile Pan-African basement (easternmost NE-Africa and Arabia; moderate μ lithospheric mantle). The compositions of the Pan-African lithospheric mantle and the MORB-type mantle of the Red Sea and Gulf of Aden spreading centers could explain the Nd-Pb-Sr isotopic compositions of the most pristine Afar flood basalts in Yemen and Ethiopia by mixtures of the isotopic composition of regional lithospheric and asthenospheric sources.

Key words: NE-Africa, intra-plate magmatism, Nd-Pb-Sr isotopes, upper mantle isotope composition, high-μ mantle

1. Introduction

The link between melt sources of continental flood basalts in the Earth's mantle at the intersection of the East African, Red Sea, and Gulf of Aden rifts in the Afar triple junction (McKenzie et al. 1972), with intra-plate magmatism of smaller volume, which is dispersed on the East African continent and the Arabian plate, and with ocean floor basalts of Red Sea and Gulf of Aden (Fig. 1) is matter of an ongoing debate. Topographic elevation and gravity field (e.g., Ebinger and Hayward 1996; Woldetinsae and Götze 2005) and seismic velocity anomalies in the mantle (e.g., Ritsema and Allen 2003; Benoit et al. 2006; Sebai et al. 2006) indicate major thermal anomalies in the mantle, which occur according to the seismic velocities in the asthenosphere and in the deep mantle. The anomalies in the deep mantle are ascribed to mantle plume activity, but the relations between deep and shallow mantle's anomalies are still unresolved (e.g., Ritsema and Allen 2003; Benoit et al. 2006).

Radiogenic isotope geochemistry (Nd, Pb, Sr) of mantle-derived rocks shows a variety of signatures in the Cenozoic to Quaternary magmatic rocks related to their setting.
(1) MORB type depleted mantle (DM) is the source for basalts on the Red Sea and Gulf of Aden ocean floor (e.g. Altherr et al. 1990; Schilling et al. 1992; Volker et al. 1993, 1997).
(2) Small to medium volume intra-plate magmatic rocks on the Arabian plate (e.g. Stein and Hofmann 1992; Bertrand et al. 2003; Shaw et al. 2003, 2007; Weinstein et al. 2006) and in Sudan (Davidson and Wilson 1989; Franz et al. 1999) pre- and postdate the Red Sea rift. They are not bound to rift structures, whereas their occurrence in the East African Rift system (EARS; e.g. Deniel et al. 1994; Bell and Tilton 2001; Kieffer et al. 2004; Furman et al. 2006 a,b; Furman 2007 for an overview) is clearly related to important continental rifting. Compared to the Red Sea MORB type depleted mantle, the isotope compositions of those rocks indicate different variably depleted mantle sources, which are characterized by less radiogenic Nd, similar or slightly more radiogenic Sr, and more radiogenic Pb isotope ratios. The Pb isotope compositions indicate variable high-μ affinities, which have been related to the activity of one or more mantle plumes and their melts interacting with asthenosphere and lithosphere (e.g., Deniel et al. 1994; Stewart and Rogers 1996; Ebinger and Sleep 1998; Franz et al. 1994, 1999; Furman et al. 2006 a, b) or to interaction of melts from asthenosphere and high-μ lithospheric mantle (e.g. Stein and Hofmann 1992; Stein et al. 1997; Bertrand et al. 2003; Shaw et al. 2003; Weinstein et al. 2006).
(3) The Ethiopian and Yemenite ('Afar') flood basalts form a third compositional group, which erupted around ca 30 Ma (Hofmann et al. 1997), before the onset of rifting in the Afar region. The variations in their isotope ratios were interpreted in terms of a slightly heterogeneous depleted sub-lithospheric mantle source without affinities to high-μ or MORB type mantle endmembers, which represents the presumable Afar plume composition, and variable contributions of lithospheric mantle and/or crust (e.g., Baker et al. 1996, 1997; Pik et al. 1999). The recent composition of the Afar plume was derived from young basalts of the Afar region (e.g., Deniel et al. 1994; Barrat et al. 1998). Geochemical evidence for the activity of deep mantle sources comes from the high $^{3}He/^{4}He$ ratios in the area of the Afar flood basalts (e.g., Marty et al. 1996; Pik et al. 2006).

The focus of this study is the isotopic composition of mafic intra-plate volcanic rocks from small to medium sized occurrences in North Sudan and South Egypt (Fig. 1) with predominantly late Cretaceous to Quaternary ages. The new data fill a large regional gap in the knowledge of intra-plate magmatism in NE-Africa in an area that is at least a thousand kilometres from the inferred axis of the Afar plume. We compare the possible compositions of the mantle sources of the volcanic rocks with evidence from the Red Sea and Gulf of Aden spreading centers (MORB), Arabian intra-plate magmatism, and the Afar flood basalts and discuss the control of the intra-plate magmatism by different Pan-African lithospheric domains.

2. Geological setting and age relations

The metamorphic and magmatic basement of north-eastern Africa including the Arabian plate formed around older cratons during a variety of Pan-African metamorphic and magmatic episodes mainly in the late Proterozoic (~900 to 550 Ma; e.g. Kröner et al. 1987; Stern 1994; Küster and Harms 1998; Küster and Liégeois 2001; Stoeser and Frost 2006). The basement comprises reworked older crust of the cratons and juvenile crust. The latter formed during the Pan-African magmatic arc activities at the respective active margins or represents accreted Pan-African island arc crust. The limits between different crustal domains are not well constrained, but the general age pattern and occurrences of rock associations as Pan-African ophiolites and juvenile magmatic rocks suggest an increase of juvenile material towards the Arabian plate (Fig.1; recent interpretations of the regional distribution in: Küster and Liégeois 2001; Teklay et al. 2002). The segmentation in swells and basins from the late Palaeozoic onwards (Klitzsch 1990; Schandelmeier and Reynolds 1997) dominates the present outcrop relations of the Pan-African basement, which is largely restricted to uplifted areas. The petrological features and age structure of the scattered outcrops in the studied area indicate intense reworking and formation of crust during the Neoproterozoic (above references; Harms et al. 1990, 1994; Denkler et al. 1994). This crust most likely continues beneath the Phanerozoic sedimentary cover.

Many intra-plate magmatic rocks occur as small, isolated monogenetic dikes, flows, or plugs with host rocks comprising Pan-African basement or younger sedimentary rocks. Extended volcanic fields exist in the Bayuda Desert and Gedaref areas with numerous smaller volcanic centres in the Bayuda and extended basalt flows in the Gedaref (Almond 1984; Wipki 1995). The volcanic province of the Darfur dome comprises several volcanic fields (e.g. Davidson and Wilson 1989; Franz et al. 1994, 1997, 1999). The occurrences of intra-plate magmatism seem to be bound to regional uplift at swells or domes (Almond 1986) with the most prominent example being the Darfur Dome. The causes of uplift for the Darfur Dome can not be attributed unambiguously to either upwelling of hot asthenospheric upper mantle or plume activity from the deep mantle (Franz et al. 1994; 1999 and references therein).

Intra-plate magmatism in the studied areas (Fig. 1) ranges from Triassic to Quaternary (compilation in Schandelmeier and Reynolds 1997). Our sample suite comprises Late Jurassic to Quaternary rocks (eTable 1) and covers the time before, during and after the ≈ 30 Ma old Afar flood basalts (Hofmann et al. 1997). For the majority of the occurrences we refer to the published age determinations (eTable 1). For one locality new K-Ar whole rock ages were obtained (eTable 2). Most of the age determinations are conventional K-Ar age determinations, often on whole rock. The application of whole rock age determinations is inevitable in many basanites due to the lack of suitable phenocrystals for dating. We are aware that K-Ar whole rock ages could include considerable uncertainties beyond their analytical precision, but they are considered as reliable enough to establish an age classification for the purpose of this study. Most samples are late Cretaceous/Early Tertiary to Quaternary and there is one exception of ~155 Ma.

3. Results

3.1 Sample selection

Many occurrences of the intra-plate magmatic rocks (Fig. 1) are small high-level subvolcanic or volcanic rocks with limited compositional variations and a simple magmatic evolution at most localities (Franz et al. 1987). Volcanic rocks, which are not affected by crustal contamination or major crystal fractionation, are also present in areas, where the magmatic

evolution is more complex, e.g., in the Darfur region (Davidson and Wilson 1989; Franz et al. 1999). The Bayuda main volcanic field and the Meidob volcanic field contain abundant lherzolite mantle xenoliths, but lherzolite inclusions are also known from other localities (eTable 1). To characterize the mantle sources, we restrict the data presentation to a selection of 65 samples from a larger data set. The latter includes compositionally evolved and variably contaminated rocks, mostly from the Darfur dome. Samples were pre-selected from the larger sample set (characterized by XRF analyses and thin sections) on the basis of the following criteria; (i) homogeneity of the sample at the scale of a handspecimen; (ii) absence or -if not applicable- smallest degree of alteration on the scale of the petrographic microscope, e.g., unaltered or least affected olivine in the thin sections; (iii) moderate crystal fractionation, i.e. MgO content > 6 wt% and SiO_2 < 49 wt% (eFig. 1a); (iv) availability of age information. Petrographic descriptions of the selected sample set are summarized in eTable 1. Sample preparation, analytical methods, and data quality are described in the eAppendix. Nd, Pb, and Sr isotope ratios are in Table 1 and geochemical data in eTable 3. A meaningful subdivision of the samples is problematic, because they are from distant outcrops and do certainly not represent common parent magmas. We subdivided the samples into five regional groups to improve the readability of the graphic presentation of the results (Fig.1; Table 1), which are South Egypt, Delgo, Bayuda (comprises the subgroups main field, Kurbei, and Arafieb), Gedaref, and Darfur.

3.2 Chemical characterization

Macroscopically, most samples are olivine basalt, with olivine and clinopyroxene as dominant phenocrysts (eTable 1). A few samples from the Darfur area are subvolcanic rocks, which are classified as gabbro. All but one samples fall within the fields of basanite, basalt, and trachy-basalt (Fig. 2) and are nepheline normative in the CIPW-norm except the Gedaref samples (eTable 3). The Gedaref samples show the lowest alkali contents. The alkalinity of most samples is dominated by the Na_2O contents (eFig. 1; eFigures show specific sample sites of the regional groups). Correlations of major element contents - except for Al_2O_3 - with the variable MgO or SiO_2 contents as indicators of magmatic fractionation are absent or weak (eFig. 1a-g), because the samples represent (1) a variety of parent magma compositions considering the spatial distribution of the samples sites and (2) only the least evolved samples are considered in this study.

Normalized trace element patterns including rare earth elements (REE) of most individual samples are similar in the different distant areas (except Gedaref). Therefore, average trace element patterns are shown (Fig. 3). Trace element contents are high compared to primitive upper mantle and enriched with decreasing compatibility in anhydrous mantle mineralogy (Fig. 3; Table 1). Similar patterns are typical of many small-volume intra-plate magmatic rocks worldwide and indicate small degrees of melting of an enriched source. K and Pb -with the exceptions of a few high Pb Bayuda samples- Pb show pronounced troughs, whereas Nb is enriched. Chondrite normalised REE patterns are L(light) REE enriched. Fractionation or accumulation of plagioclase played no or minor role in the samples as indicated by the absence of both, plagioclase phenocrysts (eTable 1) in most samples and Eu anomalies. Normalized La/Yb and Dy/Yb ratios vary between ~10 to 30 and 1.5 to 2.5 respectively. The correlations between the two ratios are cloudy or absent in some groups despite considerable variation in La/Yb (Fig. 4). Correlations among the increasing contents of incompatible trace (Ba, Sr, Nb, Th, U, Pb, light to medium REE), minor elements (P), and ratios including such elements (e.g. La/Yb) are pronounced (examples: eFig.1 k, l, m). Correlations of these elements and ratios with other more compatible trace elements or variable major elements contents as possible indicators of crystal fractionation, crustal contamination, or variable degrees of melting are cloudy or absent (eFig. 1h, i, j, m, n, o). Variable enrichment of the mantle sources in incompatible elements, variable small degrees of

melting, and variations in the mineralogy of the sources, e.g. presence of garnet, could contribute as single variable condition or process or in combinations to the variations of the trace element contents.

The normalized average trace element pattern of the Gedaref samples (except samples TUY 1879 and 2349) is variable with relative enrichment and depletion of various incompatible elements (Fig. 3). The pattern, compared to those of the enriched samples, is flatter and indicates much lower trace element contents (Fig. 3; Table 1). Incompatible trace elements and LREE of the TUY samples are slightly more enriched, e.g. their La/Yb_N is ~5 compared with $La/Yb_N < 2$ in the other Gedaref samples (Fig. 4). The flat patterns of normalized trace element contents likely indicate higher degrees of melting for all Gedaref samples and -except for the TUY samples - a less enriched source compared with the enriched samples (Fig. 3). Garnet played no role in the source of the Gedaref samples evidenced by low Dy/Yb_N (Fig.4).

Rb, Sr, and U are trace elements of special interest for the interpretation of the isotopic data. These elements can be fluid mobile during low grade alteration and losses or gains of these elements can occur during alteration. The small to medium volume volcanic rocks were never buried after deposition, therefore, alteration is largely restricted to low temperature processes, e.g. formation of vermiculite and montmorillonite after olivine. In the desert climate in NE-Africa it was in several outcrops impossible to obtain material without alteration (eTable 1). The loss on ignition (LOI) is used as a measure of such alteration. 46 samples (out of 65 samples) with a LOI below ~1.5 wt% ($\leq$ 1 wt% in 32 samples) serve as examples of fresh rocks. The LOI is not systematically correlated with Rb, Sr, U, and Ba contents or ratios of these elements with fluid-immobile elements in the denominator (eFig. 2 a-d). Samples with high and low LOI show similar trace element contents and Sr and Pb isotope ratios (eFig. 2 f, g).

3.2 Isotopic compositions and age relations

Sr and Nd isotope ratios are presented in Figure 5a, Pb isotope ratios in Figures 6a and b. The isotope ratios are corrected for in-situ radioactive decay to the respective ages of the rocks. Propagated errors on the initial isotope ratios (eFig. 3; eTable 3) are dominated by the errors on the K-Ar ages and the values of $^{87}Rb/^{86}Sr$, $^{147}Sm/^{144}Nd$, $^{238}U/^{204}Pb$, and $^{232}Th/^{204}Pb$ ratios used in the correction for radioactive decay. The errors on the $^{207}Pb/^{204}Pb$ ratios are dominated by the analytical error (eFig. 3) due to the near-exhaustion of the ^{235}U parent isotope. The propagated errors do not bias any conclusion drawn from the data. The interpretation of the isotope data, e.g. the comparison with published data from surrounding areas, remains robust even if very large errors on the K-Ar ages are assumed in order to assess a possible impact of undetected disturbance of the K-Ar isotope system in whole rock samples (eFig. 3).

Initial Sr isotope ratios and ε Nd plot within the depleted mantle array and indicate long-term depletion in the history of their dominant source with respect to the composition of bulk silicate earth. The samples form an array (ε Nd ~1.7 - 6.7 most samples > 3.0; $^{87}Sr/^{86}Sr$ ~0.7027 – 0.7036) with a weak negative correlation within each regional group except the Bayuda samples (Fig. 5a; eFig. 4a).

Initial Pb isotope ratios of the majority of the samples (Darfur, Southern Egypt, Delgo; Fig. 6a, b) are radiogenic $^{206}Pb/^{204}Pb$ ~19.5 – 20.5, $^{207}Pb/^{204}Pb$ ~15.63 - 15.73, $^{208}Pb/^{204}Pb$ ~ 39-40, and form arrays slightly oblique to the Northern Hemisphere Reference Line (NHRL; Hart 1984). A smaller number of samples mainly from Bayuda (Kurbei and Arafieb areas), Gedaref, and Delgo groups define a trend parallel and close to the NHRL, which extends the compositional field of the intra-plate magmatic rocks to considerable less radiogenic Pb isotope ratios. However, the Bayuda, Gedaref, and Delgo regions also include samples with radiogenic Pb compositions (Fig. 6a, b). Pb isotope compositions at the individual sample

locations are not correlated with Sr isotope ratios (eFig. 4b) and a weak correlation with ε Nd is only seen in the samples from the Bayuda main volcanic field (eFig. 4c).

The relations between crystallization ages and isotope compositions of our samples are important for the interpretation of sources. Effects of correction for in-situ decay on the isotope ratios are small except for the $^{143}Nd/^{144}Nd$ ratios, which are correlated with age (eFig.4 d, e, f, g; eTable 3). Therefore, Nd isotopes are reported in the ε Nd notation. The variable initial isotope compositions of samples with $^{206}Pb/^{204}Pb > 19.5$ and ages show no systematic relation, i.e. similar compositions occur in the Cenozoic and Cretaceous and also one of the two the late Jurassic samples is radiogenic (eFig. 4 g). Samples with relatively unradiogenic $^{206}Pb/^{204}Pb$ are with two exceptions ~33 Ma and younger (eFig. 4g).

4. Discussion: Nd-Pb-Sr isotope signatures of mantle sources beneath NE Africa

4.1 *Isotope signature of the Pan-African basement*

The knowledge of the isotopic composition of the crust is crucial for the discussion of its possible influence on the composition of intra-plate magmatic rocks. Two groups of isotope signatures are distinguished within the Pan-African basement on a larger scale. One crustal reservoir is characterized by recycled Early Proterozoic material of the craton mostly west of the river Nile and the inferred Pan-African suture (Fig. 1; e.g. Black and Liégois 1993; Abdelsalam et al. 2002; Küster et al. 2008). The second reservoir is dominant east of the suture and on the Arabian Peninsula. The latter is characterized by juvenile material from Pan-African magmatic arcs and accretion of island-arcs (e.g. Küster and Liégois 1998; Stern and Abdelsalam 1998; Teklay et al. 2001; Bailo et al. 2003; Stoeser and Frost 2006). Beyond this large scale subdivision, local occurrences of juvenile basement are known west of the Pan-African suture (e.g. Laquia Arbain area; Abdel Rahman et al. 1990) and of reworked craton east of the suture (e.g., locations in Saudi Arabia and north Yemen; Hegner and Pallister 1989; Baker et al. 1997).

The Sr and Nd isotopic compositions of recycled Early Proterozoic cratonic basement in NE-Africa (Fig. 5b) are known from published evidence and characterized by moderate to high Sr isotope ratios (> 0.705, most values > 0.708) and unradiogenic Nd isotope ratios (< 0.512; Fig. 5b; e.g. Davidson and Wilson 1989; Harms et al. 1990; Stern 2002; our unpublished data 2006). Pb isotope signatures are unconstrained in many areas except in the Bayuda area (Küster et al. 2008) and for a few samples from the Darfur (Davidson and Wilson 1989). Therefore, Pb isotope data were supplemented for Pan-African post-orogenic granites in the Darfur region (Fig. 1; Fig. 6c, our unpublished data 2006: eTable 3). The Pb isotope signatures are variable but the majority of the basement samples show radiogenic $^{207}Pb/^{204}Pb$ ratios at given $^{206}Pb/^{204}Pb$ ratios (Fig. 6c). The initial Pb isotope compositions of the post-orogenic granites likely approximate the modern composition of the deeper crust: depletion of U during melt extraction is common and hence a retarded evolution of the uranogenic Pb.

In comparison, the Pan-African juvenile (meta) igneous basement including ophiolites is characterized by variable but generally more radiogenic Nd (> 0.5124) and less radiogenic Sr isotopes (< 0.708; higher in (meta) granitoids; Hegner and Pallister 1989). Particularly intermediate to mafic (meta) igneous rocks, with low Rb/Sr ratios and without major contamination by cratonic material, have modern Nd and Sr isotope compositions similar to those of the selected intra-plate samples (Fig. 5b). Pb isotope compositions of the juvenile Pan-African basement including ophiolites are substantially less radiogenic than those of the reworked craton (Fig. 6c; Pallister et al. 1988; Brueckner et al. 1995; Zimmer et al. 1995; Stern and Abdelsalam 1998; Bailo et al. 2003). The widespread juvenile Pan-African magmatic crust of the Arabian Plate shows a similar isotope composition (Stacey and Stoeser 1984; new data and compilation in Stoeser and Frost 2006).

4.2 Crustal contamination by reworked cratonic basement

Assimilation of reworked cratonic crust should be visible in the Pb, Nd and Sr isotope signatures of the intra-plate volcanic rocks, because the signatures of this crust differ significantly from mantle signatures (Figs. 5b, 6c). The complete data set of intra-plate magmatic rocks from our sampling area includes compositionally evolved and crust-contaminated samples (Davidson and Wilson 1989; Franz et al. 1999; our unpublished data 2006). Nd and Sr isotope ratios of the contaminated samples scatter towards the compositional field of reworked cratonic crust with relatively unradiogenic $^{87}Sr/^{86}Sr$, i.e. Pan-African Rb depletion (Fig. 5b). Their Pb isotope ratios scatter towards the low $^{206}Pb/^{204}Pb$ ratios of the reworked cratonic crust (Fig. 6d). Radiogenic Pb isotope compositions near NHRL are considered to represent original mantle composition or a blend of mantle compositions (Fig. 6). Mixing of common crustal compositions with mantle material cannot explain these radiogenic Pb signatures. Possible exotic crustal compositions, as represented by single basement samples, are apparently not important for the Pb-isotope signature of contaminated intra-plate rocks. A similar pattern of crustal contamination by reworked cratonic crust was described for late Cenozoic rift-related volcanic rocks from the Red Sea in Saudi Arabia (Hegner and Pallister 1989) and intra-plate magmatic rocks from a single volcanic field in northern Yemen (Baker et al. 1997).

The Pb contents of many intra-plate rocks are by factors of up to ~5 lower than in average crust (Rudnick and Gao 2004) and even small amounts of crustal contamination should be visible in the $^{206}Pb/^{204}Pb$ ratios. The discussion of the extent of crustal contamination is restricted to samples with $^{206}Pb/^{204}Pb$ >19.5, which are still close to NHRL and likely experienced minor contamination, i.e. allow inferences on the composition of their mantle sources (one should keep in mind that source heterogeneities also could contribute to this relatively small scatter). The estimation of crustal contamination by bulk mixing or an AFC process, which assumes a magma chamber and crystal fractionation in the crust, depends critically on the chosen parameters for the calculation, i.e. the composition of crust and mantel magma endmember (mixing and AFC) and fractionating mineral phases, related solid/melt distribution coefficients, and model specific variables (AFC). A major uncertainty remains the estimation of the abundance of trace elements in the crustal endmember, because the compositions of high grade metamorphic rocks are highly variable and those of granites are biased e.g. by crystal fractionation.

Correction of the selected intra-plate samples for crystal fractionation to a uniform Mg# of 73 by adding incremental olivine of equilibrium composition (constant Fe/Mg K_D = 0.3; Roeder and Emslie 1970) results in variable olivine additions of up to 50 wt% (< 35 wt% in most samples; eTable 3) and gives an estimate of possible crystal fractionation. We consider samples with olivine additions < 20 wt% as reasonable approximations to initial magma compositions (eTable 3). Correlation of isotope compositions with the possible degree of crystal fractionation (e.g., variable Mg contents) is not observed. Details of AFC modelling (DePaolo 1981) are given in Figures 5 and 6. Ratios of r ~0.2 (rate of assimilating mass/fractionating mass; DePaolo 1981) and crystal fractionation to F ~0.7 (remaining fraction of the original magma) change the Pb isotope composition from $^{206}Pb/^{204}Pb$ 20.2 (initial composition of our proposed intra-plate endmember) to 19.5. This is equivalent to ~5 wt% of Bayuda crust in a bulk mixing model. For more extreme crustal compositions, as the Kas granite, these values are even lower. Nd and Sr contents of the intra-plate magmatic rocks exceed the contents of average crust (Rudnick and Gao 2004) by factors up to ~2 (except the Gedaref samples). Small crustal additions of crust (~5%), as required if the variations of the Pb isotope system are explained by crustal contamination, have only minor effects on the Nd and Sr isotope systems (Fig. 5a). The explanation of the observed variation in the Nd-Sr system of the selected samples would require crustal contributions >between 5 % up to 20% if

one of the most depleted intra-plate samples and the average Kas granite with very low ε Nd are considered as the endmembers. This amount would increase if the crustal endmember is more similar to the average Bayuda basement with higher ε Nd and assumed unradiogenic (initial) $^{87}Sr/^{86}Sr$. Furthermore, the strong vertical variation of ε Nd is not easily explained by the combination of one or two mantle and crust endmembers. Additions > 5% of reworked cratonic crust should force $^{206}Pb/^{204}Pb < 19.5$ (Fig. 6a). Finally, systematic correlations between variable Pb and Sr or Nd isotope ratios are not observed (eFig 4 b, c). Crustal additions are likely not the main cause for the variations in the Nd and Sr compositions.

Correlations between isotope ratios, variable mobile and immobile trace elements are absent with few inconsistent exceptions (eFig. 5). Some incompatible trace element ratios including fluid mobile and refractive elements (e.g., Ba/Nb, Th/Nb, Nb/U, La/Nb, and Ce/Pb; eFig. 5) show systematic differences between lower and upper crust compositions (Taylor and McLennan 1995; Rudnick and Gao 2004) and mantle. Ba/Nb, La/Nb, and Th/Nb ratios of the samples are within the compositional range of depleted and primitive (PUM) mantle compositions (Sun and McDonough 1989; Palme and O'Neill 2004; Salters and Stracke 2004; Workman and Hart 2005) and extend variably to OIB compositions, i.e. rocks from enriched mantel sources (Fig. 7; eFig.5 a-l; e.g., Hofmann et al. 1986; Weaver, 1991; Willbold and Stracke 2006). Nb/U ratios of the samples with radiogenic $^{206}Pb/^{204}Pb$ are systematically displaced from DM and PUM values to higher values known from some OIB and show no relation to the low crustal values of average crust (eFig.5 m-o) and local basement. Ce/Pb ratios between ~2.5 to 50 are highly variable and cover low crustal to high mantle values (Fig. 7; eFig. 2e). Most samples show no traces of hydrothermal alteration or weathering, and correlations of possible fluid mobile Ba and Pb with LOI are absent (eFig. 2 c, d) and we consider a secondary mobility of Pb or Ba as unlikely. Ba/Nb and Ce/Pb ratios and combinations of the latter with isotope ratios are not correlated (e.g., Bayuda main field samples: Ce/Pb ~3 – 42, Ba/Nb ~2.7 - 4.3; Fig. 7; eFig. 5a-f; eFig. 2e). Highly variable Ce/Pb ratios are described from some OIB localities and attributed to small amounts of residual sulphide minerals (Halliday et al. 1995). Three samples of the Gedaref area (samples MIR 1302, GIR 1291, SUD 1456 out of 65 samples; Table 1) approximate crustal Ce/Pb and Ba/Nb ratios similar to crust-contaminated Ethiopian plateau basalts (Fig. 7).

Possible contamination by the reworked cratonic crust can be readily detected in the Pb isotope composition of the contaminated rocks and is small or absent in the selected sample set. Covariation between the Sr, Nd, and Pb isotope systems and of the latter with trace element contents or ratios is absent or mostly inconsistent. The variable canonical element ratios plot mainly in the broad range of DM-PUM-OIB compositions and could reflect source variability of the enriched sources as known for OIB (e.g. Willbold and Stracke 2006). A systematic and substantial contamination by reworked cratonic crust is not detected.

4.2 Crustal contamination by juvenile crust

The possible assimilation of juvenile crust is difficult to discern in the isotope signatures. Modern Nd and Sr isotope compositions of the juvenile basement either resemble compositions of the intra-plate magmatic rocks or scatter to unradiogenic (Nd) and radiogenic (Sr) isotope compositions (Fig. 5b). Uranogenic Pb isotope ratios of the juvenile crust are similar or less radiogenic than in average modern MORB mantle (DM; Fig. 6c). The Pb isotope ratios of samples from some localities within the Bayuda (J. Kurbei and J. Umm Arafieb localities), Delgo (Laquia Arbain locality), and Gedaref (Merciba, El Gira, and Qualat Umm Debiba localities) groups scatter sub-parallel to NHRL towards the compositions of juvenile Pan-African basement or DM (Fig. 6c). The Bayuda area is located in the transition zone between craton and juvenile crust and Gedaref area east of the inferred Pan-African suture (Fig. 1). Juvenile crust is dominant in the area of the Laquia Arbain localities (LA in Fig. 1; Abdel Rahman et al. 1990).

Three samples from the Gedaref group show crust-like Ce/Pb and Ba/Nb ratios (Fig. 7; samples MER 1302, SUD 1443, 14565 in eFig. 5) comparable to the low Ti Afar flood basalts, which were considered to be crust-contaminated (Pik et al. 1999). Further, the La/Nb ratios of MER 1302 and SUD 14565 are more crust-like compared with the composition of all other samples (eFig.5 i-l). The REE patterns of the possibly contaminated samples are flat (Fig. 4) and without Eu anomaly and trace element contents are low (Fig. 3). Such REE patterns are unlikely if low fractions of partial melts from a plagioclase, hornblende or clinopyroxene (±garnet depending on the depth of contamination) bearing source are involved. The observed trace element patterns indicate either bulk assimilation of a compositionally similar crustal material (flat REE patterns, low trace element contents) or no or minor crustal contributions and, therefore, variations in the mantle sources. However, Sr isotope compositions of the three samples are comparable radiogenic, those of Nd isotopes unradiogenic. Juvenile Pan-African crust could have the appropriate Pb isotope composition for a contaminant (Fig. 6 c). The meaning of both, isotope signatures and trace element patterns of the three Gedaref samples remains ambiguous. The comparable radiogenic Nd and unradiogenic Sr isotope ratios of the two other samples from the Gedaref group (with unradiogenic Pb isotope compositions: GIR 1291 and 1295) are more similar to the Bayuda samples (Jebel Kurbei and Umm Arafieb; eFig. 5). The radiogenic Pb isotope compositions of the two samples from the Jebel Abu Tuyur (TUY) locality of the Gedaref area are indistinguishable from other NE-African samples with radiogenic Pb (Figs. 5 and 6) and not readily explained by crustal contributions in the known compositional framework (Fig. 6c). A higher degree of melting of an enriched mantle source similar to that of other radiogenic samples is assumed for these samples: their still flat element distribution pattern is more enriched than in the other Gedaref samples (Fig. 3).

One of the Laquia Arbain samples (12-12, Table 1) has a radiogenic isotope composition similar to the three high Ce/Pb and Ba/Nb samples from Gedaref, but does not resemble their trace element characteristics. The weak and variable correlation of isotope ratios with Ce/Pb and Ba/Nb for the Laquia Arbain samples could be tentatively interpreted as contamination by crust (eFig. 5). The Jebel Kurbei and Umm Arafieb samples of the Bayuda group show no correlations with indicators of possible crustal contamination. Their Sr isotope ratios are slightly less, their Nd isotope composition slightly more radiogenic than in the samples from the Bayuda main volcanic field.

In summary, contamination by juvenile Pan-African could be prominent in some samples from the Gedaref area, considering their crust-like Ce/Pb and Ba/Nb ratios and could be present in the Laquia Arbain samples. However, the isotope compositions of the Jebel Kurbei, Umm Arafieb and Laquia Arbain localities and of some of the Gedaref samples can be also discussed within the regional framework of mantle compositions (see below).

4.3 *Lithospheric versus convective mantle sources in the intra-plate rocks*

Major element compositions of experimentally produced melts from fertile peridotite are indicative of the degree and pressure of melting (Herzberg and Zang, 1996; Herzberg and O'Hara, 2002; Herzberg, 2004). For a comparison with experimental results, we selected samples with a low degree of crystal fractionation (Mg# > ~64), which minimizes the possible effect of the correction for crystal fractionation to Mg# ~73 by addition of olivine only (< 20 wt% olivine added). The fractionation-corrected samples are compared with the compositions of low melt fractions derived from experimental work using the equations of Herzberg and Zang (1996). Calculated pressures for various localities are between ~3.3 - 4 GPa for Al_3O_3, CaO, FeO, and MgO whereas Na_2O yields variable pressures (eTable 3). The calculated small P range indicates relatively uniform conditions and protoliths. The absolute P values should be considered as an approximation only and would indicate melting in the lower lithosphere

assuming a thickness of ~100-120 km. Such thickness was proposed for the pre-tectonic lithosphere of the Ethiopian plateau (Dugda et al. 2007).

Trace element compositions, especially the relations among REE could indicate changing mineralogical makeup in the source with increasing P. Increasing depth of melting could sample compositionally different sources, e.g. the asthenosphere (DM composition) as shown for some intra-plate basalts in Jordan (Dy/Yb ratios up to ~6 correlate with increasing DM influence on the isotopic composition; Shaw et al. 2003). Ranges of La/Yb - Dy/Yb in samples, which were interpreted to represent the composition of the Arabian mantle lithosphere, and the NE-African samples are very similar (Fig. 4) and do not extend to the high Dy/Yb ratios known from the some Jordan basalts. Further, correlations between La/Yb and Dy/Yb, as indicators of increasing depth of melt generation, and isotope signatures (eFig. 4 h-m) or of both with indicative incompatible element ratios are absent. Respective element ratios (e.g., Ce/Pb, Nb/U, Ba/Nb, La/Nb and Th/Nb) scatter within the DM - OIB mantle range (eFig.5). Therefore, the following discussion of possible convective - lithospheric mantle interaction relies on the isotopic composition of both in the regional context.

The presence of convective DM is confirmed by the isotopic compositions of young basalts from the Red Sea and Gulf of Aden spreading centers (e.g. Altherr et al. 1990; Volker et al. 1997; Schilling et al. 1992). The arrays of Sr-Nd and Pb isotopic compositions of the ridge basalts (Fig. 8; eFig 6) indicate one mixing component, which is similar to average MORB depleted mantle reservoirs (e.g., Zindler and Hart 1986; Weaver 1991; Halliday et al. 1995; Hofmann 1997; Salters and Stracke 2004; Workman and Hart 2005). The isotopic compositions of the Afar flood basalts could represent a second regionally important compositional type of convective mantle (Fig. 8; eFig. 6). Possible distinctive isotopic compositions of the Afar-plume have been extracted from the flood basalts by Baker et al. (1996) and Pik et al. (1999) and younger rocks occurring in the area influenced by the Afar-plume (Djibouti; Vidal et al. 1991; Deniel et al. 1994; Barrat et al. 1998). Pb isotope compositions of the plume material are less (most samples: $^{206}Pb/^{204}Pb<19$) and Sr isotopes more radiogenic (most samples $^{87}Sr/^{86}Sr>0.7035$) than of intra-plate magmatic rocks from NE-Africa (Fig. 8; eFig. 6). The isotopic composition of the NE-African and Arabian intra-plate magmatism shows affinities to high-μ sources (Fig. 8; eFig. 6). Therefore, we consider high-μ mantle compositions derived from distant OIB settings as a general option for contributions from the convective mantle. The selection of a compositional type is somewhat arbitrary and we refer to the FOZO (Focus Zone) type, which is considered to represent a ubiquitous compositional component in the convective mantle and was recently redefined by Stracke et al. (2005).

The isotopic compositions of lithospheric mantle have been described from the Arabian plate using young intra-plate magmatic rocks (e.g. Altherr et al. 1990; Baker et al. 1997; Bertrand et al. 2003; Shaw et al. 2003; Weinstein et al. 2006) and peridotite mantle xenoliths (Henjes-Kunst et al. 1990; Blusztajn et al. 1995; Baker et al. 1998; Shaw et al. 2007). The results from xenoliths and magmatic rocks are broadly similar, but we restrict to the Arabian intra-plate rocks (Fig. 8; eFig. 6), because they represent sample volumes of their mantle sources comparable to those of NE African samples. The existence of enriched mantle of EM1 and EM2 type endmember compositions (e.g., Zindler and Hart 1986; Hofmann 1997; Stracke et al. 2005; Willbold and Stracke 2006) has not been confirmed in the studied area, but they are considered as a general option. Sr and Nd isotope compositions of EM1 type mantle have been described from southern Yemen (Menzies and Murthy 1980).

The isotopic compositions of most radiogenic NE-African samples ($^{206}Pb/^{204}Pb> 19.5$) are different from the inferred Afar-plume, DM, and Arabian lithospheric mantle compositions (Fig. 8; eFig. 6). They can not be explained by mixing of the Afar-plume component and DM, i.e. by regional convective mantle sources. Mixing of Afar-plume component and DM sources with Arabian lithospheric mantle or – hypothetically - mantle of

the EM1 and EM2 types (e.g., Zindler and Hart 1986; Hart 1988; Stracke et al. 2005) fails to explain the radiogenic Pb isotope ratios of the NE-African samples. The ranges of $^{206}Pb/^{204}Pb$ in FOZO and the NE-African samples are similar (Fig. 8) but the $^{207}Pb/^{204}Pb$ and $^{208}Pb/^{204}Pb$ ratios of the latter are commonly higher (eFig. 6b, c) and ε Nd at given $^{87}Sr/^{86}Sr$ and $^{206}Pb/^{204}Pb$ is systematically lower than in FOZO (Fig. 8; eFig. 6a). These differences preclude FOZO as a mixing endmember for the radiogenic NE-African samples, if the other regional sources including the reworked cratonic basement are considered as potential additional 'endmembers' for mixing. Further, compositional trends in FOZO and the Red Sea and Gulf of Aden ridge basalts are inconsistent (Fig. 8; eFig.6) and preclude the published range of FOZO compositions for binary mixing with DM in the regional convective mantle.

A hidden source with the regional high-μ flavour of the NE-African magmatism located in the convective mantle (or magmas from a deep source passing through convective mantle) would require a sophisticated model of magma generation and transport in the given time - space framework of the intra-plate magmatism. Such model has to explain (1) the exclusive occurrence of the most distinctive compositions in small to medium volume magmatism, which is randomly distributed over a wide area (Fig. 1) and has ages from late Jurassic to Quaternary (eTable 1); (2) the regional compositional pattern of intra-plate magmatism on continental crust, which appears to be related to lithospheric boundaries in the Pan-African orogen (outlined in the following chapter); (3) the dominance of DM in the ridge basalts and the near contemporaneous magmatism with high-μ affinities in the Bayuda area and -with considerable spatial extension- on the Arabian plate.

The assumption of stationary high-μ sources in the subcontinental lithospheric mantle allows a straightforward explanation of these observations. The distinctive isotope compositions of the radiogenic NE-African samples likely reflect the compositions of mantle sources *sui generis* in the regional context, which have despite affinities to published FOZO compositions a distinctive regional flavour.

4.4 Origin of the radiogenic Pb in the lithospheric mantle and its relation to the regional geology

Lithospheric mantle sources similar to high-μ mantle require changes in the trace elements budget compared to the composition of asthenospheric depleted mantle. The two endmember processes are (1) metasomatism by an isotopically different material from an external source, e.g., by melt from a high-μ type mantle plume and (2) the relative enrichment of Rb, U, and Nd, resulting in higher Rb/Sr and U/Pb and lower Sm/Nd ratios in this enriched mantle compared to a depleted mantle. Process (1) has immediate effect on the isotope composition whereas the effect of (2) is related to the character of the enrichment and elapsed time since the compositional change occurred (Fig. 9). Substantial contributions of material from the Afar-plume indicating young metasomatism according to process (1) are precluded for NE-African and Arabian (discussion in Bertrand et al. 2003) intra-plate magmatic rocks, because a high-μ signature of this plume has not been established (e.g., Vidal et al. 1991; Schilling et al. 1992; Deniel et al. 1994; Baker et al. 1996, 1997, 1998; Pik et al. 1999).

The occurrence of systematic variations in the isotopic compositions between NE-African and W-Arabian intra-plate magmatic rocks indicate different enriched mantle sources. The compositional variations seem to be related to first order changes in the make-up of the Pan-African crust (Fig. 1). The Proterozoic basement of the Arabian plate consists of Pan-African arc assemblages and comprises numerous crustal blocks (terranes) with abundant juvenile material from island arcs, which were accreted to the continental margin (e.g., Stern 1994; Teklay et al. 2001; Bailo et al. 2003; Stoeser and Frost 2006). The lithospheric mantle beneath island arcs is expected to represent depleted oceanic mantle and the former mantle wedge. In the studied area west of the inferred suture in Figure 1, the influence of cratonic

crust reworked by Pan-African metamorphism and magmatism increases. This area could represent a continental magmatic arc and the transition to the ancient continent west of the Pan-African collision zones (Fig. 1; e.g., Küster and Liégeois 2001). The sub-continental lithospheric mantle could be strongly modified in the sub-arc regions (1) by the formation of the mantle wedge and percolating melts from the latter and (2) delamination of the lower crust and lithospheric mantle beneath collision zones with crustal thickening (e.g., Meissner and Mooney 1998). Delamination has been invoked for the Pan-African orogen (Black and Liégeois 1993). Both processes place asthenospheric material in the realm of lithospheric mantle. This mantle is modified by the transfer of elements from subducted material.

Stein et al. (1997) proposed a model for the isotopic evolution of the lithospheric mantle beneath Arabia and NE-Africa by metasomatism during Pan-African subduction and subsequent radiogenic growth in the fossilized sub-arc mantle (Fig. 9). They explain the variable composition of the lithospheric mantle by variable enrichment of trace elements, e.g. U and LREE, in a mantle with the starting composition of the contemporaneous asthenosphere. Variable initial mantle compositions above the subduction zones, e.g. emplacement of Pan-African plume derived enriched mantle (Stein and Hofmann 1992; Stein, 2003), would not change the conceptual model (Fig.9). The possible Pan-African metasomatism in the lithospheric mantle caused different characteristic Pb isotope compositions beneath NE-Africa (most radiogenic Pb isotope compositions) and the Arabian plate (less radiogenic, but still high Pb isotope ratios and slightly more radiogenic Nd compositions than in NE-Africa; Fig. 8; eFig. 6; see discussion in Bertrand et al. 2003). The compositional differences could reflect differences in intensity and age of the metasomatism, composition of the metasomatizing agent, and initial composition of the pristine mantle. The transition between these different compositional domains relates to the transition between reworked craton and island arc terranes. The Bayuda area is located near the inferred transition and the Gedaref area is located east of the suture (Fig.1). The unradiogenic Pb isotope compositions of the Umm Arafieb, Jebel Kurbei, and two Laquia Arbain samples plot into the compositional field of the Arabian lithospheric mantle (Fig. 8 b). $^{206}Pb/^{204}Pb$ compositions of the Gedaref and two Laquia Arbain samples are slightly less radiogenic than the Arabian lithospheric mantle, but at least two Gedaref samples with radiogenic Nd isotope compositions are not substantially different from the Arabian mantle (Fig.8 b). The intra-plate magmatic rocks of Jebel Umm Arafieb and Kurbei localities could represent Arabian lithospheric mantle. The same can be assumed for the Gedaref samples with radiogenic Nd isotope compositions (Figs. 1, 8). The Laquia Arbain area is dominated by juvenile Pan-African crust (Abdel Rahman et al. 1990).

High-μ compositions similar those described in this work are also described from the EARS in southern Ethiopia (e.g. George and Rogers 2002), in the Turkana area of Kenya (Fig.8, eFig.6; Furman et al. 2006), and in the Kenya rift further to the south (e.g., MacDonald et al. 2001). The tectonic setting of the EARS is that of an active continental rift and very different from the situation in NE Africa. High-μ signatures in the EARS are integrated in the thermo-tectonic models of one or more mantle plumes, roughly active since the pre-rift Afar event. The physical source of the high-μ signature is variably located in the sublithospheric (e.g. Furman et al. 2006a) or lithospheric mantle (e.g. George and Rogers 2001; MacDonald et al. 2001) and a localization of the source in the highly dynamic rift region appears to be complex. A comparison of the off-rift situation in Sudan and south Egypt and the EARS scenarios is beyond the scope of this contribution. Widespread intra-plate magmatism on the Arabian plate is certainly triggered by the thermal disturbance induced by continental separation and spatially related to the Red Sea rift, but rifting at the locations of magmatism appears to be absent. However, the thermal trigger of magmatism is less clear on the African side, e.g. the young volcanism in the Bayuda area could be ascribed to thermal activation by the Red Sea rift, but the nearby Cretaceous intra-plate magmatism (Satir et al. 1991) not. High-μ

magmatism at the reworked cratonic margin occurs at least since the Jurassic, i.e. long before the onset of plume activity. The scattered distribution of this magmatism does not allow an assignment to certain tectonic directions. This scenario of occasional disturbances of the local thermal regime in the mantle is documented since the Early Palaeozoic in the isolated, but widespread magmatic activity in the largely unexplored alkaline ring complexes (e.g. Schandelmaier and Reynolds 1997; El-Said et al. 2007).

4.5 Implications for the composition of the Afar flood basalts

The Afar flood basalts erupted in a short time interval (< 2 Myr) at ca. 30 Ma (Hofmann et al. 1997; Pik et al. 1998) before the rifting and plate-separation at the Afar triple junction. The flood basalts appear to be a singular, short-lived event in the region. Isotope compositions of the Afar-plume at ~30 Ma (e.g. Baker et al. 1996; Pik et al. 1999) and younger rocks ascribed to the activity of this plume (Deniel et al. 1994; Barrat et al. 1998 are not substantially different (Furman et al. 2006 b). These isotope compositions can be explained by (1) mixing between melts from the convective MORB-type mantle and the regional lithospheric mantle sources, (2) as melts from the lithospheric mantle, and (3) as melts from a source *sui generis* related to the plume. Option (3) has been recently discussed on the basis of noble gas compositions of the Afar flood basalts and younger intra-plate rocks from this area (Scarsi and Craig 1996; Marty et al. 1996; Pik et al. 2006 and references therein). The unusual high $^{3}He/^{4}He$ ratios ($20 > R/Ra > 10$) appears to be spatially restricted to the occurrence of the Afar flood basalts and younger intra-plate rocks from this area. They are considered as a contribution from deep undegassed primordial mantle near the Earth's core, i.e. a plume contribution.

Options (1) and (2) are complementary in the given framework of upper mantle compositions (Fig. 8) and could lead to the same results. MORB source endmember compositions are absent in the Afar flood basalts, but could be camouflaged by the final mixed compositions and a contribution of such source is possible (e.g., Pik et al. 1999). The minor role of the convective mantle endmember (including 'plume signatures'), dominance of lithospheric mantle signatures, and variable crustal contamination in the isotopic compositions has been discussed for the Afar flood basalts (e.g. Baker et al. 1996; Pik et al. 1999) and is also well documented in other continental flood basalt provinces (e.g. Paraná-Etendeka and Karoo provinces; Peate and Hawkesworth, 1996; Marques et al., 1999; Ewart et al., 2004; Ellam, 2006 and references therein). Considering the compositions of the regional lithospheric mantle and the Nd, Sr, and Pb isotope composition of the Afar flood basalts and young Afar plume related magmatism, the compositional variation in these isotope systems can be entirely explained by options (1) and/or (2) plus variable crustal contamination and a source *sui generis* for the flood basalts seems not to be mandatory.

5 Summary and Conclusions

Our new data provide evidence for a wide spatial distribution of enriched lithospheric mantle beneath NE-Africa. This mantle has an isotopic composition with a distinctive regional flavour despite its similarity to high-μ FOZO type mantle. Two kinds of lithospheric mantle, one mainly beneath the Arabian plate, a second one mainly beneath NE-Africa, and DM asthenosphere describe the variations in the Nd-Pb-Sr isotope compositions of Jurassic to Quaternary small volume intra-plate magmatic rocks, Afar flood basalts, and basalts of the Red Sea and Gulf of Aden spreading centers.

The major conclusions from the new and published data of the isotopic composition of the lithospheric and convective mantle are:

(1) The regional distribution of the compositional domains suggests a relation between the lithospheric mantle compositions and the growth pattern of the Pan-African orogen. In the

western domain, Pb isotope ratios are significantly more and those of Nd are slightly less radiogenic than in the eastern domain. The western domain comprises the older sections of the orogen, possibly a continental magmatic arc on cratonic crust, whereas the eastern domain is dominated by juvenile crust and accreted island arcs (Fig. 1).
(2) Compositional domains of the lithospheric mantle appear to be isotopically relatively uniform at the scale of sampling of the mantle by low-volume intra-plate magmatism. This indicates together with wide spatial distribution of this magmatism the existence of a volumetrically important compositional reservoir in the lithospheric mantle. Both lithospheric mantle domains likely represent Proterozoic Pan-African sub-arc or oceanic mantle, with relative enrichment of U and light REE and long-term separation from the convective reservoir.
(3) The regional compositional framework of the lithospheric mantle domains and MORB-type asthenospheric mantle approximates mantle signatures known from OIB settings (e.g. Hofmann 1997; Stracke et al. 2005), comprising high-μ mantle (in the western domain) or moderate-μ mantle types (in the eastern domain and in mixtures of both domains with convective depleted mantle) in the Nd, Sr, and Pb isotope space. As a prospect, such relatively young lithospheric mantle, if returned to the convective mantle system under specific conditions (e.g., O'Reilly et al. 2001; Poudjom Djomani et al. 2001), could contribute to the compositional variability of magmatism on the oceanic crust.

Acknowledgments
Cathrin Schulz and Birgit Zander are thanked for their help with the analytical work at GFZ-Potsdam. Samples were collected between 1978 and 1995 in the frame of the research project SFB 69, and we thank G. Steiner, T. Denkler, B. El Hur, E. Klitzsch and C. Breitkreuz for their help in sampling. The logistical help of GRAS at Khartoum is gratefully acknowledged. Special thanks to U. Harms for providing samples for Pb isotope analyses of the basement and to Klaus Wemmer, GZG Universität Göttingen, for the K-Ar age determinations. Rosemarie Geffe, TU-Berlin is thanked for improving the presentation of the Figures. We thank Tanya Furman, David W. Peate, and Andreas Stracke for their thorough reviews, which considerably improved the paper and Jochen Hoefs for the editorial handling. The work was financed by DFG grant FR 557/20-1.

References

Abdel Rahman EM, Harms U, Schandelmeier H, Franz G, Darbyshire DPF, Horn P, Müller-Sohnius D (1990) A new ophiolite occurrence in NW Sudan - constraints on Late Proterozoic tectonism. Terra Nova 2: 363-376

Abdelsalam MG, Liégeois J-P, Stern RJ (2002) The Saharan Metacraton. Journal of African Earth Sciences 34: 119-136

Allégre CJ, Birck JL, Fourcade S, Semet MP (1975) Rubidium-87/strontium-87 age of Juvinas basaltic achondrite and early igneous activity in the solar system. Science 187: 436-438

Almond DC (1986) Geological evolution of the Afro-Arabian dome. Tectonophysics 131: 301-331

Almond DC, Kheir OM, Poole S (1984) Alkaline basalt volcanism in the northeastern Sudan: a comparison of the Bayuda and Gedaref areas. Journal of African Earth Sciences 2: 233-245

Altherr R, Henjes-Kunst F, Puchelt H, Baumann A (1988) Volcanic activity in the Red Sea axial trough—evidence for a large mantle diapir. Tectonophysics 150: 121-133

Altherr R, Henjes-Kunst F, Baumann A (1990) Asthenosphere versus lithosphere as possible sources for basaltic magmas erupted during formation of the Red Sea: constraints from Sr, Pb and Nd isotopes. Earth and Planetary Science Letters 96: 269-286

Bailo T, Schandelmeier H, Franz G, Sun C-H, Stern RJ (2003) Plutonic and metamorphic rocks from the Keraf Suture (NE Sudan): a glimpse of Neoproterozoic tectonic evolution on the NE margin of W. Gondwana. Precambrian Research 123: 67-80

Baker JA, Thirlwall MF, Menzies MA (1996) Sr-Nd-Pb isotopic and trace element evidence for crustal contamination of plume-derived flood basalts: Oligocene flood volcanism in western Yemen. Geochimica et Cosmochimica Acta 60: 2559-2581

Baker JA, Menzies MA, Thirlwall MF, Macpherson CG (1997) Petrogenesis of Quaternary intraplate volcanism, Sana'a,Yemen: implications for plume – lithosphere interaction and polybaric melt hybridization. Journal of Petrology 38: 1359-1390

Baker JA, Chazot G, Menzies M, Thirlwall MF (1998) Metasomatism of the shallow mantle beneath Yemen by the Afar plume—implications for mantle plumes, flood volcanism, and intraplate volcanism. Geology 26: 431-434

Barrat JA, Fourcade S, Jahn BM, Cheminee JL, Capdevila R (1998) Isotope (Sr, Nd, Pb, O) and trace-element geochemistry of volcanics from the Erta'Ale range (Ethiopia). Journal of Volcanology and Geothermal Research 80, 85-100

Barth H, Meinhold KD (1979) Mineral prospecting in the Bayuda Desert. Bundesanstalt Geowiss. Rohstoffe, Hannover (unpublished report)

Bell K, Tilton GR (2001) Nd, Pb and Sr isotopic compositions of East African Carbonatites: Evidence for mantle mixing and plume inhomogeneity. Journal of Petrology 42: 1927-1945

Benoit MH, Nyblade AA, Owens TJ, Stuart G (2006) Mantle transition zone structure and upper mantle S velocity variations beneath Ethiopia: Evidence for a broad, deep-seated thermal anomaly. Geochemistry Geophysics Geosystems 7: doi:10.1029/2006GC001398.

Bernau R, Darbyshire DPF, Franz G, Harms U, Huth A, Mansour N, Pasteels P, Schandelmeier H (1987) Petrology, geochemistry and structural development of the Bir Safsat-Aswan Uplift/Southern Egypt. Journal of African Earth Science 6: 79-90

Bertrand H, Chazot G, Blichert-Toft J, Thoral S (2003) Implications of widespread high-μ volcanism on the Arabian plate for Afar mantle plume and lithosphere composition. Chemical Geology 198: 47-61

Black J, Liégeois J-P (1993) Cratons, mobile belts, alkaline rocks and continental lithospheric mantle: the Pan-African testimony. Journal of the Geological Society London 150: 89-98

Brueckner HK, Elhaddad MA, Hamelin B, Hemming S, Kröner A, Reisberg L, Seyler M, (1995) A Pan African origin and uplift for the gneisses and peridotites of Zabargad island, Red Sea: a Nd, Sr, Pb, and Os isotope study. Journal of Geophysical Research 100: 22283-22297

Blusztajn J, Hart SR, Shimizu N, McGuire AV (1995) Trace-element and isotopic characteristics of spinel peridotite xenoliths from Saudi Arabia. Chemical Geology 123: 53-65

Cahen L, Snelling NJ, Delhal J, Vail JR, (1984) The Geochronology and evolution of Africa. Oxford Clarendon Press, 512p

Chaffey DJ, Cliff RA, Wilson BM (1989) Characterization of the St. Helena magma source, . In: Magmatism in the Ocean Basins. Saunders AD, Norry MJ (editors) Geological Society London Special Publication 42: 257-276

Davidson JP, Wilson IR (1989) Evolution of an alkali basalt–trachyte suite from Jebel Marra volcano, Sudan, through assimilation and fractional crystallization. Earth and Planetary Science Letter 95: 141-160

Deniel C, Vidal P, Coulon C, Vellutini PJ, Piguet P (1994) Temporal evolution of mantle sources during continental rifting: the volcanism of Djibouti (Afar). Journal of Geophysical Research 99: 2853-2869

Denkler T, Franz G, Schandelmeier H (1994) Tectonometamorphic evolution of the Neoproterozoic Delgo suture zone, northern Sudan. Geologische Rundschau 83: 578-590

DePaolo DJ (1981) Trace element and isotopic effects of combined wallrock assimilation and fractional crystallization. Earth and Planetary Science Letters 53, 189-202

Dugda MT, Nyblade AA, Julia J (2007) Thin lithosphere beneath the Ethiopian Plateau revealed by a joint inversion of Rayleigh wave group velocities and receiver functions. Journal of Geophysical Research 112: doi:10.1029/2006JB004918

Dulski P (2001) Reference materials for geochemical studies: New analytical data by ICP-MS and critical discussion of reference values. Geostandards Newsletters 25: 87-125

Ebinger CJ, Hayward N (1996) Soft plates and hot spots: Views from Afar. Journal of Geophysical Research 101: 21859-21876

Ebinger CJ, Sleep N (1998) Cenozoic magmatism throughout East Africa resulting from impact of a single plume. Nature 395: 788-791

El-Sayed MM, Furnes H, Abou Shagar S (2007) Alexandria Growth of the Egyptian crust in the northern East African Orogen: A review of existing models and proposed modifications Neues Jahrbuch für Mineralogie Abhandlungen 183:317–341

Ellam RM (2006) New constraints on the petrogenesis of the Nuanetsi picrite basalts from Pb and Hf isotope data. Earth and Planetary Science Letters 245: 153-161

Ewart A, Marsh JS, Milner SC, Duncan AR, Kamber BS, Amstrong RA (2004) Petrology and Geochemistry of Early Cretaceous Bimodal Continental Flood Volcanism of the NW Etendeka, Namibia. Part 1: Introduction, Mafic Lavas and Re-evaluation of Mantle Source Components. Journal of Petrology 45: 59-105

Franz G, Puchelt H, Pasteels P (1987) Petrology, geochemistry and age relations of Triassic and Tertiary volcanic rocks from SW Egypt and NW Sudan. Journal of African Earth Sciences 6: 335-352

Franz G, Pudlo D, Urlacher G, Haußmann U, Boven A, Wemmer K (1994) The Darfur Dome, western Sudan: the product of a subcontinental mantle plume. Geologische Rundschau 83: 614-623

Franz G, Steiner G, Volker F, Puldo D, Hammerschmidt K (1999) Plume related alkaline magmatism in central Africa—the Meidob Hills (W Sudan). Chemical Geology 157: 27-47

Franz G, Breitkreuz C, Coyle DA, El Hur B, Heinrich W, Paulick H, Pudlo D, Steiner G, Smith R (1997) Geology of the Alkaline Meidob Volcanic Field, Late Cenozoic, Sudan. Journal of African Earth Sciences 25: 263-291

Fuhrmann U, Lippolt HJ, Hess JC (1987) Examination of some proposed K±Ar standards:40Ar/39Ar analyses and conventional K-Ar data. Chemical Geology (Isotope Section) 66: 41-51

Furman T (2007) Geochemistry of East African Rift basalts: an overview. Journal of African Earth Sciences 48: 147-160

Furman T, Kaleta KM, Bryce JG, Hanan BB (2006a) Tertiary Mafic Lavas of Turkana, Kenya: Constraints on East African Plume Structure and the Occurrence of High-μ Volcanism in Africa. Journal of Petrology 47: 1221-1244

Furman T, Bryce J, Rooney T, Hanan B, Yirgu G, Ayalew D (2006b) Heads and tails: 30 million years of the Afar plume. In: Yirgu G, Ebinger CJ, Maguire PKH (eds). The Afar Volcanic Province within the East African Rift System. Geological Society, London, Special Publications 259:95-119

George RM, Rogers NW (2002) Plume dynamics beneath the African plate inferred from the geochemistry of the Tertiary basalts of southern Ethiopia. Contributions to Mineralogy and Petrology 144:286–304.

Govindaraju K (1994) 1994 compilation of working values and sample description for 383 geostandards. Geostandards Newsletter 18 (Special Issue): 158p

Halliday AN, Lee, DC, Tommasini S, Davies GR, Paslick CR, Fitton JG, James DE (1995) Incompatible trace elements in OIB and MORB and source enrichment in the sub-oceanic mantle. Earth and Planetary Science Letters 133: 379-395

Harms U, Schandelmeier H, Darbyshire DPF (1990) Pan-African reworked early to middle Proterozoic crust in NE-Africa west of the Nile: Sr and Nd isotope evidence. Journal of the Geological Society London 147: 859-872

Harms U, Darbyshire DPF, Denkler T, Hengst M, Schandelmeier H (1994) Evolution of the Neoproterozoic Delgo suture zone and crustal growth in Northern Sudan: geochemical and radiogenic isotope constraints. Geologische Rundschau 83: 591–603

Hart SR (1984) A large-scale isotope anomaly in the southern hemisphere mantle. Nature 309: 753-757

Hart SR (1988) Heterogeneous mantle domains: Signatures, genesis and mixing chronologies. Earth and Planetary Science Letters 90: 273-296

Hegner E, Pallister JS (1989) Pb, Sr, and Nd isotopic characteristics of Tertiary Red Sea rift volcanics from the Central Saudi Arabian Coastal plain. Journal of Geophysical Research 94: 7749-7755

Heinrichs H, Herrmann AG (1990) Praktikum der Analytischen Geochemie. Springer, Berlin, 669 p

Henjes-Kunst F, Altherr R, Baumann A (1990) Evolution and composition of the western Arabian peninsula: constraints from Sr-Nd isotope systematics of mantle xenoliths. Contributions to Mineralogy and Petrology 105: 460-472

Herzberg C, Zhang J (1996) Melting experiments on anhydrous peridotite KLB-1: Compositions of magmas in the upper mantle and transition zone. Journal of Geophysical Research 101: 8271-8295

Herzberg C, O'Hara MJ (2002) Plume-associated ultramafic magmas of Phanerozoic age. Journal of Petrology 43:1857-1883

Herzberg C (2004) Geodynamic information in peridotite petrology. Journal of Petrology 45:2507–2530

Hofmann AW (1997) Mantle chemistry: the message from oceanic volcanism. Nature 385: 219-228

Hofmann AW, Jochum KP, Seufert M, White WM (1986) Nb and Pb in oceanic basalts: New constraints on mantle evolution. Earth and Planetary Science Letters 79: 33-45

Hofmann C, Courtillot V, Féraud G, Rochette P, Yirgu G, Ketefo E, Pik R (1997) Timing of the Ethiopian flood basalt event and implications for plume birth and global change. Nature 389: 838-841

Imai N, Terashima S, Itho S, Ando A (1995) 1995 compilation of analytical data for minor and trace elements in seventeen GSI geochemical reference samples 'Igneous Rock Series'. Geostandards Newsletter 19: 135-213

Kieffer B, Arndt N, Lapierre H, Bastiene F, Bosch D, Pecher A, Yirgu G, Ayalew D, Weis D, Jerram DA, Keller F, Meugniot C (2004) Flood and Shield Basalts from Ethiopia: Magmas from the African Superswell. Journal of Petrology 45: 793-834.

Klitzsch E (1990) Paleogeographical development and correlation of Continental Strata (former Nubian Sandstone) in northeast Africa. Journal of African Earth Sciences 10: 199-213

Kröner A, Stern RJ, Dawoud AS, Compston W, Reischmann T (1987) The Pan-African continental margin in northeastern Africa: evidence from a geochronological study of granulites at Sabaloka, Sudan. Earth and Planetary Science Letters 85: 91-104

Küster D, Harms U (1998) Post-collisional potassic granitoids from the southern and northwestern parts of the Late Neoproterozoic East African Orogen: a review. Lithos 45: 177-195

Küster D, Liégeois JP (2001) Isotopic and geochemical study of high-grade metamorphic lithologies from Bayuda Desert, Sudan: new insights into the Neoproterozoic evolution of the East Sahara Craton. Precambrian Research 109: 1-23

Küster D, Liégeois J-P, Matukov D, Sergeev S, Lucassen F (2008) Zircon geochronology and Sr, Nd, Pb isotope geochemistry of granitoids from Bayuda Desert and Sabaloka (Sudan):

evidence for a Bayudian event (920-900 Ma) preceding the Pan-African orogenic cycle (860 – 590 Ma) at the eastern boundary of the Saharan Metacraton. Precambrian Research in press
Le Maitre RW (ed.) (1989) A classification of igneous rocks and glossary of terms. Blackwell Scientific Publications, London, 183p
Marques LS, Dupré B, Piccirillo EM (1999) Mantle source compositions of the Paraná Magmatic Province (southern Brazil): evidence from trace element and Sr-Nd-Pb isotope geochemistry. Journal of Geodynamics 28: 439-458
Marty B, Pik R, Yirgu G (1996) Helium isotopic variations in Ethiopian plume lavas: nature of magmatic sources and limit on lower mantle contribution. Earth and Planetary Science Letters 144: 223–237
MacDonald R, Rogers, NW, Fitton JG, Black S, Smith M (2001) Plume-lithosphere interactions in the generation of the basalts in the Kenya rift, East Africa. Journal of Petrology 42, 877-900
McDonough WF, Sun S-S (1995) Composition of the Earth. Chemical Geology 120: 223-253
McKenzie DP, Davies D, Molnar P (1972) Plate tectonics of the Red Sea and East Africa. Nature 224: 125-133
Meneisy MY, Kreuzer H (1974) Potassium-argon ages of Egyptian basaltic rocks. Geologisches Jahrbuch 9: 21-31
Menzies M, Murthy VR (1980) Nd and Sr Geochemistry of hydrous mantle nodules and their host alkali basalts: implications for local heterogeneities in metasomatically veined mantle. Earth and Planetary Science Letters 46: 323-334
Meissner R, Mooney W (1998) Weakness of the lower continental crust: a condition for delamination, uplift and escape. Tectonophysics 296: 47-60
O'Reilly SY, Griffin WL, Poudjom Djomani YH, Morgan P (2001) Are Lithospheres Forever? Tracking changes in sub-continental lithospheric mantle through time. GSA Today 11: 4-10
Pallister JS, Stacey JS, Fischer LB, Premo WR (1988) Precambrian ophiolites of Arabia: Geologic settings, U-Pb geochronology, Pb-isotope characteristics, and implications for continental accretion. Precambrian Research 38: 1-54
Palme H, O'Neill HStC 2004. Cosmochemical estimates of Mantle Composition. In: Treatise on Geochemistry. Holland HD, Turrekian KK (Eds.), Elsevier, Amsterdam, The Netherlands, Vol. 2, 1-38
Peate DW, Hawkesworth CJ (1996) Lithospheric to asthenospheric transition in Low-Ti flood basalts from southern Paraná, Brazil. Chemical Geology 127: 1-24
Pik R, Deniel C, Coulon C, Yirgu G, Hofmann C, Ayalew D (1998) The Northwestern Ethiopian plateau flood basalts: classification and spatial distribution of magma types. Journal of Volcanology and Geothermal Research 81: 91-111
Pik R, Deniel C, Coulon C, Yirgu G, Marty B (1999) Isotopic and trace element signatures of Ethiopian flood basalts: evidence for plume–lithosphere interactions. Geochimica Cosmochimica Acta 63: 2263-2279
Pik R, Marty B, Hilton DR (2006) How many mantle plumes in Africa? The geochemical point of view. Chemical Geology 226: 100-114
Poudjom Djomani YH, O'Reilly SY, Griffin WL, Morgan P (2001) The density structure of subcontinental lithosphere through time. Earth and Planetary Science Letters 184: 605-621.
Reisberg L, Zindler A, Marcantonio F, White W, Wyman D, Weaver B (1993) Os Isotope Systematics in Ocean Island Basalts. Earth and Planetary Science Letters 120:149-167
Ritsema J, Allen RM (2003) The elusive mantle plume. Earth and Planetary Science Letters 207: 1-12
Roeder PL, Emslie PF (1970) Olivine-Liquid equilibrium. Contributions to Mineralogy and Petrology 29: 275-289
Romer RL, Heinrich W, Schröder-Smeibidl B, Meixner A, Fischer CO, Schulz C (2005) Elemental dispersion and stable isotope fractionation during reactive fluid-flow and fluid

immiscibility in the Bufa del Diente aureole, NE-Mexico: Evidence from radiographies and Li, B, Sr, Nd, and Pb isotope systematics. Contributions to Mineralogy and Petrology 149: 400-429
Rudnick RL, Fountain DM (1995) Nature and composition of the continental crust: a lower crustal perspective. Reviews of Geophysics 33: 267-309
Rudnick RL, and Gao S (2004) Composition of the continental crust. In: Treatise on Geochemistry volume 3, The Crust, Rudnick RL (editor) Elsevier, New York, 1–64
Salters VJM, White WM (1998) Hf isotope constraints on mantle evolution. Chemical Geology 145: 447-460
Salters VJM, Stracke A (2004) Composition of the depleted mantle. Geochemistry Geophysics Geosystems 5: doi:10.1029/2003GC000597.
Satir M, Morteani G, Fuganti A, Drach vV (1991) K-Ar ages, Sr isotopic compositions and chemistry of late Cretaceous – Tertiary basalts from the Nubian Desert (northern Sudan). European Journal of Mineralogy 3: 943-955
Scarsi P, Craig H (1996) Helium isotope ratios in Ethiopian Rift basalts. Earth and Planetary Science Letters 144: 505-516
Schandelmeier H, Reynolds P-O (Eds.) (1997) Paleogeographic-paleotectonic atlas of north-eastern Africa, Arabia, and adjacent areas. Rotterdam: Balkema.
Schilling J, Kingsley RH, Hanan BB, McCully BL (1992) Nd-Sr-Pb isotopic variations along the Gulf of Aden: Evidence for Afar mantle plume–continental lithosphere interaction. Journal of Geophysical Research 97: 10927-10966
Schuhmacher E (1975) Herstellung von 99.9997% 38Ar für die 40K/40Ar Geochronologie. Chimia 24: 441-442
Sebai A, Stutzmann E, Montagner J-P, Sicilia D, Beucler E (2006) Anisotropic structure of the African upper mantle from Rayleigh and Love wave tomography. Physics of the Earth and Planetary Interiors 155: 48-62
Shaw JE, Baker JA, Menzies MA, Thirlwall MF, Ibrahim KM (2003) Petrogenesis of the largest intraplate volcanic field on the Arabian Plate (Jordan): a mixed lithosphere– asthenosphere source activated by lithospheric extension. Journal of Petrology 44, 1657–1679.
Shaw JE, Baker JA, Kent AJR, Ibrahim KM, Menzies MA (2007) The geochemistry of the Arabian lithospheric mantle - a source for intraplate volcanism? Journal of Petrology, in press
Stacey JS, Kramers JD (1975) Approximation of terrestrial lead evolution by a two-stage model. Earth and Planetary Science Letters 26: 207-221
Stacey JS, Stoeser DB (1983) Distribution of oceanic and continental leads in the Arabian–Nubian Shield. Contributions to Mineralogy and Petrology 84: 91-105
Steiger RH, Jäger E (1977) Subcommission on geochronology: convention on the use of decay constants in geo- and cosmochronology. Earth and Planetary Science Letters 36: 359-362
Stein M (2003) Tracing the plume material in the Arabian-Nubian shield. Precambrian Research123: 223–234
Stein M, Hofmann AW (1992) Fossil plumes beneath the Arabian lithosphere? Earth and Planetary Science Letters 114: 193-209
Stein M, Navon O, Kessel R (1997) Chromatographic metasomatism of the Arabian–Nubian lithosphere. Earth and Planetary Science Letters 152: 75-91
Stern RJ (1994) Neoproterozoic (900–550 Ma) arc assembly and continental collision in the East African Orogen: implications for the consolidation of Gondwanaland. Annual Review of Earth Planetary Sciences 22: 319-351
Stern RJ (2002) Crustal evolution in the East African Orogen: a neodymium isotopic perspective. Journal of African Earth Sciences 34: 109-117
Stern RJ, Abdelsalam MG (1998) Formation of juvenile continental crust in the Arabian–Nubian Shield: evidence from Granitic rocks of the Nakasib Suture, NE Sudan. Geologische
Rundschau 87: 150-160

Stoeser DB, Frost CD (2006) Nd, Pb, Sr, and O isotopic characterization of Saudi Arabian Shield terranes. Chemical Geology 226: 163-188

Stracke A, Hofmann AW, Hart SR (2005) FOZO, HIMU, and the rest of the mantle zoo, Geochemistry Geophysics Geosystems 6: doi:10.1029/2004GC000824

Stewart K and Rogers N (1996) Mantle plume and lithosphere contributions to basalts from southern Ethiopia. Earth and Planetary Science Letters 139, 195-211

Sun SS, McDonough WF (1989) Chemical and isotopic systematics of oceanic basalts: Implications for mantle composition and processes. In: Magmatism in the Ocean Basins. Saunders AD, Norry MJ (editors) Geological Society London Special Publication 42: 313-345

Taylor SR, McLennan SM (1985) The Continental Crust: Its Composition and Evolution. Blackwell Publisher, Oxford

Teklay M, Kröner A, Mezger K (2002) Enrichment from plume interaction in the generation of Neoproterozoic arc rocks in northern Eritrea: implications for crustal accretion in the southern Arabian–Nubian Shield. Chemical Geology 184: 167-184

Vidal P, Deniel C, Vellutini PJ, Piguet P, Coulon C, Vincent J, Audin J (1991) Changes of mantle sources in the course of a rift evolution: the Afar case. Geophysical Research Letter 18: 1913-1916

Volker F, McCulloch MT, Altherr R (1993) Submarine basalts from the Red Sea: New Pb, Sr, and Nd isotopic data. Geophysical Research Letter 20: 927-930

Volker F, Altherr R, Jochum K-P, McCulloch MT (1997) Quaternary volcanic activity of the southern Red Sea: new data and assessment of models on magma sources and Afar plume-lithosphere interaction. Tectonophysics 278: 15-29

Weaver BL (1991) The origin of ocean island basalt end-member compositions: trace element and isotopic constraints. Earth and Planetary Science Letters 104: 381-397

Weinstein Y, Navon O, Altherr, R, Stein M (2006) The Role of Lithospheric Mantle Heterogeneity in the Generation of Plio-Pleistocene Alkali Basaltic Suites from NW Harrat Ash Shaam (Israel) Journal of Petrology 47: 1017 - 1050

Wemmer K, Ahrendt H (1991) Comparative K–Ar and Rb–Sr age determinations of retrograde processes on rocks from the KTB deep drilling project. Geologische Rundschau 86 (supplement): S272-S285

Willbold M, Stracke A (2006) Trace element composition of mantle end-members: Implications for recycling of oceanic and upper and lower continental crust. Geochemistry Geophysics Geosystems 7, doi:10.1029/2005GC001005

Wipki M (1995) Eigenschaften, Verbreitung und Entstehung von Kaolinlagerstätten im Nordsudan. PhD thesis, Technische Universität Berlin, Verlag Dr. Köster, Berlin, 213 p

Woldetinsae G, Götze HJ (2005) Gravity field and isostatic state of Ethiopia and adjacent areas. Journal of African Earth Sciences (and the Middle East) 41: 103-117

Workman RK, Hart SR (2005) Major and trace element composition of the depleted MORB mantle (DMM). Earth and Planetary Science Letters 231: 53-72

Zimmer M, Kröner A, Jochum KP, Reischmann T, Todt W (1995) The Gabal Gerf complex: A Precambrian N-MORB ophiolite in the Nubian Shield, NE Africa. Chemical Geology 123: 29-51

Zindler A, Hart SR (1986) Chemical geodynamics. Annual Review of Earth and Planetary Sciences 14: 493-571

Figures

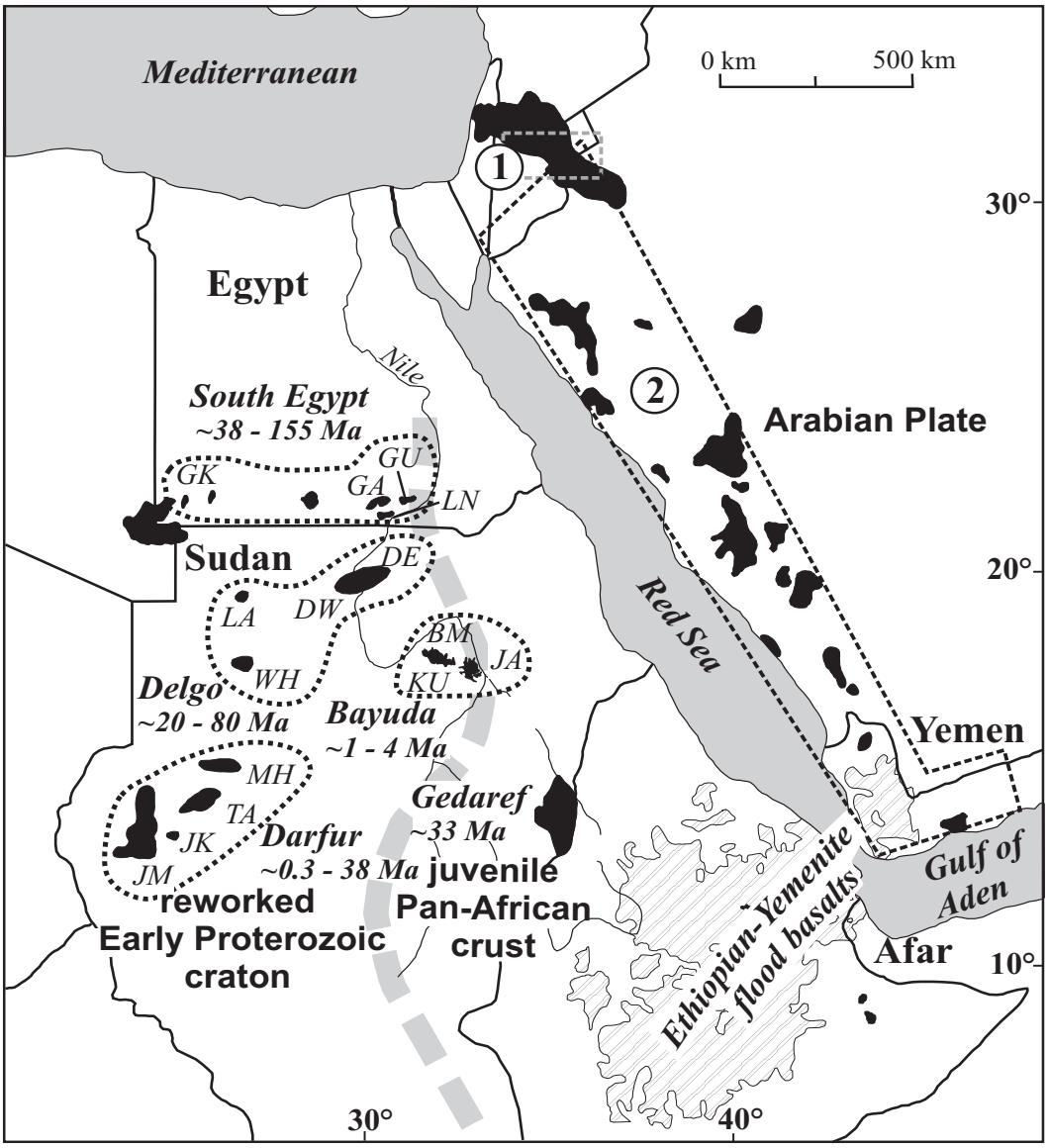

Figure 1

Figure 1 Distribution of intra-plate magmatism in NE Africa and the western Arabian plate and the Ethiopian – Yemenite 'Afar' flood basalt province. Compiled from Schandelmeier and Reynolds (1997). The extent of the intra-plate volcanism in the map is schematic and most localities comprise a number of small isolated outcrops. Key to sample locations and regional grouping of the NE-African samples: Group 'South Egypt' GK = Gilf Kebir; GA = Gebel el Asr; GU = Gebel um Shagir; LN = Lake Nasser; Group 'Delgo' DW = Delgo west; DE = Delgo east; LA = Laqia Arbain; WH = Wadi Howar; Group 'Bayuda' BM = Bayuda main volcanic field; KU = Gebel Kurbei; JA=Jebel Umm Arafieb; Group 'Darfur' JM = Gebel Marra; JK = Gebel Kussa; TA = Tagabo Hills; MH = Meidob Hills; Group 'Gedaref'. The suture zone in the Pan-African orogen (thick grey dashed line) separates mainly reworked Early Proterozoic craton from mainly Pan-African juvenile crust (e.g. Küster and Liégeois 2001; Abdelsalam et al. 2002); note however, that also west of this line juvenile and east of it cratonic crust can be found. Approximate areas for comparison with intra-plate magmatic rocks on the Arabian Plate are indicated by dotted lines from (1) Shaw et al. (2003) and (2) Bertrand et al. (2003).

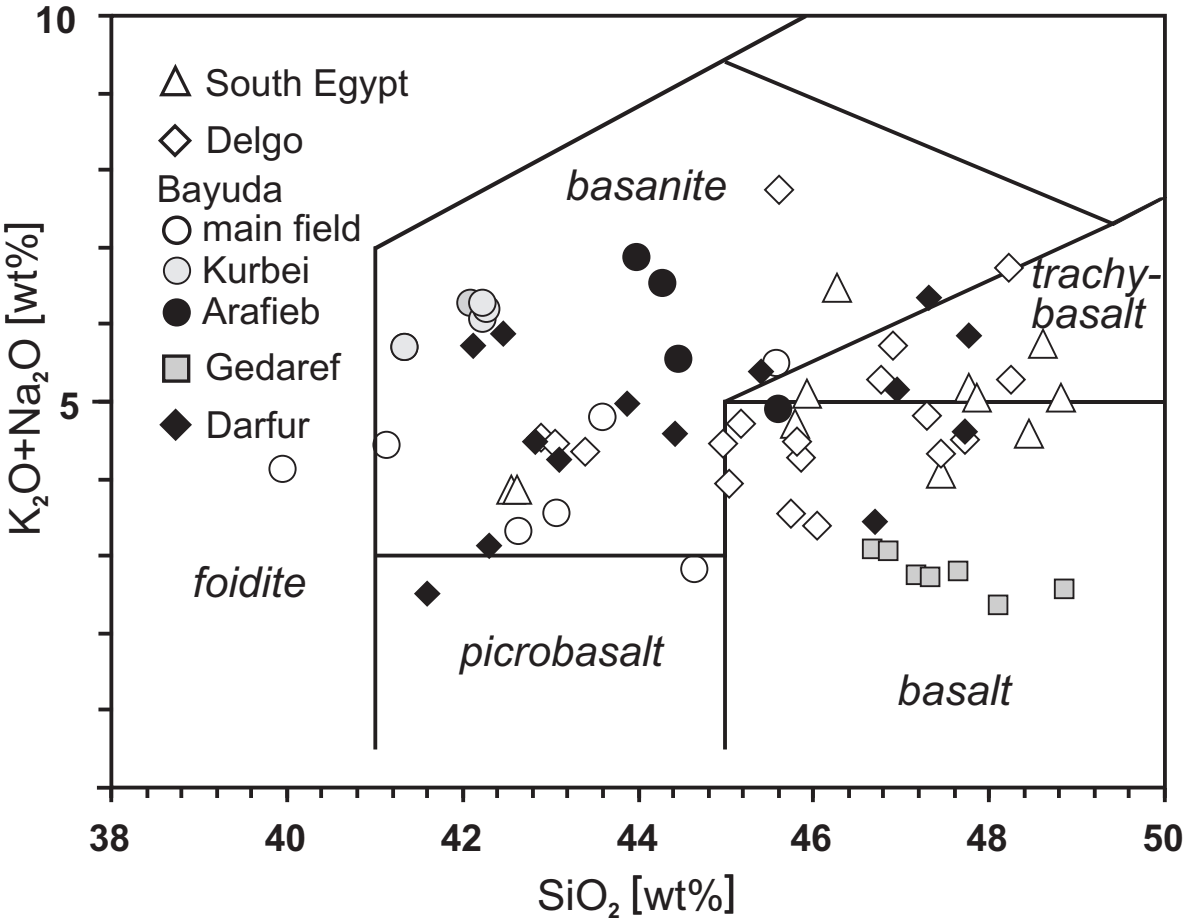

Figure 2

Figure 2 TAS-diagram (Le Maitre 1989) of the selected intra-plate magmatic rocks from Sudan and Egypt. Sample compositions are recalculated to dry 100%.

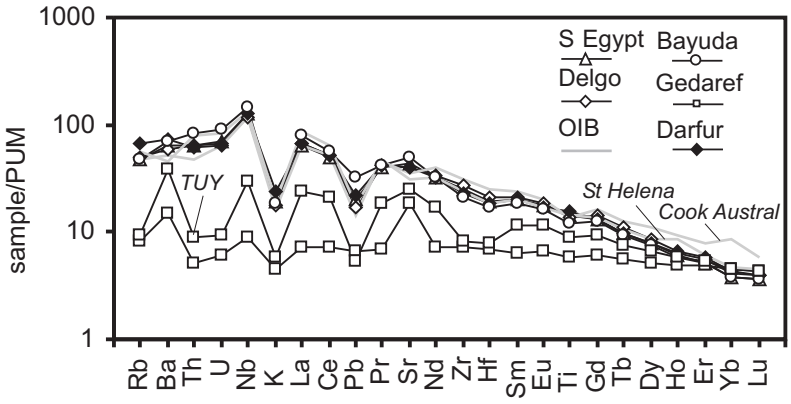

Figure 3

Figure 3. Primitive upper mantle (PUM; Palme and O'Neill 2004) normalized trace element patterns of the South Egypt, Delgo, Darfur, and Bayuda areas are very similar. The TUY-samples of the Gedaref area show a similar flat pattern as the other Gedaref samples, but are more enriched in incompatible trace elements. Average compositions of St. Helena and Cook Austral OIBs (Oceanic Island Basalts) are shown for comparison.

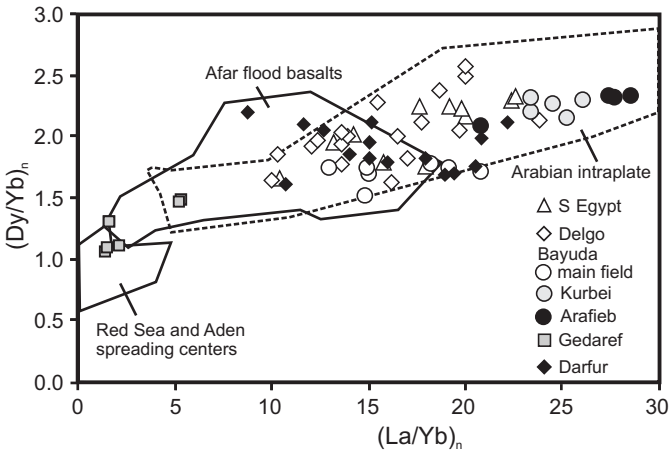

Figure 4

Figure 4 Dy/Yb and La/Yb normalized to C1 chondrite. The compositions of the NE-African samples and Arabian intra-plate magmatic rocks overlap. The compositional fields of Red Sea and Gulf of Aden spreading centers basalts and Afar flood basalts are also shown (references see the text). C1 chondrite (McDonough and Sun 1995)

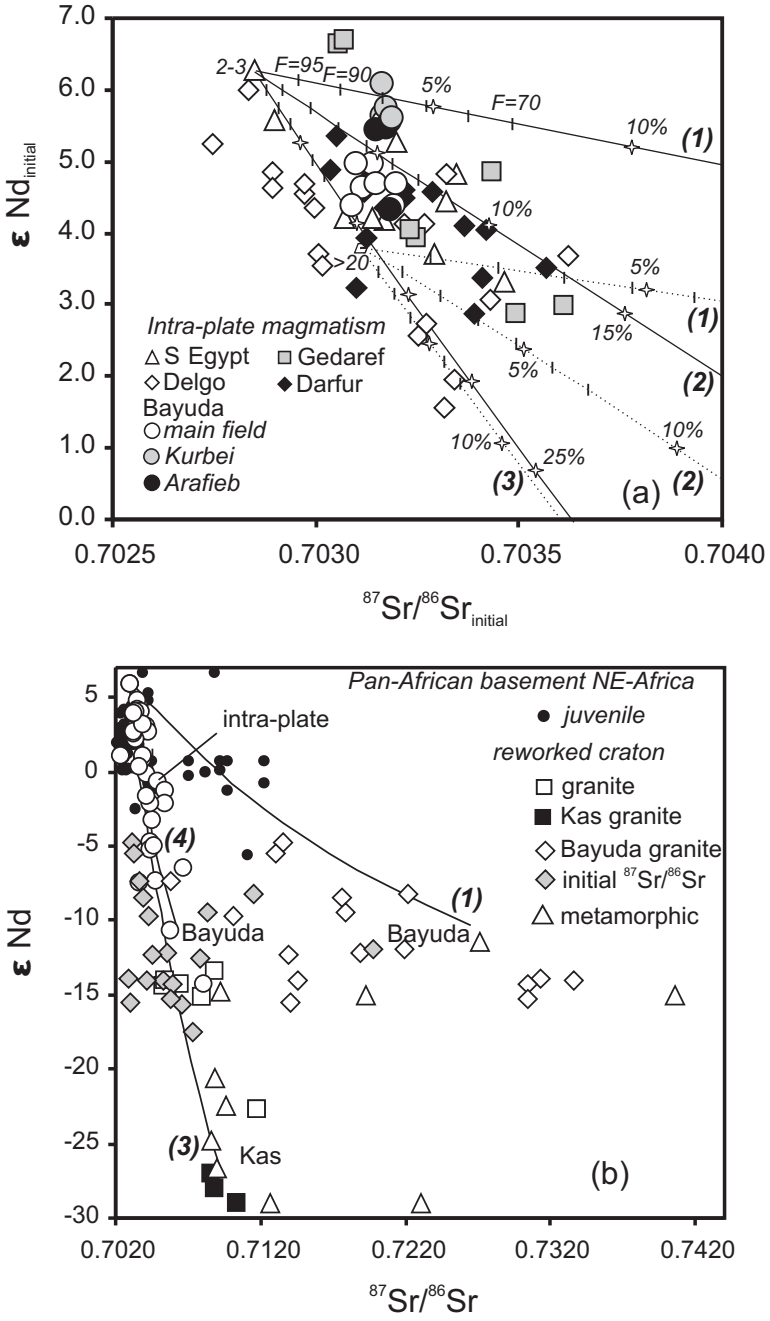

Figure 5

Figure 5 a, b, Sr and Nd isotope composition and possible contamination by crustal material. (a) Initial Sr and Nd isotope ratios of the selected intra-plate magmatic rocks from NE-Africa (Sudan and Egypt).

Endmembers used in the AFC modelling of crustal contamination (DePaolo. 1981) and binary mixing lines are described below. Sample 2-3 (labelled 2-3) is an example of radiogenic Nd and unradiogenic Sr isotope composition ($^{87}Sr/^{86}Sr_{initial}$=0.7028, $\varepsilon Nd_{initial}$=5.3, $^{206}Pb/^{204}Pb_{initial}$= 19.86, $^{207}Pb/^{204}Pb_{initial}$=15.64, Sr=891ppm, Nd=45.1ppm, Pb=2.9ppm). The second endmember is the average composition of samples with $^{206}Pb/^{204}Pb$>20 (labelled >20), i.e. the possible high-μ endmember ($^{87}Sr/^{86}Sr_{initial}$=0.7031, $\varepsilon Nd_{initial}$=3.8, $^{206}Pb/^{204}Pb_{initial}$= 20.2, $^{207}Pb/^{204}Pb_{initial}$=15.72, Sr=604ppm, Nd=31ppm, Pb=2.5ppm). Element contents of the

intra-plate 'endmembers' were corrected for olivine fractionation, which implies that unfractionated mantle magma enters the crust and enhances the effect of crustal contamination by the lower trace element abundances in the corrected mantle magma compositions. Two crustal endmembers are considered, the average isotope composition of the Bayuda granite ($^{87}Sr/^{86}Sr$=0.7265, $^{87}Sr/^{86}Sr_{initial}$=0.7061, ε Nd -11.3, $^{206}Pb/^{204}Pb$=19.38, $^{206}Pb/^{204}Pb_{initial}$=18.18, $^{207}Pb/^{204}Pb$=15.78, $^{207}Pb/^{204}Pb_{initial}$=15.71; Sr=320ppm, Nd=27ppm, and Pb=17ppm; element contents are for average upper crust; Rudnick and Gao 2004) and the average Kas granite with a more extreme isotope composition and measured elemental abundances ($^{87}Sr/^{86}Sr$=0.7093, $^{87}Sr/^{86}Sr_{initial}$=0.7071, ε Nd_0=-28, $^{206}Pb/^{204}Pb$=16.89, $^{207}Pb/^{204}Pb$=15.64; Sr=779 ppm, Nd=28.1 ppm, Pb=24.1 ppm). Bulk distribution coefficients are assumed to be uniformly low (solid/melt K_D=0.1), because olivine is considered as the main fractionating mineral up to F (remaining melt) of ~0.7. The assimilated crust/fractionated mineral ratio is set to 0.2 derived from the possible contamination of the Pb isotope system in the intra-plate rocks to values of $^{206}Pb/^{204}Pb$ = 19.5 (see Figure 6).

Lines **(1)** represent trajectories of AFC and binary mixing with Bayuda granite, **(2)** with Kas granite and measured element abundances, and **(3)** Kas granite and element abundances of average upper crust. The Kas and possible Bayuda endmember with initial $^{87}Sr/^{86}Sr$ plot along a similar trajectory and the Bayuda line **(4** in Fig. b**)** is not shown in (a). Tick-marks indicate the amounts of remaining melt during progression of ACF, stars the amount of crust from binary mixing (both in 5% steps).

(b) Juvenile and reworked cratonic basement of Pan-African age from NE-Africa and Mesozoic-Quaternary intra-plate magmatic rocks from the studied area including crust-contaminated samples. Data sources: Davidson and Wilson (1989), Harms et al. (1990), Zimmer et al. (1995), Küster and Liégois (1998), Stern and Abdelsalam (1998), Teklay et al. (2001), Bailo et al. (2003), Küster et al. (2008) and our unpublished data (2006). Mesozoic to Cenozoic intra-plate magmatic rocks of the studied area include crust-contaminated samples. Data sources: Davidson and Wilson (1989), Franz et al. (1999), and our unpublished data (2006). The field of basement composition extends to higher $^{87}Sr/^{87}Sr$.

The trajectories of crustal contamination from sample 2-3 are toward reworked cratonic crust of the Kas type (line **3**) or, if the initial their initial Sr isotope ratios are considered, of the Bayuda type (line **4**). The required low Sr isotope ratios (< 0.71) indicate involvement of Rb-deficient, Pan-African high-grade crust. Substantial contribution of radiogenic Sr isotopes (upper crust line **1**) is unlikely.

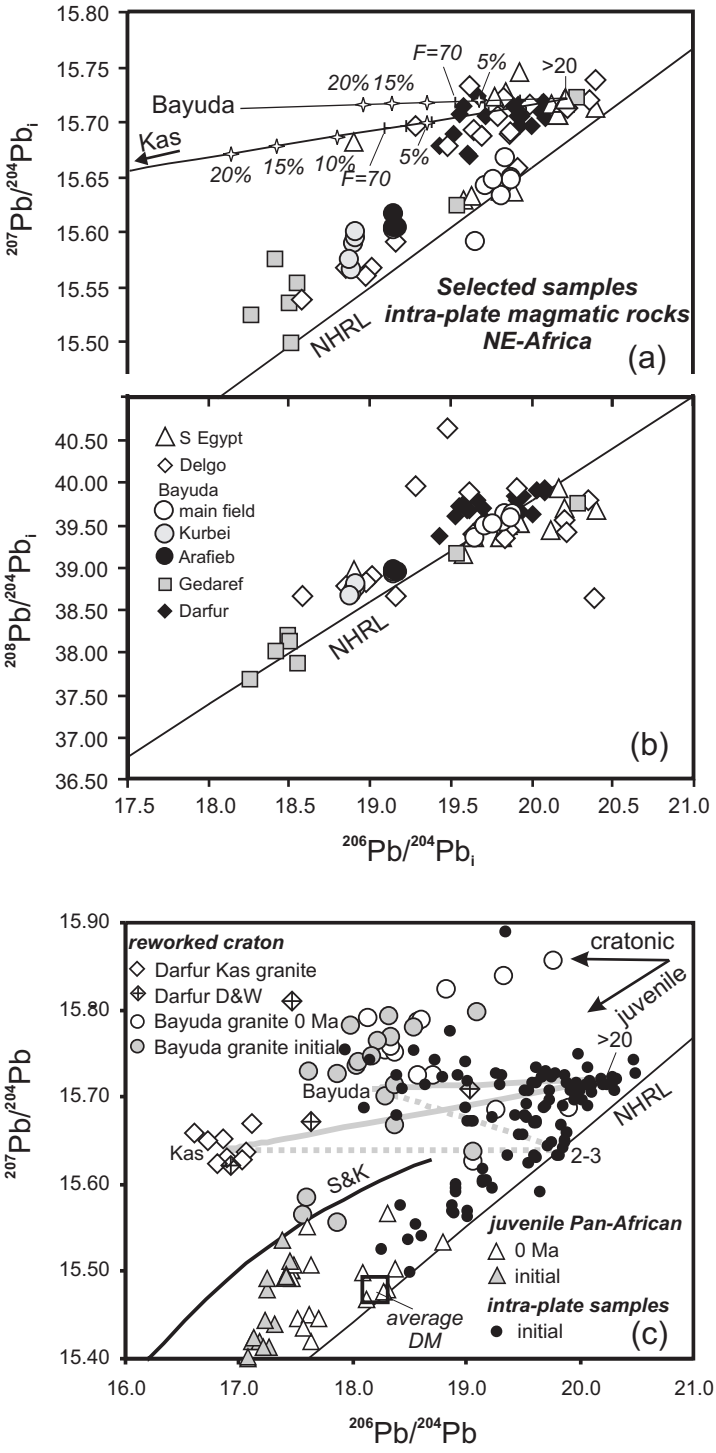

Figure 6

Figure 6 a, b, c, Pb isotope composition of intra-plate magmatic and basement rocks of NE-Africa. (a) and (b) Pb-isotope compositions of the selected intra-plate magmatic rocks from NE-Africa (Sudan and Egypt). (a) Trajectories of possible crustal contamination for AFC up to F=0.7 and bulk mixing (% crust added) for the average intra-plate samples ($^{206}Pb/^{204}Pb>20$) and the Bayuda (initial isotope ratios) and the Kas crustal endmembers assuming Pb contents of average upper crust (see caption Figure 5 for setup of the model). ~ 5% of crustal material is sufficient to explain the observed variation in $^{206}Pb/^{204}Pb$ in the radiogenic samples.

(c) Pb-isotope compositions of Pan-African basement and intra-plate magmatism in NE-Africa. The reworked craton is represented by post-orogenic Pan-African granites and four metamorphic rocks. In the Darfur area, measured compositions of whole rock and leached feldspars of the Kas granite are very similar and not distinguished in the diagram (our unpublished data, 2006, eTable 3; one data point of the granites from D&W: Davidson and Wilson 1989). Measured and initial ratios are shown for granites from the Bayuda area (whole rock; Küster et al. 2008). Four metamorphic rocks of the Darfur area represent measured ratios (no initial ratios given, one sample plots outside the panel with $^{207}Pb/^{204}Pb$=16.01; Davidson and Wilson 1989). The $^{207}Pb/^{204}Pb$ ratios of most samples from the reworked craton are substantially higher than in average continental crust (S&K; Stacey and Kramers 1975). The Pan-African juvenile basement is represented by the measured and initial composition of ophiolite (Zimmer et al. 1995) and igneous rocks (Stern and Abdelsalam 1998; Bailo et al. 2003). Late Mesozoic to Cenozoic intra-plate magmatic rocks of the studied area include crust contaminated samples. The arrows indicate typical trajectories of possible crustal contamination by cratonic and juvenile basement. Mixing lines are indicated as in (a) and in addition for sample 2-3 (see Fig. 5 for details). Data sources as in Fig. 5. NHRL= northern hemisphere reference line (Hart 1984).

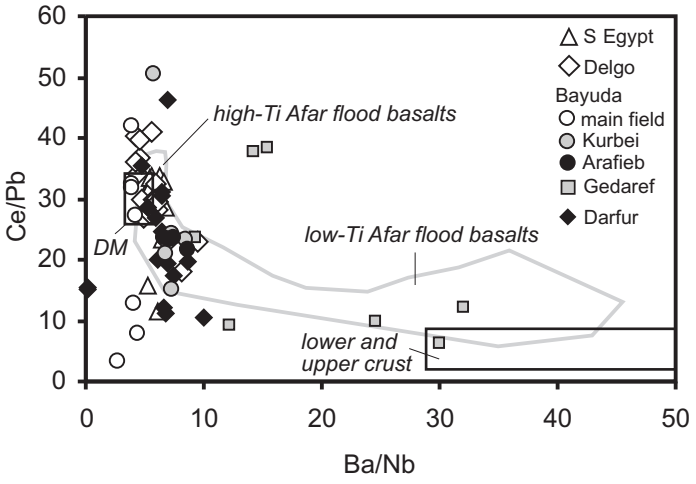

Figure 7

Figure 7 Ce/Pb and Ba/Nb distinguish crust and mantle compositions. The field of depleted mantle compositions is based on values from Hoffman et al. (1986), Weaver (1991), Salters and Stracke (2004), Workman and Hart (2005). The field of lower and upper crust is from Taylor and McLennan (1985) and Rudnick and Gao (2004). The field of Ethiopian flood basalts (Pik et al. 1999) indicates strong crustal contributions to many samples of the low Ti series, whereas many samples of the high Ti series resemble mantle compositions.

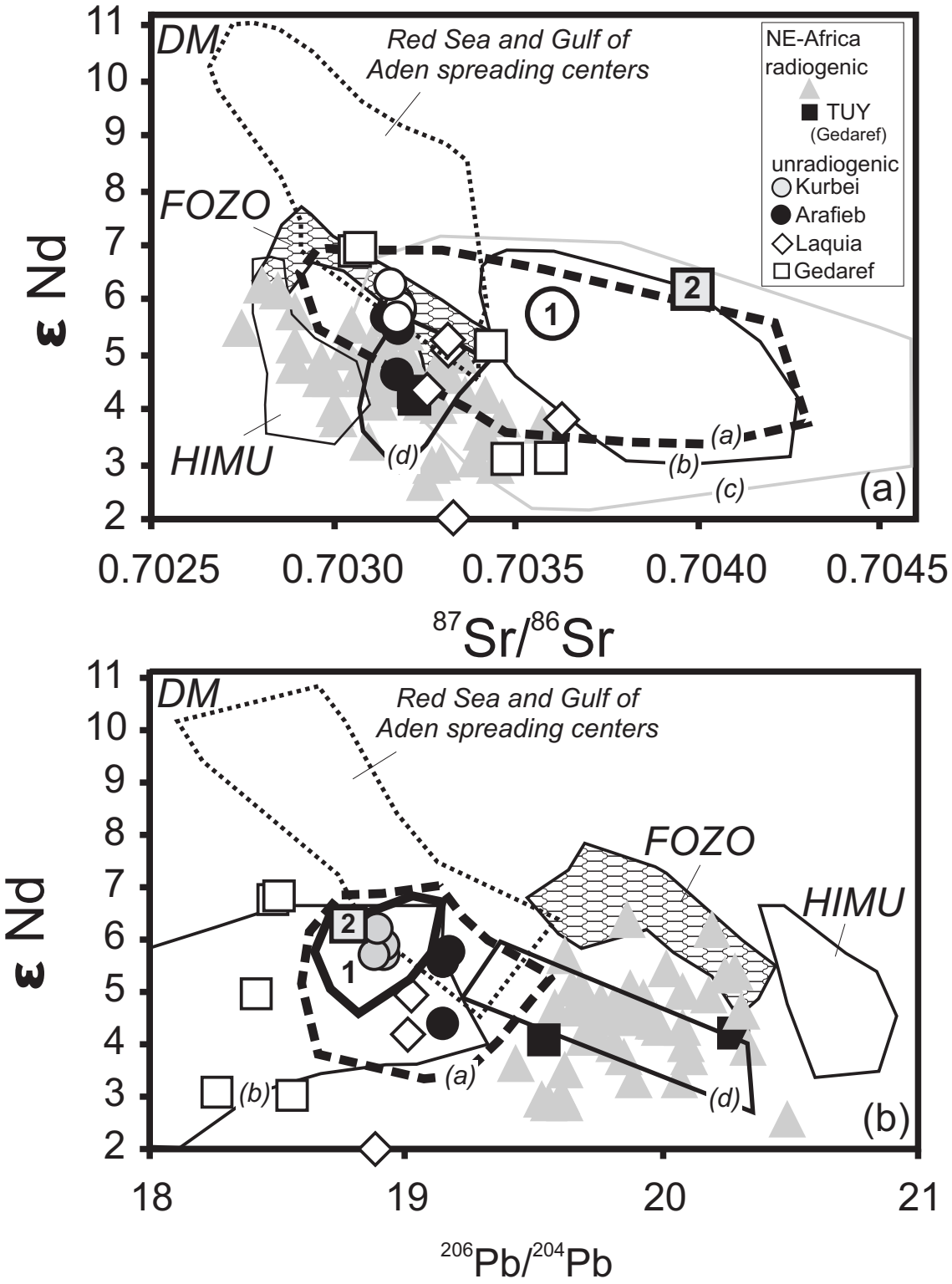

Figure 8

Figure 8 a, b Nd, Sr and Pb isotope compositions of the NE-African intra-plate magmatic rocks with radiogenic ($^{206}Pb/^{204}Pb$> 19.5) and unradiogenic (Jebel Kurbei, Umm Arafieb, Laquia Arbain, and most Gedaref samples) Pb isotope compositions are compared with

compositional fields of various regional groups of mantle derived magmatic rocks. Field *(a)* includes Arabian intra-plate magmatic rocks (Bertrand et al. 2003; Shaw et al. 2003); Afar flood basalts and younger basalts ascribed to Afar plume activity are in field *(b)* with high data density and field *(c)*, which includes all data (Deniel et al. 1994; Baker et al. 1996; Barrat et al. 1998; Pik et al. 1999; Kieffer et al. 2004); proposed Afar plume compositions (1) (Baker et al. 1996 mainly based on data of Deniel et al. 1994) and (2) (Pik et al. 1999); basalts from the Red Sea and Gulf of Aden spreading centres (Altherr et al. 1988, 1990; Schilling et al. 1992; Volker et al. 1993, 1997); field *(d)* includes data of high-μ rocks from the EARS (Turkana; Furman et al. 2006a). The FOZO compositional field is drawn from the Austral Cook OIB data in Stracke et al. (2005); the HIMU field is drawn after the St. Helena OIB (Chaffey et al. 1989); DM: depleted mantle; EM 1 and EM 2 compositions plot far out of the Nd and Sr isotope diagram and contributions of such sources were likely absent or minute. The distribution of data points in the compositional fields and additional variation diagrams are shown in eFigure 6.

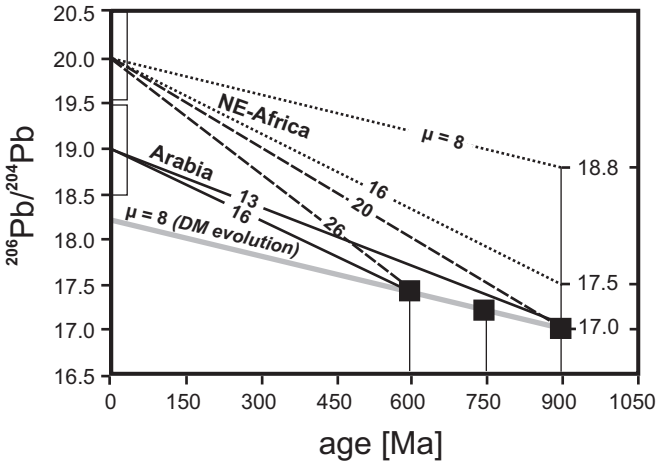

Figure 9

Figure 9 Conceptual model for the evolution of the lithospheric mantle beneath NE-Africa and the Arabian plate (modified from Stein et al., 1997). The starting composition of the subarc mantle is the average isotopic composition of the Gerf ophiolite 750 m.y. ago (Zimmer et al. 1995), which is similar to MORB-type DM mantle. The depleted mantle composition is extrapolated using μ = 8. The average present $^{206}Pb/^{204}Pb$ compositions of the NE-African and Arabian lithospheric mantle domains (small rectangular boxes) require μ values between 13 and 26 assuming the initial $^{206}Pb/^{204}Pb$ ratios of the depleted mantle and ages between 600 and 900 Ma for possible formation of the Pan-African lithospheric mantle from such mantle. The initial composition of the lithospheric mantle is an additional parameter in this conceptual model. The example is for an age of the lithospheric mantle of 900 Ma. A $^{206}Pb/^{204}Pb$ of 17.0 represents the initial depleted mantle value and would require a μ of 20 to accomplish the average Pb isotope composition of the NE-African intra-plate magmatic rocks. A more radiogenic initial value of $^{206}Pb/^{204}Pb$ 17.5 (Pan-African plume related high-μ mantle; Stein 2003) would require a μ-value of 16. The assumption of a typical mantle-μ-value of 8 in the source of the NE-African samples would relate to an initial $^{206}Pb/^{204}Pb$ ratio of 18.8, which appears to be unlikely.

Table 1 Sample localities, crystallization ages, and measured and initial isotope Sr, Nd, and Pb ratios of intra-plate magmatic rocks from NE-Africa. The 2σ uncertainty on the measured Pb isotope ratios is assumed to be 0.1% including the uncertainty in the correction for instrumental mass fractionation. References to the K-Ar ages: see eTable 1.

Table 1 Sample localities, crystallization ages, and measured and initial (i) Sr, Nd, and Pb isotope ratios of intra-plate magmatic rocks from NE-Africa. The 2σ uncertainty on the measured Pb isotope ratios is assumed to be 0.1% including the uncertainty in the correction for instrumental mass fractionation. References to the K-Ar ages: see eTable 1; all errors are 2 σ.

Group	Location /coordinates	sample No	age Ma	$^{87}Rb/^{86}Sr$	$^{87}Sr/^{86}Sr$	$^{87}Sr/^{86}Sr$ i	$^{147}Sm/^{144}Nd$	$^{143}Nd/^{144}Nd$	$^{143}Nd/^{144}Ndi$	ε - Nd_0	ε - Nd_t	μ	ω	$^{206}Pb/^{204}Pb$	$^{206}Pb/^{204}Pbi$	$^{207}Pb/^{204}Pb$	$^{207}Pb/^{204}Pbi$	$^{208}Pb/^{204}Pb$	$^{208}Pb/^{204}Pbi$
S-EGYPT	Gilf Kebir (GK)																		
	23°15'; 26°00'	2-1	37.9±2.0	0.0657	0.702933±7	0.702897	0.1209	0.512904±5	0.512874	5.19	5.58	33	123	19.81	19.62	15.64	15.63	39.45	39.22
		2-3	37.9±2.0	0.0654	0.702885±7	0.702849	0.1230	0.512940±5	0.512910	5.89	6.27	37	142	20.08	19.86	15.65	15.64	39.70	39.43
	23°03'; 27°38'	2-7	59±1.7	0.0897	0.703368±8	0.703293	0.1260	0.512810±5	0.512761	3.36	3.72	36	118	20.14	19.81	15.65	15.63	39.88	39.53
	Lake Nasser (LN)																		
	~22°00; 30°50'	P-7	79±3.0	0.1153	0.703301±8	0.703171	0.1169	0.512811±5	0.512751	3.37	4.19	35	129	20.43	20.00	15.77	15.75	40.11	39.60
		P-8	79±3.0	0.0752	0.703430±7	0.703346	0.1282	0.512849±5	0.512783	4.12	4.82	33	122	20.59	20.19	15.74	15.72	39.99	39.51
	Gebel um Shagir (GU)																		
	~ 23°20'; 32°	GU-12	155±4.0	0.1856	0.703606±11	0.703197	0.1181	0.512826±5	0.512706	3.67	5.27	19	78	20.72	20.25	15.74	15.71	40.63	40.03
		GU18	155±4.0	0.1942	0.703745±11	0.703317	0.1293	0.512795±6	0.512664	3.06	4.44	23	105	19.56	19.00	15.71	15.69	39.90	39.09
	Gebel el Asr (GA)																		
	~22°50'; 31°	GA-02	87±2.0	0.1100	0.703208±11	0.703072	0.1273	0.512827±5	0.512755	3.69	4.22	29	112	20.16	19.76	15.74	15.72	39.89	39.41
		GA-04	87±2.0	0.0832	0.703242±10	0.703139	0.1153	0.512822±7	0.512756	3.59	4.21	31	102	20.73	20.31	15.73	15.71	40.01	39.57
		GA-21	87±2.0	0.0198	0.703489±13	0.703465	0.1098	0.512774±5	0.512711	2.65	3.32	35	110	20.57	20.10	15.74	15.71	40.08	39.61
	Laquia Arbain (LA)																		
DELGO	~20°; 28°	12-2	19.6±1.0	0.0705	0.703362±7	0.703342	0.1286	0.512726±7	0.512710	1.72	1.94	20	72	18.94	18.88	15.57	15.57	38.88	38.81
		12-3	19.6±1.0	0.0503	0.703334±8	0.703320	0.1282	0.512877±6	0.512861	4.66	4.84	31	126	19.12	19.02	15.57	15.57	39.03	38.91
	~19°50'; 28°15	12-10	21.4±0.8	0.0763	0.703291±8	0.703269	0.1290	0.512838±7	0.512820	3.90	4.13	31	116	19.12	19.01	15.57	15.56	38.99	38.87
		12-12	21.4±0.8	0.3270	0.703721±7	0.703621	0.1320	0.512815±7	0.512797	3.45	3.67	24	89	18.69	18.61	15.54	15.54	38.81	38.71
	Wadi Howar (WH)																		
	18°; 30°	WH-1	37.6±0.9	0.0624	0.703005±11	0.702972	0.1186	0.512841±7	0.512812	3.96	4.56	37	131	20.19	19.97	15.73	15.71	39.95	39.71
	17°50', 29°40'	WH-2	71.9±1.8	0.1198	0.703127±8	0.703004	0.1216	0.512799±6	0.512742	3.14	3.72	37	136	20.75	20.33	15.74	15.72	40.25	39.76
		WH-31	71.9±1.8	0.1435	0.703575±10	0.703428	0.1165	0.512764±6	0.512709	2.46	3.07	33	122	20.26	19.89	15.68	15.66	40.35	39.92
	Delgo basement west of the Nile (DW)																		
	~19°49'; 30°	NB 9a	76.7±1.9	0.1197	0.703403±13	0.703273	0.1288	0.512747±5	0.512682	2.13	2.73	26	105	19.94	19.63	15.75	15.73	40.31	39.91
		NB 10	80.9±2.0	0.1226	0.703159±14	0.703018	0.1241	0.512787±6	0.512721	2.91	3.56	32	116	20.25	19.85	15.71	15.69	39.90	39.43
		NB 11	80.9±2.0	0.1339	0.702987±10	0.702833	0.1339	0.512917±7	0.512846	5.44	6.00	31	106	20.60	20.20	15.73	15.71	39.97	39.55
		RC-101	59±1.7	0.1577	0.703386±8	0.703254	0.1145	0.512732±4	0.512688	1.83	2.57	28	106	20.74	20.48	15.76	15.74	39.05	38.75
		7-51	59±1.7	0.0656	0.702801±8	0.702746	0.1167	0.512876±6	0.512831	4.64	5.26	46	185	20.72	20.29	15.74	15.72	40.04	39.50
		7-55	59±1.7	0.0689	0.703054±8	0.702997	0.1251	0.512833±6	0.512785	3.80	4.35	26	95	19.97	19.73	15.71	15.70	39.76	39.48
		7-56	59±1.7	0.0870	0.703043±7	0.702970	0.1246	0.512850±7	0.512802	4.14	4.69	31	108	20.16	19.88	15.74	15.72	39.72	39.40
	Delgo basement east of the Nile (DE)																		
	~20°10'; 30°40'	RC-411	82±2.9	0.0998	0.703009±10	0.702893	0.1263	0.512854±5	0.512786	4.21	4.84	34	121	20.13	19.68	15.71	15.69	39.99	39.50

Table 1 Sample localities, crystallization ages, and measured and initial (i) Sr, Nd, and Pb isotope ratios of intra-plate magmatic rocks from NE-Africa. The 2σ uncertainty on the measured Pb isotope ratios is assumed to be 0.1% including the uncertainty in the correction for instrumental mass fractionation. References to the K-Ar ages: see eTable 1; all errors are 2 σ.

Group	Location /coordinates	sample No	age Ma	$^{87}Rb/^{86}Sr$	$^{87}Sr/^{86}Sr$	$^{87}Sr/^{86}Sr$ i	$^{147}Sm/^{144}Nd$	$^{143}Nd/^{144}Nd$	$^{143}Nd/^{144}Ndi$	ε - Nd_0	ε - Nd_t	μ	ω	$^{206}Pb/^{204}Pb$	$^{206}Pb/^{204}Pbi$	$^{207}Pb/^{204}Pb$	$^{207}Pb/^{204}Pbi$	$^{208}Pb/^{204}Pb$	$^{208}Pb/^{204}Pbi$
		RC-418	66.1±2.4	0.0678	0.702959±8	0.702895	0.1256	0.512843±5	0.512789	4.00	4.63	37	127	19.61	19.24	15.61	15.59	39.16	38.74
		RC-414	82±2.9	0.1225	0.703459±8	0.703316	0.1110	0.512679±3	0.512619	0.80	1.57	35	121	20.94	20.49	15.75	15.73	40.79	40.30
		RC 415	82±2.9	0.0500	0.703277±7	0.703219	0.1282	0.512818±4	0.512749	3.51	4.12	28	94	20.43	20.08	15.75	15.73	40.07	39.68
BAYUDA	Main Volcanic Field (M) ~ 18°25'; 32°40'	BD-88a	1.44±.01	0.0888	0.703116±8	0.703114	0.1137	0.512875±5	0.512874	4.62	4.64	5	3	19.82	19.82	15.63	15.63	39.55	39.55
		BD-67	1.44±.01	0.0865	0.703093±7	0.703091	0.1103	0.512861±7	0.512860	4.35	4.37	46	175	19.85	19.84	15.67	15.67	39.64	39.63
		BD-21c	1.44±.01	0.1136	0.703144±8	0.703142	0.1109	0.512891±7	0.512890	4.94	4.95	18	69	19.88	19.88	15.65	15.65	39.64	39.63
		BD-62	1.44±.01	0.0835	0.703103±11	0.703101	0.1162	0.512892±6	0.512891	4.95	4.97	29	128	19.66	19.65	15.59	15.59	39.36	39.35
		BD-77a	1.44±.01	0.0833	0.703151±8	0.703149	0.1173	0.512878±6	0.512877	4.68	4.70	27	120	19.72	19.71	15.64	15.64	39.50	39.49
		BD-44b	1.44±.01	0.1894	0.703196±8	0.703192	0.1087	0.512861±6	0.512860	4.35	4.37	11	36	19.87	19.87	15.65	15.65	39.58	39.58
		BG-93	1.44±.01	0.1284	0.703201±18	0.703198	0.1108	0.512878±4	0.512877	4.68	4.70	34	130	19.77	19.76	15.65	15.65	39.53	39.52
	Jebel Kurbei (KU) ~18°10'; 33°38'	BD-100a	4.0±0.2	0.0462	0.703169±7	0.703166	0.1158	0.512925±5	0.512922	5.60	5.64	29	95	18.92	18.91	15.59	15.59	38.76	38.74
		BD-100b	4.0±0.2	0.0683	0.703171±7	0.703167	0.1171	0.512921±4	0.512918	5.52	5.56	31	115	18.94	18.92	15.60	15.60	38.79	38.76
		BD-100e	4.0±0.2	0.0569	0.703167±13	0.703163	0.1165	0.512948±4	0.512945	6.05	6.09	20	76	18.90	18.89	15.57	15.57	38.71	38.69
		BD-101	4.0±0.2	0.0855	0.703179±7	0.703174	0.1142	0.512931±6	0.512928	5.72	5.76	72	274	18.96	18.92	15.60	15.60	38.86	38.81
		BD-101a	4.0±0.2	0.0995	0.703189±8	0.703183	0.1146	0.512921±5	0.512918	5.52	5.56	33	125	18.90	18.88	15.58	15.58	38.70	38.68
	Jebel Umm Arafib (JA) ~ 18°05' 33°48'	BD-103a	4.0±0.2	0.0618	0.703189±8	0.703185	0.1162	0.512858±6	0.512855	4.29	4.33	28	124	19.16	19.15	15.60	15.60	38.96	38.93
		BD-103b	4.0±0.2	0.0557	0.703179±7	0.703176	0.1169	0.512916±4	0.512913	5.42	5.46	32	122	19.17	19.15	15.61	15.60	38.97	38.94
		BD-104	4.0±0.2	0.0686	0.703150±10	0.703147	0.1149	0.512914±6	0.512911	5.38	5.43	34	126	19.17	19.15	15.62	15.62	39.00	38.98
		BD-105	4.0±0.2	0.0719	0.703190±10	0.703186	0.1224	0.512924±5	0.512921	5.58	5.62	22	114	19.19	19.18	15.61	15.61	38.98	38.95
GEDAREF	Mercibia 14°25'; 35°53'	MER 1302	33±3.3	0.0719	0.703525±8	0.703491	0.1732	0.512781±4	0.512744	2.79	2.88	8	24	18.60	18.56	15.55	15.55	37.89	37.86
	El Gira 14°13'; 36°08'	GIR 1291	33±3.3	0.0206	0.703065±8	0.703056	0.1835	0.512976±7	0.512936	6.59	6.64	5	18	18.53	18.50	15.54	15.54	38.22	38.19
		GIR 1295	33±3.3	0.0169	0.703076±10	0.703068	0.1786	0.512978±5	0.512939	6.63	6.70	10	37	18.56	18.51	15.50	15.50	38.19	38.13
	Jebel Abu Tuyur 13°46'; 36°19'	TUY 1879	33±3.3	0.0310	0.703260±10	0.703245	0.1385	0.512828±5	0.512798	3.71	3.93	13	50	19.61	19.54	15.63	15.62	39.24	39.15
		TUY 2349	33±3.3	0.0308	0.703249±7	0.703235	0.1365	0.512834±6	0.512805	3.82	4.05	13	54	20.36	20.29	15.73	15.72	39.84	39.75

Table 1 Sample localities, crystallization ages, and measured and initial (i) Sr, Nd, and Pb isotope ratios of intra-plate magmatic rocks from NE-Africa. The 2σ uncertainty on the measured Pb isotope ratios is assumed to be 0.1% including the uncertainty in the correction for instrumental mass fractionation. References to the K-Ar ages: see eTable 1; all errors are 2 σ.

Group	Location /coordinates	sample No	age Ma	$^{87}Rb/^{86}Sr$	$^{87}Sr/^{86}Sr$	$^{87}Sr/^{86}Sr$ i	$^{147}Sm/^{144}Nd$	$^{143}Nd/^{144}Nd$	$^{143}Nd/^{144}Ndi$	ε - Nd_0	ε - Nd_t	μ	ω	$^{206}Pb/^{204}Pb$	$^{206}Pb/^{204}Pbi$	$^{207}Pb/^{204}Pb$	$^{207}Pb/^{204}Pbi$	$^{208}Pb/^{204}Pb$	$^{208}Pb/^{204}Pbi$
	Qualat Umm Debiba																		
	14°08'; 35°32'	SUD 1443	33±3.3	0.0799	0.703470±7	0.703433	0.1682	0.512881±6	0.512845	4.74	4.85	9	31	18.47	18.42	15.58	15.58	38.06	38.01
		SUD 14565	33±3.3	0.0310	0.703625±7	0.703610	0.1798	0.512787±6	0.512748	2.91	2.97	4	13	18.28	18.26	15.53	15.52	37.70	37.67
DARFUR	Tagabo (T)																		
	14°30; 25°50'	DT 26B	11.5±0.3	0.1575	0.703391±8	0.703365	0.1090	0.512840±8	0.512832	3.94	4.11	28	127	19.79	19.74	15.71	15.71	39.68	39.61
		DT 5	11.5±0.3	0.1351	0.703122±12	0.703100	0.1122	0.512795±12	0.512787	3.06	3.22	37	116	20.13	20.06	15.72	15.71	40.02	39.95
		GM-29G	11.5±0.3	0.1402	0.703193±11	0.703170	0.1172	0.512853±5	0.512844	4.19	4.35	26	105	20.01	19.96	15.71	15.71	39.92	39.86
	Jebl Kussa (JK)																		
	13°40'; 24°40'	DF 6 O	25.5±0.7	0.3071	0.703400±10	0.703289	0.1476	0.512865±7	0.512840	4.43	4.58	9	32	19.93	19.90	15.72	15.72	39.89	39.85
		DF 6 X	25.5±0.7	0.0986	0.703153±11	0.703117	0.1225	0.512860±4	0.512840	4.33	4.57	28	140	19.70	19.59	15.72	15.72	39.95	39.78
		DF-6j	25.5±0.7	0.0340	0.703229±8	0.703217	0.1325	0.512863±7	0.512841	4.39	4.59	4	20	19.68	19.66	15.72	15.72	39.82	39.79
	Meidob Hills (MH)																		
	15°18'; 26°30'	Me-3 e	0.3±0.1	0.1614	0.703411±7	0.703410	0.1092	0.512811±5	0.512811	3.37	3.39	35	140	19.62	19.62	15.67	15.67	39.68	39.68
		Me-3 g	0.21±0.1	0.1636	0.703391±10	0.703390	0.1090	0.512785±5	0.512785	2.87	2.88	33	134	19.61	19.60	15.67	15.67	39.69	39.69
		Me-5	6.8±0.2	0.1652	0.703585±8	0.703569	0.1153	0.512814±5	0.512809	3.43	3.51	30	114	19.46	19.43	15.68	15.68	39.42	39.38
		GU-3	3.3±0.3	0.1835	0.703228±8	0.703219	0.1156	0.512865±4	0.512863	4.43	4.50	37	146	19.98	19.96	15.70	15.70	39.72	39.70
	Jebel Marra area (JM)																		
	12°50'; 24°20'	DM-10	23.1±0.7	0.0957	0.703449±8	0.703418	0.1267	0.512834±4	0.512815	3.82	4.05	10	42	19.74	19.70	15.69	15.69	39.76	39.71
		D-2	23.1±0.7	0.1406	0.703169±11	0.703123	0.1231	0.512828±5	0.512809	3.71	3.94	17	62	20.16	20.10	15.71	15.71	40.03	39.95
		DF-1B	22.9±0.7	0.1051	0.703086±17	0.703052	0.1293	0.512902±5	0.512883	5.15	5.37	18	69	20.08	20.02	15.70	15.70	39.72	39.64
		GK-2a	23.1±0.7	0.1739	0.703185±8	0.703128	0.1233	0.512870±6	0.512851	4.53	4.76	19	70	19.99	19.92	15.71	15.71	39.90	39.82

Electronic Appendix

Nd, Pb, and Sr isotope composition of Late Mesozoic to Quaternary intra-plate magmatism in NE-Africa (Sudan, Egypt): high-μ signatures from the mantle lithosphere

by

Friedrich Lucassen, Gerhard Franz, Rolf L. Romer, Dieter Pudlo, Peter Dulski

Contents:

(1) eTable 1 Sample localities, description, and crystallization ages.

Locality	NE coordinates	Abbreviation Fig. 1	Sample Nos.	Field relations xenoliths occurrences	Fabric and mineralogy	Age
Regional group				**S-EGYPT**		
Gilf Kebir		**GK**				
	23°15';26°00'		2-1; 2-3	plug with lava flows, olivine basalts; lherzolite xenoliths	cpx, opx, ol, sp ol variable alteration verm. montm.	2-1: 37.9±2Ma [(1)]
	23°03';27°38'		2-7; 2-10	plug; olivine basalts	cpx, ol, pl, mt	2-10: 59±1.7 Ma [(1)]
Lake Nasser		**LN**				
	~22°00;30°50'		P-7; P-8	plug; olivine basalts	cpx, ol, (pl in P-7 only); P-8 partly serp, chl in groundmass	79±3 Ma[(2)]
Gebel Umm Shagir		**GU**				
	~ 23°20'; 32°		GU-12,GU-18	plug; olivine basalts	aphanitic groundmass (flow texture in GU-18) pl, pyx, opaque min; phenocrysts: ol, cpx (rare in GU-12); pl (only GU-18)	GU-12 155±4 Ma[(3)]
Gebel el Asr		**GA**				
	~22°50'; 31°		GA-2, -4, -21	plugs; olivine basalts	aphanitic groundmass: pl. pyx, opaque min.(GA-02; very fine grained in GA-21); phenocrysts: ol, cpx (pl in GA-04); GA-21: ol, pl, cpx in relatively coarse grained groundmass of pyx, ol, pl, opaque min.	GA-2: 87±2 Ma[(3)]
Regional group				**DELGO**		
Laquia Arbain		**LA**				
	~20°; 28°		12-2; 12-3	plug; olivine basalts	aphanitic groundmass pl, pyx, ol,	12-2: 19.6±1 Ma[(1)]

					opaque; phenocrysts: ol, cpx; secondary filled amygdales; some ol show serp.	
	~19°50';28°15'		12-10; 12-12	plug; olivine basalts	aphanitic groundmass pl, pyx, ol, opaque; phenocrysts: ol, cpx; ol phenocrysts show variable alteration, which does nor affect the groundmass	12-12 21.4±0.8 Ma[1]
Wadi Howar		**WH**				
	WH-1: 18°, 30° WH-2, WH31: 17°50', 29°40'		WH-1,WH-2,WH-31	dikes; olivine basalts	ol, cpx; aphanitic groundmass: pl lath, pyx, ol opaque minerals, flow texture; WH-1 small cpx-ol-sp xenoliths	WH1: 37.6±0.9 Ma[4] WH2: 71.9±1.8Ma[4]
Delgo basement west of the Nile	~19°49'; 30°	**DW**	NB-9a, NB-10, NB-11; RC-101; 7-51, 7-55, 7-56	plugs; olivine basalt; lherzolite xenoliths	aphanitic groundmass: pl lath, pyx, opaque min.(flow texture: NB 10); ol, cpx, rare pl phenocrysts; NB 11 sub-volcanic rel. coarse grained (cpx, ol, pl, minor secondary amph; no groundmass)	NB-9b: 76.7±1.9 Ma[4] NB-10: 80.9±2 Ma[4] 7-55: 59±1.7 Ma [1]
Delgo basement east of the Nile	~20°10'; 30°40'	**DE**	RC-411, 415, 418 RC-414	plugs; olivine basalt; dike; olivine basalt	aphanitic groundmass pl, cpx, opaque min. with or without (RC-418) flow texture; variable ol, cpx phenocrysts (RC-414 also xenocrysts cpx, sp); RC-415 small xenolith ol, cpx, opx, sp	RC-411: 82±2.9 Ma[5] RC-418: 66.1±2.4 Ma[5]
Regional group			**BAYUDA**			
Bayuda Main Volcanic Field		**BM**				
	~32°40'; 18°25'		BD-88a, BD-	various volcanic	very fine grained aphanitic to	1.44±0.07 Ma[6]

			67, BD-21c, BD-62, BD-77a, BD-44b, BD-93	centers; lava flows; olivine basalt; abundant lherzolite an pyroxenite xenolith	glassy groundmass with variable amount of olivine and cpx phenocrysts; BG 93 nearly void of phenocrysts; BD44b flow texture, small spinel lherzolite xenolith; BD88a with abundant vesicles without secondary fill	0.88±0.07 Ma[6]
Jebel Kurbei		**KU**				
	~33°38', 18°10'		BD-100a, BD-100b, BD-100e, BD-101, BD-101a	plugs; olivine basalt; lherzolite xenoliths	very fine grained aphanitic groundmass (BD 101 glassy) with cpx and ol phenocrysts; all samples contain small fragments of spinel lherzolite and xenocrysts (cpx, ol, opx, sp) from lherzolite (<15 vol%).	age similar to other young Bayuda samples (0-4 Ma) from field relations
Jebel Umm Arafieb		**JA**				
	~33°48', 18°05'		BD-103a, BD-103b, BD-104, BD-105	shield volcano; lava flows, olivine basalt; lherzolite xenoliths	aphanitic relatively coarse grained matrix (pyx, pl, ol, opaque min.), cpx and ol phenocrysts; phenocrysts form aggregates in BD 104; patchy carbonate (<1 vol%) occurs in the matrix of BD 105, but no related alteration of phenocrysts.	4.0±0.2 Ma[6]
Regional group	Gedaref		**GEDAREF**			
Mercibia	14°25'; 35°53'		MER 1302,	extended lava flow sheets; olivine basalts;	aphanitic groundmass of pl and pyx; cpx, variable amount of ol, and rare pl are the phenocrysts ; SUD samples show weathering of ol and the formation of clay	33 Ma - 34Ma [7,8] ages given without errors
El Gira	14°13'; 36°08'		GIR 1295, GIR 1291,			

Jebel Abu Tuyur	13°46'; 36°19'		TUY 1879, TUY 2349,		minerals around ol.	
QualatUmm Debiba	14°08'; 35°32'		SUD 1443, SUD 14565			
Regional group			**DARFUR**			
Tagabo	14°30; 25°50'	**TA**	DT-26B, DT-5, GM-29G	lava flows; olvine basalt (GM29g; DT-5); subvolcanic 'gabbro' (DT-26b)	aphanitic relatively coarse matrix of pl, pyx, ol, and opaque min; ol, cpx, and rare hbl form phenocrysts. DT-5 with flow texture; DT-26b coarse grained cpx minor ol (>70 vol%) in groundmass of opaque min., pl, pxy	DT-26B: 11.5±0.3 Ma[9]; DT-5: 11.1±0.3 Ma[9]
Jebel Kussa	13°40'; 24°40'	**JK**	DF-6O, DF-6X, DF-6J	subvolcanic 'gabbro'	cpx, opx, pl, opaque min., and minor hbl; DF-6O has some ol and no hydrous phases	35.8±2 Ma[9] 25.5±0.7 Ma[9]
Meidob Hills	15°18'; 26°30'	**MH**	Me-3e, Me-3g, Me-5; GU-3;	lava flows, olivine basalt; lherzolite xenoliths	Me3 g, e: mainly cpx, some ol and pl phenocrysts in a glassy groundmass; Me5 pxy, pl, and ol phenocrysts in aphanitic groundmass	Me-3e: 0.3±0.05 Ma[9] ME-5: 6.8±0.2 Ma[9] GU-3: 3.3±0.3 Ma[9]
Jebel Marra area	12°50'; 24°20'	**JM**	DM-10, D-2, DF-1B, GK-2a	lava flows; olivine basalts	ol, cpx phenocrysts in aphanitic groundmass of pl, pyx, ol, and opaque min.; contents of opaque min. is variable between the samples; GK-2a contains small ol-cps-opx-sp xenolith.	GK-2a: 23.1±0.7Ma[9]; DF1-b: 22.9±0.7 Ma [9]

Data sources: (1) Franz et al. (1987); (2) Meneisy and Kreuzer (1974); (3) Bernau et al. (1987); (4) unpublished data Pasteels & Franz; for the method see Franz et al., 1987; (5) this work, eTable 2; (6) Barth and Meinold (1979); (7) Whiteman 1971 in Cahen et al. 1984; (8) Wipki (1995); (9) Franz et al. (1994)

(2) eTable 2 New K-Ar age data.

The analytical procedure is given in: **(4) Sample preparation, analytical methods, and data quality**

Geowissenschaftliches Zentrum der Universität Göttingen, Goldschmidtstr. 3, 37077 GÖTTINGEN

K/Ar - Age Determinations

Ar - Isotopic Abundance		Spike-Isotopic Comp.		Decay Constants [1/a]:		Potassium	
40 Ar :	99.6000%	40 Ar :	0.0099980%	λ ε :	5.810E-11	40K :	0.011670%
38 Ar :	0.0630%	38 Ar :	99.9890000%	λ β :	4.962E-10	K2O/K :	0.8302
36 Ar :	0.3370%	36 Ar :	0.0009998%			**Atomic Weight [g/mol]:**	
Standard Temperature Pressure (STP)				λ tot:	5.543E-10	tot Ar :	39.9477
0° C; 760 mm Hg				**Molar Volume**		40Ar :	39.9624
Normal Atmosphere (DIN 1343)				[ml] :	22413.8	tot K :	39.1027
273,15K; 1013,25 mbar							

Sample	K2O [Wt. %]	40 Ar * [nl/g] STP	40 Ar * [%]	Age [Ma]	2s-Error [Ma]	2s-Error [%]
RC 411	0.99	2.680	58.25	**82.0**	2.9	3.5
RC 411	0.99	2.677	57.94	**82.0**	2.9	3.5
RC 418	1.08	2.346	55.67	**66.1**	2.4	3.6
RC 418	1.08	2.401	57.48	**67.7**	2.4	3.5

(3) eTable 3

Major and trace element composition, ICPW-norm minerals, measured and initial isotope ratios, major and trace element composition corrected for olivine fractionation, international standards run with the samples, key data of XRF calibration.The 2-sigma error on the initial ratios includes the error propagation from the crystallization ages. Pressure estimates follow the approach of Herzberg & Zhang (1996).

The analytical procedures are given in: **(4) Sample preparation, analytical methods, and data quality**

Group		S-EGYPT						
Location		Gilf Kebir (GK)		Lake Nasser (LN)			Gebel um Shagir (GU)	
coordinates N/E		23°15'; 26°00'		23°03'; 27°3	~22°00; 30°50'		~ 23°20'; 32°	
sample No		2-1	2-3	2-7	P-7	P-8	GU-12	GU18
SiO2	wt%	42.5	42.5	45.0	46.9	43.9	47.3	47.9
TiO2	wt%	2.7	2.7	3.9	2.8	3.5	2.7	2.6
Al2O3	wt%	10.7	10.9	14.8	14.9	14.9	14.8	14.2
Fe2O3	wt%	13.5	13.6	12.1	13.1	13.9	10.7	12.4
MnO	wt%	0.19	0.19	0.15	0.17	0.15	0.15	0.16
MgO	wt%	15.5	14.8	4.2	6.4	7.2	7.4	7.6
CaO	wt%	10.1	10.2	9.7	8.1	7.3	7.9	7.7
Na2O	wt%	2.7	2.7	4.0	3.5	3.3	3.7	3.7
K2O	wt%	1.1	1.1	2.3	1.5	1.3	1.9	1.3
P2O5	wt%	0.90	0.91	1.08	0.77	0.49	0.75	0.42
LOI		nd	1.2	1.9	1.8	4.4	1.5	0.7
Total		99.9	100.8	99.2	100.0	100.1	98.7	98.8
Mg#		69.48	68.39	40.53	48.91	50.53	57.90	54.88
CIPW norm								
Plagioclase	wt%	19.05	19.7	34.37	49.4	49.4	45.57	49.68
Orthoclase	wt%	6.68	6.8	14.06	9.4	7.8	11.88	7.8
Nepheline	wt%	9.88	9.73	9.29	1.28	1.93	3	0.85
Leucite	wt%	0	0	0	0	0	0	0
Diopside	wt%	24.62	24.96	21.73	12.49	9.17	13.55	14.44
Hypersthene	wt%	0	0	0	0	0	0	0
Olivine	wt%	30.49	29.39	8.35	18.19	21.32	17.27	19.21
Ilmenite	wt%	5.18	5.28	7.79	5.45	7.05	5.34	5.17
Magnetite	wt%	1.99	2	1.83	1.97	2.13	1.61	1.86
Apatite	wt%	2.11	2.15	2.59	1.83	1.2	1.78	1
Ba	ppm	510	459	552	484	300	472	336
Rb	ppm	25	23	35	32	22	52	36
Sr	ppm	1112	996	1131	787	850	805	538
Cs	ppm	0.44	0.39	0.42	0.57	0.51	1.50	0.36
Ta	ppm	4.1	6.7	8.1	7.9	4.8	7.7	5.6
Nb	ppm	74.5	81.7	107.7	76.9	55.7	89.5	51.5
Hf	ppm	6.7	6.4	6.4	6.3	4.6	7.3	5.1
Zr	ppm	313	288	318	285	203	338	214
Y	ppm	26.9	25.2	28.9	24.0	20.5	27.1	24.7
Th	ppm	7.4	6.8	6.0	5.5	3.5	7.1	4.3
U	ppm	2.01	1.83	1.89	1.57	0.96	1.82	0.97
Pb	ppm	4.1	3.3	3.5	3.0	2.0	6.3	2.8
La	ppm	59.9	56.5	54.8	49.8	30.5	50.5	32.1
Ce	ppm	115.2	110.1	108.6	100.1	62.8	98.7	64.9
Pr	ppm	13.5	12.9	13.1	11.9	7.8	11.6	8.0
Nd	ppm	53.6	50.4	53.1	46.9	31.9	44.7	32.0
Sm	ppm	10.7	10.2	11.1	9.1	6.8	8.7	6.8
Eu	ppm	3.4	3.2	3.5	3.1	2.4	2.8	2.2
Gd	ppm	9.5	8.7	9.4	8.0	6.2	7.6	6.6
Tb	ppm	1.28	1.18	1.27	1.04	0.86	1.05	0.95
Dy	ppm	6.4	6.0	6.7	5.6	4.7	5.9	5.4
Ho	ppm	1.09	1.04	1.16	0.97	0.84	1.07	0.97
Er	ppm	2.61	2.50	2.75	2.40	2.09	2.76	2.64
Tm	ppm	0.32	0.30	0.35	0.29	0.26	0.37	0.34
Yb	ppm	1.82	1.70	1.94	1.69	1.57	2.17	2.10
Lu	ppm	0.27	0.24	0.27	0.25	0.23	0.32	0.31
age Ma		37.9	37.9	59	79	79	155	155
2σ error		2.0	2.0	1.7	3.0	3.0	4.0	4.0
87/86 Sr		0.702933	0.702885	0.703368	0.703301	0.703430	0.703606	0.703745
±2σ(m) error*		0.000007	0.000007	0.000008	0.000008	0.000007	0.000011	0.000011
87Rb/86Sr		0.0657	0.0654	0.0897	0.1153	0.0752	0.1856	0.1942
87/86Sr i		0.702897	0.702849	0.703293	0.703171	0.703346	0.703197	0.703317
2σ error*		0.000008	0.000008	0.000012	0.000014	0.000011	0.000036	0.000028
143/144Nd		0.512904	0.512940	0.512810	0.512811	0.512849	0.512826	0.512795
±2σ(m) error*		0.000006	0.000005	0.000005	0.000005	0.000005	0.000005	0.000006
147Sm/144Nd		0.1209	0.1230	0.1260	0.1169	0.1282	0.1181	0.1293

Group		S-EGYPT						
Location		Gilf Kebir (GK)			Lake Nasser (LN)		Gebel um Shagir (GU)	
coordinates N/E		23°15'; 26°00'		23°03'; 27°3	~22°00; 30°50'		~ 23°20'; 32°	
sample No		2-1	2-3	2-7	P-7	P-8	GU-12	GU18
143/144 Nd i		0.512874	0.512910	0.512761	0.512751	0.512783	0.512706	0.512664
2σ error*		0.000010	0.000009	0.000013	0.000014	0.000011	0.000006	0.000007
e-Nd_0		5.2	5.9	3.4	3.4	4.1	3.7	3.1
e_Nd_t		5.6	6.3	3.7	4.2	4.8	5.3	4.4
μ		33	37	36	35	33	19	23
ω		123	142	118	129	122	78	105
206Pb/204Pb		19.81	20.08	20.14	20.43	20.59	20.72	19.56
206Pb/204Pbi		19.62	19.86	19.81	20.00	20.19	20.25	19.00
2σ error*		0.03	0.03	0.04	0.05	0.05	0.05	0.06
207Pb/204Pb		15.64	15.65	15.65	15.77	15.74	15.74	15.71
207Pb/204Pbi		15.63	15.64	15.63	15.75	15.72	15.71	15.69
2σ error*		0.02	0.02	0.02	0.02	0.02	0.02	0.02
208Pb/204Pb		39.45	39.70	39.88	40.11	39.99	40.63	39.90
208Pb/204Pbi		39.22	39.43	39.53	39.60	39.51	40.03	39.09
2σ error*		0.05	0.05	0.06	0.07	0.06	0.08	0.09
Correction for crystal fractionation to Mg#=73 by olivine addition								
olivine added	wt%	8.5	11	46.5	39.5	40	23.5	30.5
SiO2	wt%	42.4	42.4	43.6	45.0	43.7	46.7	46.4
TiO2	wt%	2.5	2.5	2.5	1.9	2.4	2.2	2.0
Al2O3	wt%	9.9	9.7	9.5	10.2	10.4	12.0	10.7
Fe2O3	wt%	13.3	13.5	14.1	14.1	14.7	11.6	13.1
MnO	wt%	0.17	0.17	0.10	0.12	0.10	0.12	0.12
MgO	wt%	18.2	18.4	19.2	19.2	20.1	15.8	17.9
CaO	wt%	9.2	9.2	6.2	5.5	5.1	6.4	5.8
Na2O	wt%	2.5	2.4	2.6	2.4	2.3	3.0	2.7
K2O	wt%	1.03	1.02	1.47	1.05	0.87	1.57	0.96
P2O5	wt%	0.83	0.82	0.69	0.53	0.34	0.60	0.31
Rb	ppm	25.3	22.6	32.2	30.9	21.7	51.6	36.0
Sr	ppm	1020	891	706	528	567	634	395
Y	ppm	24.7	22.6	18.0	16.1	13.7	21.4	18.1
Zr	ppm	287	258	198	191	135	267	157
Nb	ppm	68.4	73.1	67.2	51.5	37.1	70.6	37.8
Cs	ppm	0.40	0.35	0.26	0.38	0.34	1.18	0.26
Ba	ppm	468	411	344	324	200	372	246
La	ppm	55.0	50.5	34.2	33.4	20.4	39.8	23.6
Ce	ppm	105.7	98.6	67.7	67.1	41.9	77.8	47.7
Pr	ppm	12.4	11.5	8.2	8.0	5.2	9.1	5.9
Nd	ppm	49.2	45.1	33.1	31.4	21.3	35.2	23.5
Sm	ppm	9.8	9.2	6.9	6.1	4.5	6.9	5.0
Eu	ppm	3.1	2.9	2.2	2.1	1.6	2.2	1.6
Gd	ppm	8.7	7.8	5.9	5.3	4.1	6.0	4.9
Tb	ppm	1.18	1.06	0.79	0.70	0.57	0.83	0.70
Dy	ppm	5.9	5.4	4.2	3.8	3.1	4.7	3.9
Ho	ppm	1.00	0.93	0.72	0.65	0.56	0.84	0.71
Er	ppm	2.39	2.24	1.72	1.61	1.40	2.18	1.94
Tm	ppm	0.29	0.27	0.22	0.20	0.17	0.29	0.25
Yb	ppm	1.67	1.52	1.21	1.13	1.05	1.71	1.54
Lu	ppm	0.25	0.21	0.17	0.16	0.15	0.25	0.23
Hf	ppm	6.19	5.75	4.02	4.21	3.05	5.77	3.78
Ta	ppm	3.72	5.95	5.05	5.30	3.23	6.06	4.12
Pb	ppm	3.72	2.92	2.17	1.98	1.31	4.97	2.05
Th	ppm	6.77	6.05	3.74	3.71	2.32	5.57	3.17
U	ppm	1.85	1.64	1.18	1.05	0.64	1.44	0.71
MG#		73.0	73.0	72.9	73.0	73.0	73.0	73.0

Pressure estimates (Herzberg and Zhang 1996)

sample		2-1	2-3
Al2O3	GPa	3.9	3.9
CaO	GPa	4.0	4.1
FeO	GPa	4.0	4.1
MgO	GPa	4.3	4.4
Na2O	GPa	5.8	6.1

Group				DELGO				
Location	Gebel el Asr (GA)			Laquia Arbain (LA)				Wadi Howa
coordinates N/E	~22°50'; 31°			~20°; 28°		~19°50'; 28°15		18°; 30°
sample No	GA-02	GA-04	GA-21	12-2	12-3	12-10	12-12	WH-1
SiO2	47.6	46.4	46.8	42.2	41.9	41.7	44.5	44.6
TiO2	2.7	2.9	2.9	2.6	2.7	2.8	2.6	3.0
Al2O3	13.6	13.8	15.3	11.7	11.4	11.6	12.5	13.9
Fe2O3	12.3	12.0	12.0	12.8	13.0	13.2	12.7	12.6
MnO	0.15	0.14	0.16	0.18	0.21	0.18	0.16	0.16
MgO	8.6	9.0	6.7	11.9	12.5	11.7	10.0	8.5
CaO	8.3	9.3	8.5	10.9	10.7	10.6	9.9	10.2
Na2O	3.5	2.8	4.0	3.2	3.5	3.2	2.9	2.5
K2O	1.0	1.2	0.9	1.0	0.9	1.1	1.3	0.8
P2O5	0.49	0.41	0.58	0.78	0.82	0.78	0.58	0.57
LOI	0.8	1.0	1.0	2.5	2.3	2.6	3.0	1.8
Total	99.1	98.9	98.7	99.7	99.9	99.4	100.0	98.5
Mg#	57.94	59.89	52.74	64.70	65.58	63.55	61.05	57.20
CIPW norm								
Plagioclase	48.83	46.05	51.1	20.95	18.34	20.07	33.5	47.49
Orthoclase	6.21	7.51	5.73	6.32	5.73	6.68	7.98	4.61
Nepheline	0.28	0.17	3.04	12.05	13.78	12.5	5.34	0.1
Leucite	0	0	0	0	0	0	0	0
Diopside	16.39	18.19	14.52	29.02	29.04	28.41	23.87	19.27
Hypersthene	0	0	0	0	0	0	0	0
Olivine	20.13	19.66	16.8	22.65	23.91	22.87	20.96	19.26
Ilmenite	5.18	5.68	5.62	5.18	5.3	5.58	5.07	5.98
Magnetite	1.84	1.8	1.8	1.93	1.96	2	1.91	1.91
Apatite	1.16	0.97	1.39	1.88	1.97	1.9	1.39	1.37
Ba	329	315	480	498	441	449	464	344
Rb	24	23	8	27	15	23	70	19
Sr	626	813	1191	1094	886	872	616	877
Cs	0.61	0.41	0.27	0	0.44	0.48	2.15	0.50
Ta	4.5	4.7	5.4	3.3	6.2	5.9	2.7	6.5
Nb	55.6	58.2	73.0	60.9	74.9	73.1	48.9	75.2
Hf	4.4	5.1	5.5	5.7	5.8	5.9	5.5	5.9
Zr	194	215	251	253	258	263	235	273
Y	20.2	16.6	21.0	25.9	25.7	25.0	23.5	24.3
Th	3.6	3.2	4.6	5.7	5.6	5.3	4.4	4.7
U	0.98	1.03	1.51	1.62	1.44	1.47	1.20	1.36
Pb	2.2	2.2	2.9	5.3	3.0	3.1	3.3	2.4
La	31.7	34.2	46.0	47.5	48.3	44.7	36.9	43.7
Ce	64.3	73.7	95.8	94.9	96.5	90.2	74.5	89.3
Pr	7.8	9.2	11.4	11.5	11.7	11.0	9.1	10.9
Nd	32.5	37.6	44.6	47.0	47.3	45.1	37.8	43.2
Sm	6.8	7.2	8.1	10.0	10.0	9.6	8.2	8.5
Eu	2.3	2.4	2.7	3.3	3.2	3.1	2.8	2.7
Gd	6.1	6.1	6.5	9.0	8.9	8.4	7.9	7.3
Tb	0.86	0.79	0.86	1.25	1.19	1.16	1.09	1.04
Dy	4.7	4.0	4.7	6.3	6.2	6.0	5.7	5.5
Ho	0.82	0.70	0.85	1.06	1.03	1.02	0.96	0.98
Er	2.04	1.70	2.19	2.52	2.44	2.34	2.34	2.45
Tm	0.26	0.20	0.28	0.30	0.29	0.28	0.29	0.30
Yb	1.51	1.17	1.74	1.73	1.64	1.52	1.62	1.80
Lu	0.21	0.17	0.26	0.25	0.23	0.21	0.24	0.25
age Ma	87	87	87	19.6	19.6	21.4	21.4	37.6
2σ error	2.0	2.0	2.0	1.0	1.0	0.8	0.8	0.9
87/86 Sr	0.703208	0.703242	0.703489	0.703362	0.703334	0.703292	0.703721	0.703005
±2σ(m) error*	0.000010	0.000010	0.000013	0.000007	0.000008	0.000008	0.000007	0.000011
87Rb/86Sr	0.1100	0.0832	0.0198	0.0705	0.0503	0.0763	0.3270	0.0624
87/86Sr i	0.703072	0.703139	0.703465	0.703342	0.703320	0.703269	0.703621	0.702972
2σ error*	0.000013	0.000013	0.000013	0.000007	0.000009	0.000009	0.000010	0.000012
143/144Nd	0.512827	0.512822	0.512774	0.512726	0.512877	0.512838	0.512815	0.512841
±2σ(m) error*	0.000005	0.000007	0.000005	0.000007	0.000006	0.000007	0.000007	0.000007
147Sm/144Nd	0.1273	0.1153	0.1098	0.1286	0.1282	0.1290	0.1320	0.1186

Group				DELGO				
Location	Gebel el Asr (GA)			Laquia Arbain (LA)				Wadi Howa
coordinates N/E	~22°50'; 31°			~20°; 28°		~19°50'; 28°15		18°; 30°
sample No	GA-02	GA-04	GA-21	12-2	12-3	12-10	12-12	WH-1
143/144 Nd i	0.512755	0.512756	0.512711	0.512710	0.512861	0.512820	0.512797	0.512812
2σ error*	0.000005	0.000007	0.000005	0.000007	0.000006	0.000007	0.000007	0.000007
e-Nd_0	3.7	3.6	2.7	1.7	4.7	3.9	3.5	4.0
e_Nd_t	4.2	4.2	3.3	1.9	4.8	4.1	3.7	4.6
μ	29	31	35	20	31	31	24	37
ω	112	102	110	72	126	116	89	131
206Pb/204Pb	20.16	20.73	20.57	18.94	19.12	19.12	18.69	20.19
206Pb/204Pbi	19.76	20.31	20.10	18.88	19.02	19.01	18.61	19.97
2σ error*	0.05	0.05	0.05	0.02	0.02	0.02	0.02	0.03
207Pb/204Pb	15.74	15.73	15.74	15.57	15.57	15.57	15.54	15.73
207Pb/204Pbi	15.72	15.71	15.71	15.57	15.57	15.56	15.54	15.71
2σ error*	0.02	0.02	0.02	0.02	0.02	0.02	0.02	0.02
208Pb/204Pb	39.89	40.01	40.08	38.88	39.03	38.99	38.81	39.95
208Pb/204Pbi	39.41	39.57	39.61	38.81	38.91	38.87	38.71	39.71
2σ error*	0.06	0.06	0.06	0.04	0.04	0.04	0.04	0.05
Correction for crystal fı								
olivine added	26.5	23.5	32	17.5	16	20	23	28.5
SiO2	46.4	45.8	45.6	42.9	42.5	42.5	44.6	44.5
TiO2	2.1	2.3	2.1	2.3	2.3	2.4	2.1	2.3
Al2O3	10.6	11.1	11.3	10.1	10.0	9.8	10.2	10.7
Fe2O3	12.9	12.5	12.9	13.1	13.2	13.5	13.1	13.3
MnO	0.11	0.11	0.12	0.16	0.18	0.15	0.13	0.12
MgO	17.6	17.1	17.6	17.9	18.0	18.5	17.9	18.2
CaO	6.5	7.5	6.3	9.4	9.3	8.9	8.1	7.9
Na2O	2.7	2.2	3.0	2.8	3.0	2.7	2.3	2.0
K2O	0.79	0.99	0.70	0.89	0.82	0.91	1.05	0.58
P2O5	0.38	0.33	0.43	0.67	0.71	0.66	0.47	0.44
Rb	23.8	23.4	8.1	26.7	15.4	23.0	69.6	18.9
Sr	479	641	861	917	754	712	488	657
Y	15.4	13.1	15.2	21.7	21.9	20.4	18.6	18.2
Zr	149	170	181	212	220	215	186	205
Nb	42.5	45.9	52.8	51.0	63.7	59.7	38.8	56.4
Cs	0.47	0.32	0.20	0.33	0.37	0.39	1.71	0.38
Ba	252	248	347	417	375	367	368	258
La	24.3	27.0	33.3	39.8	41.1	36.5	29.2	32.7
Ce	49.2	58.1	69.3	79.5	82.1	73.7	59.1	66.9
Pr	6.0	7.2	8.3	9.6	10.0	9.0	7.2	8.2
Nd	24.9	29.6	32.2	39.4	40.3	36.8	29.9	32.4
Sm	5.2	5.6	5.9	8.4	8.5	7.9	6.5	6.3
Eu	1.7	1.9	2.0	2.8	2.8	2.5	2.2	2.0
Gd	4.7	4.8	4.7	7.5	7.6	6.9	6.2	5.5
Tb	0.66	0.62	0.62	1.05	1.01	0.95	0.86	0.78
Dy	3.6	3.2	3.4	5.3	5.3	4.9	4.5	4.1
Ho	0.63	0.55	0.62	0.89	0.87	0.83	0.76	0.74
Er	1.56	1.34	1.58	2.11	2.08	1.91	1.86	1.83
Tm	0.20	0.16	0.21	0.25	0.24	0.23	0.23	0.23
Yb	1.16	0.93	1.26	1.45	1.39	1.24	1.29	1.35
Lu	0.16	0.13	0.19	0.21	0.20	0.18	0.19	0.19
Hf	3.39	4.01	3.97	4.81	4.94	4.78	4.33	4.44
Ta	3.48	3.74	3.87	2.76	5.25	4.84	2.10	4.84
Pb	1.68	1.74	2.11	4.42	2.53	2.50	2.59	1.83
Th	2.74	2.56	3.35	4.77	4.78	4.34	3.50	3.49
U	0.75	0.81	1.09	1.36	1.23	1.20	0.95	1.02
MG#	73.0	73.1	72.9	73.0	73.0	73.0	73.0	73.1
Pressure estimates (H								
sample				12-2	12-3	12-10		
Al2O3				3.8	3.9	3.9		
CaO				3.9	4.0	4.3		
FeO				3.9	3.9	4.1		
MgO				4.2	4.2	4.4		
Na2O				4.8	4.0	4.9		

Group									
Location	r (WH)		Delgo basement west of the Nile (DW)						
coordinates N/E	17°50', 29°40'		~19°49'; 30°						
sample No	WH-2	WH-31	NB 9a	NB 10	NB 11	RC-101	7-51	7-55	7-56
SiO2	44.2	45.7	46.6	47.9	44.1	45.9	46.4	47.3	47.7
TiO2	3.7	2.1	2.9	2.7	2.9	3.5	2.4	2.0	2.4
Al2O3	13.1	13.1	15.1	16.3	14.9	15.4	14.6	14.4	14.9
Fe2O3	13.9	12.9	13.0	14.3	13.5	13.5	13.1	12.4	12.8
MnO	0.16	0.12	0.16	0.19	0.16	0.16	0.19	0.15	0.15
MgO	8.7	9.6	6.9	3.7	7.6	6.1	7.3	9.8	7.2
CaO	10.0	8.3	8.8	6.2	8.4	7.1	9.0	8.2	7.8
Na2O	2.7	3.7	3.3	5.1	3.3	4.0	3.3	3.4	3.8
K2O	1.2	1.4	1.0	1.6	1.0	1.6	1.4	1.1	1.4
P2O5	0.51	0.81	0.46	1.35	0.45	0.66	0.51	0.46	0.61
LOI	0.7	0.9	0.5	0.2	2.5	0.8	1.7	1.4	1.6
Total	98.8	98.7	98.6	99.5	98.8	98.7	99.8	100.5	100.4
Mg#	55.39	59.67	51.22	34.04	52.58	47.36	52.51	60.95	52.56
CIPW norm									
Plagioclase	38.31	36.21	52.83	54.12	46.58	47.91	44.74	47.17	48.84
Orthoclase	7.15	8.81	5.79	9.51	6.32	9.46	8.45	6.56	8.33
Nepheline	3.28	6.37	0.18	3.81	3.69	3.97	3.1	1.82	2.27
Leucite	0	0	0	0	0	0	0	0	0
Diopside	21.82	17.66	14.11	4.45	13.82	9.93	17.14	13.8	13.09
Hypersthene	0	0	0	0	0	0	0	0	0
Olivine	18.82	22.98	18.42	17.5	20.72	18.35	18.67	23.88	19.42
Ilmenite	7.33	4.08	5.6	5.3	5.72	6.78	4.73	3.84	4.71
Magnetite	2.09	1.93	1.96	2.12	2.06	2.03	1.96	1.84	1.9
Apatite	1.2	1.95	1.11	3.17	1.11	1.58	1.23	1.09	1.44
Ba	311	401	284	470	216	470	537	342	345
Rb	31	39	26	41	26	47	20	17	23
Sr	741	775	637	953	557	857	897	692	752
Cs	0.31	0.95	1.36	2.89	1.49	9.11	0.39	0.34	0.27
Ta	6.1	6.2	6.1	7.0	5.0	6.8	9.1	2.7	5.3
Nb	72.9	80.9	52.5	83.9	48.5	76.7	112.8	49.8	59.7
Hf	6.1	5.6	5.1	7.2	5.3	6.7	6.5	6.1	6.4
Zr	274	278	219	328	230	299	305	272	280
Y	27.8	25.9	24.0	35.8	24.3	23.4	29.3	23.9	21.3
Th	4.3	6.2	3.7	4.8	2.8	5.7	9.6	4.8	4.3
U	1.24	1.73	0.94	1.36	0.84	1.53	2.50	1.35	1.28
Pb	2.2	3.5	2.4	2.9	1.8	3.7	3.6	3.4	2.8
La	42.5	50.5	32.3	54.4	29.0	51.0	59.9	40.0	40.2
Ce	89.1	95.1	66.3	117.3	61.8	103.7	107.6	78.1	82.2
Pr	11.1	10.9	8.2	14.9	7.9	12.2	11.8	9.2	10.1
Nd	44.7	41.8	33.8	62.7	32.6	48.0	44.1	36.2	40.6
Sm	9.0	8.1	7.2	12.9	7.2	9.1	8.5	7.5	8.4
Eu	2.9	2.6	2.4	4.4	2.4	2.9	2.7	2.5	2.7
Gd	8.2	7.3	6.9	11.5	6.9	7.9	7.5	7.0	7.4
Tb	1.15	1.04	0.95	1.53	0.98	1.03	1.10	1.00	1.01
Dy	6.3	5.6	5.4	8.1	5.4	5.5	6.3	5.4	5.0
Ho	1.10	1.03	0.96	1.42	1.01	0.98	1.15	0.97	0.87
Er	2.80	2.58	2.45	3.54	2.54	2.39	3.10	2.55	2.10
Tm	0.36	0.35	0.31	0.44	0.32	0.29	0.41	0.33	0.26
Yb	2.12	2.02	1.83	2.65	1.92	1.76	2.51	2.00	1.54
Lu	0.29	0.29	0.27	0.39	0.29	0.25	0.37	0.30	0.22
age Ma	71.9	71.9	76.7	80.9	80.9	59	59	59	59
2σ error	1.8	1.8	1.9	2.0	2.0	1.7	1.7	1.7	1.7
87/86 Sr	0.703127	0.703575	0.703403	0.703159	0.702987	0.703386	0.702801	0.703054	0.703043
±2σ(m) error*	0.000008	0.000010	0.000013	0.000014	0.000010	0.000008	0.000008	0.000008	0.000007
87Rb/86Sr	0.1198	0.1435	0.1197	0.1226	0.1339	0.1577	0.0656	0.0689	0.0870
87/86Sr i	0.703004	0.703428	0.703273	0.703018	0.702833	0.703254	0.702746	0.702997	0.702970
2σ error*	0.000013	0.000015	0.000016	0.000020	0.000014	0.000015	0.000010	0.000009	0.000009
143/144Nd	0.512799	0.512764	0.512747	0.512787	0.512917	0.512732	0.512876	0.512833	0.512850
±2σ(m) error*	0.000006	0.000006	0.000005	0.000006	0.000007	0.000004	0.000006	0.000006	0.000007
147Sm/144Nd	0.1216	0.1165	0.1288	0.1241	0.1339	0.1145	0.1167	0.1251	0.1246

Group									
Location	ır (WH)		Delgo basement west of the Nile (DW)						
coordinates N/E	17°50', 29°40'		~19°49'; 30°						
sample No	WH-2	WH-31	NB 9a	NB 10	NB 11	RC-101	7-51	7-55	7-56
143/144 Nd i	0.512742	0.512709	0.512682	0.512721	0.512846	0.512688	0.512831	0.512785	0.512802
2σ error*	0.000006	0.000006	0.000005	0.000007	0.000007	0.000004	0.000006	0.000006	0.000007
e-Nd_0	3.1	2.5	2.1	2.9	5.4	1.8	4.6	3.8	4.1
e_Nd_t	3.7	3.1	2.7	3.6	6.0	2.6	5.3	4.4	4.7
μ	37	33	26	32	31	28	46	26	31
ω	136	122	105	116	106	106	185	95	108
206Pb/204Pb	20.75	20.26	19.94	20.25	20.60	20.74	20.72	19.97	20.16
206Pb/204Pbi	20.33	19.89	19.63	19.85	20.20	20.48	20.29	19.73	19.88
2σ error*	0.05	0.04	0.04	0.05	0.05	0.03	0.05	0.03	0.04
207Pb/204Pb	15.74	15.68	15.75	15.71	15.73	15.76	15.74	15.71	15.74
207Pb/204Pbi	15.72	15.66	15.73	15.69	15.71	15.74	15.72	15.70	15.72
2σ error*	0.02	0.02	0.02	0.02	0.02	0.02	0.02	0.02	0.02
208Pb/204Pb	40.25	40.35	40.31	39.90	39.97	39.05	40.04	39.76	39.72
208Pb/204Pbi	39.76	39.92	39.91	39.43	39.55	38.75	39.50	39.48	39.40
2σ error*	0.06	0.06	0.06	0.06	0.06	0.05	0.08	0.05	0.05
Correction for crystal fı									
olivine added	33	25	36.5	60.5	36.5	42.5	35	22.5	34
SiO2	43.5	45.2	45.0	44.0	43.9	44.3	45.0	46.1	45.7
TiO2	2.7	1.7	2.0	1.5	2.1	2.3	1.7	1.6	1.7
Al2O3	9.6	10.4	10.7	8.8	10.7	10.2	10.4	11.6	10.7
Fe2O3	14.2	13.3	13.8	16.0	14.3	14.5	13.8	12.7	13.5
MnO	0.12	0.09	0.11	0.10	0.12	0.11	0.14	0.12	0.11
MgO	19.4	18.0	18.9	21.9	19.5	19.8	18.8	17.4	18.4
CaO	7.3	6.6	6.2	3.4	6.1	4.7	6.4	6.6	5.6
Na2O	2.0	3.0	2.3	2.8	2.4	2.7	2.4	2.7	2.7
K2O	0.85	1.14	0.67	0.86	0.73	1.03	0.99	0.88	0.99
P2O5	0.37	0.65	0.33	0.73	0.32	0.44	0.36	0.37	0.44
Rb	30.6	38.4	26.3	32.2	25.7	44.7	20.3	16.5	22.5
Sr	531	602	440	515	385	557	630	551	533
Y	19.9	20.1	16.6	19.3	16.8	15.2	20.6	19.0	15.1
Zr	196	216	151	177	159	194	214	216	198
Nb	52.2	62.8	36.3	45.3	33.5	49.9	79.1	39.6	42.3
Cs	0.22	0.74	0.94	1.56	1.03	5.92	0.27	0.27	0.19
Ba	223	312	196	254	150	306	377	273	245
La	30.4	39.2	22.3	29.4	20.0	33.1	42.0	31.9	28.5
Ce	63.8	73.9	45.8	63.4	42.7	67.4	75.5	62.2	58.3
Pr	7.9	8.4	5.7	8.1	5.4	7.9	8.3	7.3	7.1
Nd	32.0	32.5	23.4	33.9	22.6	31.2	30.9	28.8	28.8
Sm	6.4	6.3	5.0	7.0	5.0	5.9	6.0	6.0	5.9
Eu	2.1	2.0	1.7	2.4	1.6	1.9	1.9	2.0	1.9
Gd	5.9	5.7	4.8	6.2	4.7	5.2	5.2	5.6	5.2
Tb	0.83	0.81	0.66	0.82	0.68	0.67	0.77	0.80	0.72
Dy	4.5	4.4	3.7	4.4	3.8	3.6	4.4	4.3	3.5
Ho	0.79	0.80	0.66	0.77	0.70	0.63	0.81	0.77	0.62
Er	2.01	2.01	1.69	1.91	1.75	1.55	2.18	2.03	1.49
Tm	0.26	0.27	0.22	0.24	0.22	0.19	0.29	0.26	0.18
Yb	1.52	1.57	1.26	1.43	1.32	1.14	1.76	1.60	1.09
Lu	0.21	0.22	0.19	0.21	0.20	0.16	0.26	0.24	0.16
Hf	4.36	4.35	3.51	3.88	3.67	4.35	4.54	4.87	4.50
Ta	4.36	4.82	4.24	3.80	3.44	4.43	6.36	2.18	3.78
Pb	1.59	2.74	1.67	1.54	1.25	2.39	2.53	2.73	1.95
Th	3.11	4.83	2.54	2.61	1.92	3.69	6.76	3.79	3.07
U	0.88	1.34	0.65	0.73	0.58	0.99	1.75	1.08	0.91
MG#	73.0	73.0	73.0	73.1	73.1	73.1	73.0	73.1	73.0
Pressure estimates (H									
sample									
Al2O3									
CaO									
FeO									
MgO									
Na2O									

Group					BAYUDA				
Location	Delgo basement east of the Nile (DE)				Main Volcanic Field (M)				
coordinates N/E	~20°10'; 30°40'				~ 18°25'; 32°40'				
sample No	RC-411	RC-418	RC-414	RC 415	BD-88a	BD-67	BD-21c	BD-62	BD-77a
SiO2	45.1	44.2	44.3	44.2	40.2	41.1	43.5	42.3	42.8
TiO2	2.6	3.2	2.6	4.2	3.7	3.0	2.5	3.1	2.2
Al2O3	12.7	13.6	13.2	14.7	13.6	13.4	13.5	13.9	12.7
Fe2O3	12.5	13.4	14.5	14.8	17.0	13.9	11.9	13.7	13.2
MnO	0.17	0.16	0.22	0.17	0.25	0.22	0.14	0.21	0.18
MgO	11.9	9.4	6.8	6.4	10.0	10.9	11.7	10.5	14.1
CaO	9.8	9.5	6.6	8.3	11.1	12.0	11.3	11.6	10.2
Na2O	2.6	3.4	4.5	3.6	3.4	3.2	3.5	2.3	2.6
K2O	0.9	0.9	3.0	1.0	0.7	1.3	1.3	0.9	0.9
P2O5	0.47	0.59	1.50	0.49	0.70	0.84	0.54	0.65	0.44
LOI	0.4	0.7	0.8	0.2	0.3	0.6	0.4	0.5	0.7
Total	99.0	99.0	97.8	98.1	101.0	100.4	100.2	99.6	99.9
Mg#	65.20	58.06	48.09	45.92	53.78	60.89	66.00	60.25	67.92
CIPW norm									
Plagioclase	38.15	37.14	23.59	46.4	21.76	18.95	20.42	32.1	26.43
Orthoclase	5.32	5.73	18.32	5.91	4.2	2.98	7.68	5.61	5.56
Nepheline	2.85	6.6	12.73	3.89	14.87	14.71	14.72	7.18	8.99
Leucite	0	0	0	0	0	3.55	0	0	0
Diopside	20.98	20.2	13.71	14.51	25.37	29.16	28.74	23.91	22.68
Hypersthene	0	0	0	0	0	0	0	0	0
Olivine	24.72	20.63	20.76	17.63	22.56	20.82	20.71	21.63	29.09
Ilmenite	4.99	6.29	5.05	8.26	7.12	5.83	4.71	6.02	4.27
Magnetite	1.87	2	2.2	2.23	2.48	2.04	1.74	2.03	1.94
Apatite	1.11	1.41	3.64	1.18	1.65	1.97	1.27	1.53	1.04
Ba	221	274	762	277	275	418	433	345	277
Rb	18	15	66	16	20	24	30	21	17
Sr	523	656	1559	919	642	800	750	737	584
Cs	0.12	0.23	1.64	0.14	0.30	0.28	0.58	0.27	0.21
Ta	5.5	6.1	7.8	2.7	7.2	7.7	8.6	6.7	6.4
Nb	52.5	59.2	129.7	45.5	99.7	107.0	106.3	88.4	65.4
Hf	5.0	6.0	15.1	5.3	0.7	4.3	5.5	4.2	3.5
Zr	216	262	743	224	35	190	242	188	153
Y	25.3	25.4	43.2	23.0	17.5	24.1	21.1	21.8	18.4
Th	3.3	3.8	12.8	3.2	1.0	6.0	7.7	4.5	4.1
U	0.98	1.12	3.84	0.96	1.53	1.62	2.10	1.06	0.96
Pb	1.9	2.0	7.4	2.3	20.1	2.3	7.7	2.4	2.3
La	32.0	37.6	109.3	32.3	33.0	51.7	54.6	39.3	33.1
Ce	68.0	79.2	221.3	68.0	68.1	97.4	98.8	76.3	63.7
Pr	8.4	9.8	26.3	8.5	8.1	11.0	10.8	8.8	7.3
Nd	34.3	40.5	102.3	35.5	31.6	42.1	39.8	34.0	28.4
Sm	7.2	8.4	18.8	7.5	5.9	7.7	7.3	6.5	5.5
Eu	2.3	2.7	5.7	2.6	1.9	2.5	2.2	2.2	1.8
Gd	6.7	7.8	15.2	7.1	5.5	6.9	6.2	6.0	5.0
Tb	0.95	1.08	2.04	1.01	0.79	0.95	0.84	0.87	0.71
Dy	5.5	5.9	10.1	5.3	4.6	5.2	4.7	4.6	4.0
Ho	1.03	1.04	1.75	0.94	0.85	0.96	0.87	0.86	0.73
Er	2.76	2.59	4.20	2.32	2.21	2.51	2.23	2.22	1.93
Tm	0.36	0.32	0.54	0.29	0.29	0.33	0.30	0.30	0.26
Yb	2.17	1.88	3.11	1.77	1.72	1.92	1.78	1.78	1.51
Lu	0.30	0.26	0.45	0.26	0.25	0.29	0.25	0.26	0.22
age Ma	82	66.1	82	82	1.44	1.44	1.44	1.44	1.44
2σ error	2.9	2.4	2.9	2.9	0.1	0.1	0.1	0.1	0.1
87/86 Sr	0.703009	0.702959	0.703459	0.703277	0.703116	0.703093	0.703144	0.703103	0.703151
±2σ(m) error*	0.000010	0.000008	0.000008	0.000007	0.000008	0.000007	0.000008	0.000011	0.000008
87Rb/86Sr	0.0998	0.0678	0.1225	0.0500	0.0888	0.0865	0.1136	0.0835	0.0833
87/86Sr i	0.702893	0.702895	0.703316	0.703219	0.703114	0.703091	0.703142	0.703101	0.703149
2σ error*	0.000012	0.000010	0.000024	0.000009	0.000008	0.000007	0.000008	0.000011	0.000008
143/144Nd	0.512854	0.512843	0.512679	0.512818	0.512875	0.512861	0.512891	0.512892	0.512878
±2σ(m) error*	0.000005	0.000005	0.000003	0.000004	0.000005	0.000007	0.000007	0.000006	0.000006
147Sm/144Nd	0.1263	0.1256	0.1110	0.1282	0.1137	0.1103	0.1109	0.1162	0.1173

Group					BAYUDA				
Location	Delgo basement east of the Nile (DE)				Main Volcanic Field (M)				
coordinates N/E	~20°10'; 30°40'				~ 18°25'; 32°40'				
sample No	RC-411	RC-418	RC-414	RC 415	BD-88a	BD-67	BD-21c	BD-62	BD-77a
143/144 Nd i	0.512786	0.512789	0.512619	0.512749	0.512874	0.512860	0.512890	0.512891	0.512877
2σ error*	0.000006	0.000005	0.000005	0.000005	0.000005	0.000007	0.000007	0.000006	0.000006
e-Nd_0	4.2	4.0	0.8	3.5	4.6	4.4	4.9	5.0	4.7
e_Nd_t	4.8	4.6	1.6	4.1	4.6	4.4	5.0	5.0	4.7
μ	34	37	35	28	5	46	18	29	27
ω	121	127	121	94	3	175	69	128	120
206Pb/204Pb	20.13	19.61	20.94	20.43	19.82	19.85	19.88	19.66	19.72
206Pb/204Pbi	19.68	19.24	20.49	20.08	19.82	19.84	19.88	19.65	19.71
2σ error*	0.05	0.04	0.05	0.04	0.02	0.02	0.02	0.02	0.02
207Pb/204Pb	15.71	15.61	15.75	15.75	15.63	15.67	15.65	15.59	15.64
207Pb/204Pbi	15.69	15.59	15.73	15.73	15.63	15.67	15.65	15.59	15.64
2σ error*	0.02	0.02	0.02	0.02	0.02	0.02	0.02	0.02	0.02
208Pb/204Pb	39.99	39.16	40.79	40.07	39.55	39.64	39.64	39.36	39.50
208Pb/204Pbi	39.50	38.74	40.30	39.68	39.55	39.63	39.63	39.35	39.49
2σ error*	0.06	0.06	0.08	0.06	0.04	0.04	0.05	0.04	0.04
Correction for crystal fı									
olivine added	16	28	43.5	47.5	40.5	24.5	14	25.5	11.5
SiO2	44.9	43.7	43.4	42.9	39.8	40.9	43.1	42.0	42.8
TiO2	2.2	2.5	1.7	2.7	2.5	2.4	2.1	2.4	2.0
Al2O3	10.9	10.4	8.7	9.3	9.0	10.5	11.7	10.8	11.4
Fe2O3	12.7	13.7	15.2	15.5	16.1	13.8	12.0	13.7	13.1
MnO	0.14	0.12	0.15	0.11	0.16	0.17	0.13	0.16	0.16
MgO	17.3	18.6	20.5	21.1	22.0	18.8	16.4	18.8	17.9
CaO	8.4	7.2	4.3	5.2	7.3	9.4	9.8	9.1	9.2
Na2O	2.3	2.6	3.0	2.3	2.3	2.5	3.1	1.8	2.3
K2O	0.76	0.72	1.97	0.61	0.46	0.98	1.11	0.72	0.83
P2O5	0.41	0.45	0.99	0.31	0.46	0.66	0.47	0.51	0.40
Rb	18.1	15.3	62.5	14.5	19.3	23.9	29.5	21.2	16.8
Sr	445	494	1003	568	426	625	651	570	520
Y	21.5	19.1	27.8	14.2	11.6	18.8	18.3	16.9	16.4
Zr	184	198	478	138	23	148	210	146	136
Nb	44.6	44.6	83.4	28.1	66.2	83.5	92.3	68.3	58.2
Cs	0.11	0.17	1.05	0.08	0.20	0.22	0.51	0.21	0.18
Ba	188	207	490	171	183	327	376	267	247
La	27.2	28.3	70.3	20.0	21.9	40.3	47.4	30.4	29.5
Ce	57.8	59.7	142.4	42.0	45.2	76.0	85.8	59.0	56.7
Pr	7.1	7.4	16.9	5.3	5.4	8.6	9.4	6.8	6.5
Nd	29.2	30.5	65.8	21.9	20.9	32.9	34.5	26.3	25.3
Sm	6.1	6.3	12.1	4.6	3.9	6.0	6.3	5.0	4.9
Eu	2.0	2.1	3.7	1.6	1.3	2.0	1.9	1.7	1.6
Gd	5.7	5.9	9.8	4.4	3.6	5.4	5.4	4.6	4.4
Tb	0.81	0.81	1.31	0.62	0.53	0.74	0.73	0.67	0.64
Dy	4.7	4.4	6.5	3.3	3.0	4.1	4.0	3.6	3.6
Ho	0.87	0.79	1.13	0.58	0.57	0.75	0.76	0.67	0.65
Er	2.34	1.95	2.70	1.43	1.47	1.96	1.94	1.72	1.72
Tm	0.30	0.24	0.35	0.18	0.19	0.26	0.26	0.23	0.23
Yb	1.84	1.42	2.00	1.10	1.14	1.50	1.55	1.38	1.34
Lu	0.26	0.19	0.29	0.16	0.17	0.23	0.21	0.20	0.20
Hf	4.26	4.55	9.70	3.25	0.46	3.38	4.79	3.27	3.11
Ta	4.64	4.59	4.99	1.69	4.79	6.04	7.47	5.20	5.73
Pb	1.60	1.50	4.76	1.42	13.37	1.81	6.66	1.82	2.09
Th	2.83	2.83	8.22	1.95	0.68	4.66	6.72	3.44	3.69
U	0.83	0.85	2.47	0.59	1.02	1.26	1.82	0.82	0.86
MG#	73.0	72.9	72.8	73.0	73.0	73.0	73.1	73.1	73.0
Pressure estimates (H									
sample							BD-21c		BD-77a
Al2O3							3.3		3.4
CaO							3.6		4.1
FeO							3.4		3.9
MgO							3.7		4.2
Na2O							3.9		6.8

Group									
Location			Jebel Kurbei (KU)					Jebel Umm Arafib (JA)	
coordinates N/E			~18°10'; 33°38'					~ 18°05' 33°48'	
sample No	BD-44b	BG-93	BD-100a	BD-100b	BD-100e	BD-101	BD-101a	BD-103a	BD-103b
SiO2	43.2	45.2	40.9	41.4	40.9	40.5	40.6	43.6	43.5
TiO2	2.2	2.4	2.6	2.6	2.5	2.4	2.5	2.3	2.3
Al2O3	12.0	14.7	12.0	12.0	11.8	10.7	12.2	13.8	13.7
Fe2O3	11.7	12.4	12.6	12.7	12.4	12.7	12.3	12.7	12.6
MnO	0.15	0.17	0.19	0.19	0.19	0.20	0.19	0.19	0.19
MgO	14.3	8.4	12.4	12.8	12.4	15.1	11.0	8.0	8.5
CaO	10.0	9.9	9.4	9.5	9.7	9.7	10.4	10.5	10.7
Na2O	1.3	3.9	4.5	4.6	4.5	4.5	4.3	4.8	3.9
K2O	1.4	1.6	1.6	1.4	1.5	1.1	1.7	1.6	1.5
P2O5	0.55	0.56	0.93	0.91	0.92	1.01	1.00	0.99	0.94
LOI	3.7	1.1	1.5	1.4	1.5	0.9	2.0	0.6	1.5
Total	100.4	100.2	98.6	99.5	98.2	98.8	98.1	99.1	99.3
Mg#	70.83	57.35	66.03	66.67	66.51	70.21	63.96	55.54	57.25
CIPW norm									
Plagioclase	33.11	30.87	8.14	9.47	8.12	5.92	9.34	18.31	24.26
Orthoclase	8.63	9.57	8.47	8.21	8.05	1.85	5.59	9.75	9.4
Nepheline	1.18	11.34	21.64	21.09	21.5	21.45	20.67	19	13.85
Leucite	0	0	0.86	0	0.92	3.6	4	0	0
Diopside	19.91	22.79	27.64	27.52	28.81	29.73	30.73	28.66	26.5
Hypersthene	0	0	0	0	0	0	0	0	0
Olivine	29.79	17.66	23.91	24.51	23.48	28.45	20.28	15.59	17.39
Ilmenite	4.29	4.62	5.18	5.13	5.03	4.69	5.07	4.44	4.46
Magnetite	1.77	1.83	1.9	1.9	1.87	1.91	1.87	1.9	1.88
Apatite	1.32	1.32	2.25	2.18	2.22	2.41	2.43	2.36	2.25
Ba	425	396	562	646	649	496	660	558	535
Rb	48	36	18	27	25	37	55	26	26
Sr	731	818	1128	1142	1251	1240	1594	1221	1355
Cs	0.97	0.38	0.26	0.54	0.65	0.65	0.80	0.22	0.30
Ta	6.7	8.9	4.6	4.1	4.9	4.7	4.9	3.7	3.7
Nb	98.1	102.2	83.1	75.6	88.6	86.2	90.3	74.8	75.6
Hf	6.8	5.7	6.0	5.7	6.2	6.0	6.1	5.1	5.1
Zr	311	271	276	259	288	269	284	235	234
Y	22.6	28.2	24.2	23.1	25.7	25.1	25.7	23.4	23.6
Th	6.8	6.3	7.7	7.6	9.0	9.9	9.6	8.7	8.6
U	2.17	1.70	2.40	2.12	2.49	2.69	2.58	2.01	2.34
Pb	12.7	3.3	5.4	4.4	7.8	2.4	5.1	4.7	4.7
La	52.1	54.5	59.5	54.2	63.5	66.2	66.4	62.8	62.6
Ce	98.2	104.5	112.3	101.7	118.4	120.8	123.3	110.0	109.4
Pr	11.0	11.9	12.8	11.7	13.5	13.5	14.1	12.1	12.0
Nd	41.2	44.7	49.1	45.4	51.5	51.7	54.2	45.9	45.8
Sm	7.4	8.2	9.4	8.8	9.9	9.8	10.3	8.8	8.8
Eu	2.3	2.6	3.1	2.9	3.2	3.2	3.4	3.0	3.0
Gd	6.4	7.1	8.3	7.8	8.7	8.4	8.9	8.0	7.9
Tb	0.89	1.01	1.13	1.08	1.20	1.15	1.20	1.08	1.08
Dy	4.9	5.8	5.8	5.6	6.1	5.9	6.1	5.6	5.5
Ho	0.91	1.11	1.00	0.95	1.06	1.01	1.02	0.96	0.96
Er	2.33	2.98	2.41	2.28	2.54	2.45	2.47	2.27	2.25
Tm	0.31	0.40	0.29	0.28	0.31	0.31	0.30	0.27	0.26
Yb	1.84	2.49	1.73	1.57	1.76	1.78	1.73	1.56	1.55
Lu	0.28	0.37	0.24	0.24	0.25	0.26	0.26	0.23	0.23
age Ma	1.44	1.44	4	4	4	4	4	4	4
2σ error	0.1	0.1	0.2	0.2	0.2	0.2	0.2	0.2	0.2
87/86 Sr	0.703196	0.703201	0.703169	0.703171	0.703167	0.703179	0.703189	0.703189	0.703179
±2σ(m) error*	0.000008	0.000018	0.000007	0.000007	0.000013	0.000007	0.000008	0.000008	0.000007
87Rb/86Sr	0.1894	0.1284	0.0462	0.0683	0.0569	0.0855	0.0995	0.0618	0.0557
87/86Sr i	0.703192	0.703198	0.703166	0.703167	0.703163	0.703174	0.703183	0.703185	0.703176
2σ error*	0.000008	0.000018	0.000007	0.000007	0.000013	0.000007	0.000008	0.000008	0.000007
143/144Nd	0.512861	0.512878	0.512925	0.512921	0.512948	0.512931	0.512921	0.512858	0.512916
±2σ(m) error*	0.000006	0.000004	0.000005	0.000004	0.000004	0.000006	0.000005	0.000006	0.000004
147Sm/144Nd	0.1087	0.1108	0.1158	0.1171	0.1165	0.1142	0.1146	0.1162	0.1169

Group									
Location			Jebel Kurbei (KU)					Jebel Umm Arafib (JA)	
coordinates N/E			~18°10'; 33°38'					~ 18°05' 33°48'	
sample No	BD-44b	BG-93	BD-100a	BD-100b	BD-100e	BD-101	BD-101a	BD-103a	BD-103b
143/144 Nd i	0.512860	0.512877	0.512922	0.512918	0.512945	0.512928	0.512918	0.512855	0.512913
2σ error*	0.000006	0.000004	0.000005	0.000004	0.000004	0.000006	0.000005	0.000006	0.000004
e-Nd_0	4.4	4.7	5.6	5.5	6.0	5.7	5.5	4.3	5.4
e_Nd_t	4.4	4.7	5.6	5.6	6.1	5.8	5.6	4.3	5.5
μ	11	34	29	31	20	72	33	28	32
ω	36	130	95	115	76	274	125	124	122
206Pb/204Pb	19.87	19.77	18.92	18.94	18.90	18.96	18.90	19.16	19.17
206Pb/204Pbi	19.87	19.76	18.91	18.92	18.89	18.92	18.88	19.15	19.15
2σ error*	0.02	0.02	0.02	0.02	0.02	0.02	0.02	0.02	0.02
207Pb/204Pb	15.65	15.65	15.59	15.60	15.57	15.60	15.58	15.60	15.61
207Pb/204Pbi	15.65	15.65	15.59	15.60	15.57	15.60	15.58	15.60	15.60
2σ error*	0.02	0.02	0.02	0.02	0.02	0.02	0.02	0.02	0.02
208Pb/204Pb	39.58	39.53	38.76	38.79	38.71	38.86	38.70	38.96	38.97
208Pb/204Pbi	39.58	39.52	38.74	38.76	38.69	38.81	38.68	38.93	38.94
2σ error*	0.05	0.04	0.05	0.05	0.05	0.05	0.05	0.05	0.05
Correction for crystal fı									
olivine added	5	27	15	13.5	14	6.5	18	30	28
SiO2	44.4	44.2	41.8	42.0	42.0	41.3	41.9	43.1	43.3
TiO2	2.1	1.8	2.3	2.3	2.3	2.3	2.2	1.7	1.7
Al2O3	11.7	11.3	10.6	10.7	10.6	10.2	10.6	10.3	10.5
Fe2O3	12.0	12.8	12.9	12.8	12.7	12.9	12.8	13.3	13.2
MnO	0.15	0.13	0.17	0.17	0.17	0.19	0.16	0.14	0.15
MgO	16.4	17.5	17.6	17.5	17.4	17.5	17.4	18.1	18.0
CaO	9.9	7.6	8.3	8.5	8.7	9.3	9.0	7.8	8.2
Na2O	1.3	3.0	4.0	4.1	4.0	4.3	3.7	3.6	3.0
K2O	1.38	1.22	1.38	1.20	1.34	1.00	1.49	1.21	1.19
P2O5	0.54	0.43	0.82	0.81	0.83	0.97	0.87	0.74	0.72
Rb	48.0	36.2	18.0	27.0	24.6	36.7	54.8	26.0	26.0
Sr	695	623	969	996	1086	1161	1329	901	1021
Y	21.5	21.5	20.8	20.2	22.3	23.5	21.4	17.3	17.8
Zr	296	206	237	226	250	252	237	174	176
Nb	93.3	77.8	71.4	65.9	77.0	80.7	75.3	55.2	56.9
Cs	0.93	0.29	0.22	0.47	0.57	0.60	0.67	0.16	0.22
Ba	404	302	483	564	563	464	550	412	403
La	49.5	41.5	51.1	47.3	55.2	62.0	55.4	46.4	47.2
Ce	93.4	79.5	96.5	88.8	102.8	113.1	102.8	81.2	82.4
Pr	10.4	9.0	11.0	10.2	11.7	12.6	11.8	8.9	9.1
Nd	39.2	34.1	42.2	39.6	44.7	48.4	45.2	33.9	34.5
Sm	7.1	6.2	8.1	7.7	8.6	9.1	8.6	6.5	6.7
Eu	2.2	1.9	2.7	2.5	2.8	3.0	2.8	2.2	2.3
Gd	6.1	5.4	7.1	6.8	7.5	7.9	7.4	5.9	5.9
Tb	0.85	0.77	0.97	0.94	1.04	1.07	1.00	0.80	0.82
Dy	4.7	4.4	5.0	4.9	5.3	5.5	5.1	4.1	4.2
Ho	0.86	0.85	0.86	0.83	0.92	0.94	0.85	0.71	0.72
Er	2.21	2.27	2.07	1.99	2.20	2.29	2.06	1.67	1.70
Tm	0.29	0.31	0.25	0.25	0.27	0.29	0.25	0.20	0.20
Yb	1.75	1.90	1.48	1.37	1.52	1.67	1.45	1.15	1.17
Lu	0.26	0.29	0.21	0.21	0.22	0.24	0.21	0.17	0.17
Hf	6.43	4.36	5.19	5.01	5.38	5.59	5.12	3.79	3.87
Ta	6.36	6.77	3.92	3.57	4.22	4.40	4.09	2.76	2.78
Pb	12.11	2.50	4.63	3.81	6.81	2.24	4.23	3.44	3.56
Th	6.46	4.79	6.64	6.62	7.84	9.27	7.99	6.39	6.48
U	2.06	1.29	2.06	1.85	2.16	2.52	2.15	1.48	1.76
MG#	73.0	73.0	73.1	72.9	73.1	72.9	73.0	72.9	73.0

Pressure estimates (H						
sample	BD-44b	BD-100a	BD-100b	BD-100e	BD-101	BD-101a
Al2O3	3.3	3.6	3.6	3.6	3.8	3.7
CaO	3.6	4.8	4.7	4.5	4.0	4.2
FeO	3.4	3.8	3.8	3.7	3.8	3.7
MgO	3.7	4.1	4.0	4.0	4.1	4.0
Na2O	74.1	2.4	2.3	2.4	2.1	2.7

Group			GEDAREF			
Location			Mercibia	El Gira		Jebel Abu T
coordinates N/E			14°25'; 35°	14°13'; 36°08'		13°46'; 36°-
sample No	BD-104	BD-105	MER 1302	GIR 1291	GIR 1295	TUY 1879
SiO2	42.8	44.3	47.8	46.0	47.0	46.0
TiO2	2.3	1.9	0.8	1.7	1.9	1.8
Al2O3	13.6	13.1	15.3	16.9	17.1	16.9
Fe2O3	12.6	12.1	10.7	12.5	12.9	12.3
MnO	0.19	0.17	0.13	0.18	0.14	0.13
MgO	7.8	10.0	11.9	8.1	8.0	7.9
CaO	10.3	10.1	10.3	9.9	10.0	9.4
Na2O	5.4	3.3	2.0	2.8	2.8	2.3
K2O	1.3	1.4	0.3	0.2	0.2	0.4
P2O5	1.04	0.68	0.11	0.19	0.21	0.43
LOI	1.0	1.2	1.4	1.1	0.4	1.5
Total	98.3	98.3	100.7	99.6	100.7	99.1
Mg#	55.12	62.14	68.75	56.00	55.14	55.95
CIPW norm						
Plagioclase	16.27	28.87	49.56	58.05	57.71	55.83
Orthoclase	7.98	8.69	2.07	1.48	1.42	2.6
Nepheline	21.93	9.63	0	0	0	0
Leucite	0	0	0	0	0	0
Diopside	29.92	24.74	15	12.5	12.42	7.66
Hypersthene	0	0	11.64	1.44	3.53	16.09
Olivine	14.97	20.77	18.39	20.83	18.99	11.34
Ilmenite	4.54	3.84	1.5	3.4	3.55	3.61
Magnetite	1.9	1.83	1.58	1.87	1.88	1.84
Apatite	2.5	1.65	0.25	0.46	0.49	1.04
Ba	540	456	114	132	62	246
Rb	29	22	5	4	2	6
Sr	1232	869	218	505	389	512
Cs	0.51	0.24	0.01	0.21	0.10	0.22
Ta	4.1	2.6	1.0	0.47	1.3	2.8
Nb	80.7	52.6	3.6	5.4	6.6	17.3
Hf	5.4	4.0	1.5	2.7	2.6	2.4
Zr	246	177	57	103	102	86
Y	24.0	18.9	18.3	21.5	22.7	22.5
Th	9.4	5.8	0.3	0	0.3	0.7
U	2.59	1.18	0.11	0.12	0.10	0.20
Pb	5.0	3.4	0.9	1.4	0.6	1.0
La	67.2	41.5	4.2	5.1	5.3	16.4
Ce	117.5	73.4	10.3	13.7	14.4	37.4
Pr	12.9	8.1	1.5	2.2	2.3	5.0
Nd	48.5	31.2	7.4	11.4	12.0	21.9
Sm	9.2	6.3	2.1	3.5	3.6	5.0
Eu	3.1	2.2	0.8	1.4	1.4	1.9
Gd	8.3	5.8	2.8	4.3	4.4	5.2
Tb	1.13	0.83	0.48	0.70	0.72	0.77
Dy	5.7	4.3	3.3	4.3	4.4	4.7
Ho	0.98	0.76	0.73	0.88	0.90	0.92
Er	2.32	1.86	2.12	2.46	2.54	2.50
Tm	0.28	0.23	0.30	0.34	0.35	0.34
Yb	1.60	1.35	2.04	2.16	2.20	2.07
Lu	0.22	0.20	0.30	0.32	0.32	0.31
age Ma	4	4	33	33	33	33
2σ error	0.2	0.2	3.3	3.3	3.3	3.3
87/86 Sr	0.703151	0.703190	0.703525	0.703066	0.703076	0.703260
±2σ(m) error*	0.000010	0.000007	0.000008	0.000008	0.000010	0.000010
87Rb/86Sr	0.0686	0.0719	0.0719	0.0206	0.0169	0.0310
87/86Sr i	0.703147	0.703186	0.703491	0.703056	0.703068	0.703245
2σ error*	0.000010	0.000007	0.000009	0.000009	0.000010	0.000010
143/144Nd	0.512914	0.512924	0.512781	0.512976	0.512978	0.512828
±2σ(m) error*	0.000006	0.000005	0.000004	0.000007	0.000005	0.000005
147Sm/144Nd	0.1149	0.1224	0.1732	0.1835	0.1786	0.1385

Group			GEDAREF			
Location			Mercibia	El Gira		Jebel Abu T
coordinates N/E			14°25'; 35°	14°13'; 36°08'		13°46'; 36°-
sample No	BD-104	BD-105	MER 1302	GIR 1291	GIR 1295	TUY 1879
143/144 Nd i	0.512911	0.512921	0.512744	0.512936	0.512939	0.512798
2σ error*	0.000006	0.000005	0.000005	0.000008	0.000006	0.000006
e-Nd_0	5.4	5.6	2.8	6.6	6.6	3.7
e_Nd_t	5.4	5.6	2.9	6.6	6.7	3.9
μ	34	22	8	5	10	13
ω	126	114	24	18	37	50
206Pb/204Pb	19.17	19.19	18.60	18.53	18.56	19.61
206Pb/204Pbi	19.15	19.18	18.56	18.50	18.51	19.54
2σ error*	0.02	0.02	0.02	0.02	0.02	0.02
207Pb/204Pb	15.62	15.61	15.55	15.54	15.50	15.63
207Pb/204Pbi	15.62	15.61	15.55	15.54	15.50	15.62
2σ error*	0.02	0.02	0.02	0.02	0.02	0.02
208Pb/204Pb	39.00	38.98	37.89	38.22	38.19	39.24
208Pb/204Pbi	38.98	38.95	37.86	38.19	38.13	39.15
2σ error*	0.05	0.04	0.04	0.04	0.04	0.04
Correction for crystal fı						
olivine added	31	20.5	8	29.5	30.5	29
SiO2	42.8	44.5	47.5	44.9	44.9	45.3
TiO2	1.7	1.6	0.7	1.3	1.4	1.4
Al2O3	10.2	10.9	14.3	12.7	12.5	12.9
Fe2O3	13.3	12.6	10.9	13.1	13.3	13.0
MnO	0.14	0.14	0.12	0.14	0.10	0.10
MgO	18.3	17.2	14.8	18.0	18.1	17.7
CaO	7.7	8.5	9.5	7.4	7.3	7.2
Na2O	4.0	2.8	1.8	2.1	2.1	1.7
K2O	0.98	1.18	0.32	0.18	0.18	0.32
P2O5	0.78	0.57	0.10	0.14	0.15	0.33
Rb	29.1	21.6	5.4	3.6	2.3	5.5
Sr	900	706	201	375	285	382
Y	17.5	15.3	16.8	15.9	16.6	16.8
Zr	180	144	52	76	75	64
Nb	59.0	42.7	3.3	4.0	4.9	12.9
Cs	0.37	0.20	0.01	0.15	0.07	0.16
Ba	395	370	105	98	45	183
La	49.1	33.7	3.9	3.8	3.9	12.2
Ce	85.9	59.6	9.5	10.2	10.6	27.9
Pr	9.4	6.6	1.4	1.6	1.7	3.7
Nd	35.5	25.3	6.8	8.5	8.8	16.4
Sm	6.7	5.1	1.9	2.6	2.6	3.7
Eu	2.3	1.8	0.8	1.0	1.0	1.4
Gd	6.1	4.7	2.6	3.2	3.2	3.9
Tb	0.83	0.67	0.44	0.52	0.53	0.58
Dy	4.1	3.5	3.0	3.2	3.2	3.5
Ho	0.72	0.62	0.67	0.65	0.66	0.69
Er	1.70	1.52	1.96	1.83	1.87	1.86
Tm	0.20	0.19	0.28	0.25	0.26	0.26
Yb	1.17	1.10	1.88	1.60	1.62	1.55
Lu	0.16	0.16	0.28	0.24	0.24	0.23
Hf	3.92	3.27	1.36	1.97	1.91	1.76
Ta	2.97	2.12	0.97	0.35	0.92	2.07
Pb	3.63	2.77	0.79	1.04	0.45	0.74
Th	6.86	4.74	0.29	0.29	0.25	0.55
U	1.90	0.96	0.10	0.09	0.07	0.15
MG#	73.0	73.0	72.9	73.1	72.9	73.0
Pressure estimates (H						
sample						
Al2O3						
CaO						
FeO						
MgO						
Na2O						

Group				DARFUR				
Location	Tuyur	Qualat Umm Debiba		Tagabo (T)			Jebl Kussa (JK)	
coordinates N/E	19'	14°08'; 35°32'		14°30; 25°50'			13°40'; 24°40'	
sample No	TUY 2349	SUD 1443	SUD 1456	DT 26B	DT 5	GM-29G	DF 6 O	DF 6 X
SiO2	45.9	46.1	47.1	43.0	41.3	41.6	41.5	46.7
TiO2	1.8	1.0	0.8	2.7	4.4	4.3	4.1	3.4
Al2O3	16.8	15.5	16.2	13.6	13.4	14.4	11.0	17.5
Fe2O3	12.3	10.4	9.9	12.3	16.0	15.0	16.4	12.3
MnO	0.13	0.16	0.16	0.15	0.19	0.16	0.14	0.20
MgO	7.8	10.1	8.8	9.0	6.7	7.3	10.4	3.5
CaO	9.3	10.7	11.0	11.7	9.2	8.7	13.5	10.0
Na2O	2.2	2.3	2.1	3.2	3.3	3.5	1.7	3.5
K2O	0.4	0.4	0.4	1.7	2.4	2.3	0.8	1.6
P2O5	0.41	0.12	0.09	0.64	1.37	0.75	0.19	0.80
LOI	1.5	3.0	2.8	1.8	1.3	1.8	0.1	0.3
Total	98.6	99.8	99.3	99.8	99.5	99.7	99.9	99.8
Mg#	55.67	65.89	63.80	59.36	45.49	49.12	55.74	35.75
CIPW norm								
Plagioclase	55.57	52.41	53.82	21.2	24.53	24.67	20.55	52.47
Orthoclase	2.6	2.54	2.3	10.46	14.42	13.83	5.02	9.75
Nepheline	0	0	0	13.42	10.44	12.66	7.72	2.94
Leucite	0	0	0	0	0	0	0	0
Diopside	7.45	18.29	17.36	30.32	18.39	18.26	37.88	14.3
Hypersthene	17.74	1.23	10.79	0	0	0	0	0
Olivine	10.18	21.73	12.5	15.87	17.83	18.17	18.09	10.28
Ilmenite	3.61	1.94	1.52	5.37	8.72	8.36	7.84	6.57
Magnetite	1.86	1.57	1.49	1.83	2.39	2.26	2.42	1.81
Apatite	1	0.3	0.21	1.53	3.29	1.81	0.44	1.88
Ba	262	91	109	589	613	562	141	551
Rb	6	7	6	44	55	45	49	32
Sr	522	264	542	812	1165	921	463	944
Cs	0.16	0.10	0.04	0.40	0.49	0.36	0.58	0.41
Ta	2.6	0.9	0.6	9.5	11.0	7.9	2.5	6.2
Nb	16.9	7.5	3.7	112.1	129.4	95.7	21.0	80.1
Hf	2.4	1.9	1.6	5.7	8.6	7.0	3.6	1.4
Zr	90	72	61	246	369	306	126	33
Y	22.4	17	17.9	25.6	34.6	28.4	14.6	30.9
Th	0.8	0.7	0.3	7.7	7.8	6.2	1.3	4.6
U	0.20	0.23	0.10	1.77	2.59	1.58	0.35	0.94
Pb	1.0	1.5	1.7	4.2	4.6	4.0	2.7	2.2
La	16.4	6.1	4.4	63.6	79.6	54.4	13.1	48.1
Ce	37.3	14.0	10.6	117.9	163.2	107.8	29.8	103.1
Pr	5.0	1.9	1.5	13.2	19.2	12.9	4.1	12.7
Nd	22.2	9.0	7.4	50.3	74.6	50.7	18.8	51.7
Sm	5.0	2.5	2.2	9.1	13.8	9.8	4.6	10.5
Eu	1.9	0.9	0.8	2.8	4.2	3.1	1.6	3.3
Gd	5.2	3.0	2.8	7.6	11.3	8.6	4.4	9.4
Tb	0.79	0.51	0.49	1.05	1.50	1.16	0.62	1.29
Dy	4.8	3.2	3.3	5.7	7.9	6.3	3.4	7.0
Ho	0.93	0.68	0.70	1.05	1.39	1.14	0.59	1.26
Er	2.52	1.99	2.10	2.68	3.55	2.99	1.46	3.08
Tm	0.35	0.29	0.30	0.34	0.45	0.40	0.17	0.39
Yb	2.14	1.89	1.99	2.10	2.60	2.31	1.02	2.16
Lu	0.31	0.29	0.30	0.31	0.39	0.34	0.14	0.29
age Ma	33	33	33	11.5	11.5	11.5	25.5	25.5
2σ error	3.3	3.3	3.3	0.3	0.3	0.3	0.7	0.7
87/86 Sr	0.703249	0.703470	0.703625	0.703391	0.703122	0.703193	0.703400	0.703153
±2σ(m) error*	0.000007	0.000008	0.000007	0.000008	0.000012	0.000011	0.000010	0.000011
87Rb/86Sr	0.0308	0.0799	0.0310	0.1575	0.1351	0.1402	0.3071	0.0986
87/86Sr i	0.703235	0.703433	0.703610	0.703365	0.703100	0.703170	0.703289	0.703117
2σ error*	0.000007	0.000009	0.000007	0.000009	0.000012	0.000011	0.000012	0.000012
143/144Nd	0.512834	0.512881	0.512787	0.512840	0.512795	0.512853	0.512865	0.512860
±2σ(m) error*	0.000006	0.000006	0.000006	0.000008	0.000012	0.000005	0.000007	0.000004
147Sm/144Nd	0.1365	0.1682	0.1798	0.1090	0.1122	0.1172	0.1476	0.1225

Group				DARFUR				
Location	Tuyur	Qualat Umm Debiba		Tagabo (T)			Jebl Kussa (JK)	
coordinates N/E	19'	14°08'; 35°32'		14°30; 25°50'			13°40'; 24°40'	
sample No	TUY 2349	SUD 1443	SUD 1456	DT 26B	DT 5	GM-29G	DF 6 O	DF 6 X
143/144 Nd i	0.512805	0.512845	0.512748	0.512832	0.512787	0.512844	0.512840	0.512840
2σ error*	0.000007	0.000007	0.000007	0.000008	0.000012	0.000005	0.000007	0.000004
e-Nd_0	3.8	4.7	2.9	3.9	3.1	4.2	4.4	4.3
e_Nd_t	4.1	4.8	3.0	4.1	3.2	4.3	4.6	4.6
μ	13	9	4	28	37	26	9	28
ω	54	31	13	127	116	105	32	140
206Pb/204Pb	20.36	18.47	18.28	19.79	20.13	20.01	19.93	19.70
206Pb/204Pbi	20.29	18.42	18.26	19.74	20.06	19.96	19.90	19.59
2σ error*	0.02	0.02	0.02	0.02	0.02	0.02	0.02	0.02
207Pb/204Pb	15.73	15.58	15.53	15.71	15.72	15.71	15.72	15.72
207Pb/204Pbi	15.72	15.58	15.52	15.71	15.71	15.71	15.72	15.72
2σ error*	0.02	0.02	0.02	0.02	0.02	0.02	0.02	0.02
208Pb/204Pb	39.84	38.06	37.70	39.68	40.02	39.92	39.89	39.95
208Pb/204Pbi	39.75	38.01	37.67	39.61	39.95	39.86	39.85	39.78
2σ error*	0.04	0.04	0.04	0.05	0.05	0.05	0.04	0.05
Correction for crystal fı								
olivine added	29.5	12.5	15	24.5	50.5	44	37	52
SiO2	45.4	46.8	47.6	43.0	41.0	41.4	41.0	43.7
TiO2	1.4	0.9	0.7	2.2	2.7	2.8	2.8	2.0
Al2O3	12.8	14.1	14.4	10.8	8.1	9.4	7.6	10.4
Fe2O3	13.1	10.9	10.6	12.7	16.2	15.4	15.8	14.5
MnO	0.10	0.15	0.14	0.12	0.12	0.10	0.10	0.12
MgO	17.8	14.8	14.5	17.4	22.0	21.0	21.6	19.9
CaO	7.1	9.8	9.8	9.3	5.6	5.7	9.3	5.9
Na2O	1.7	2.1	1.9	2.5	2.0	2.3	1.2	2.1
K2O	0.32	0.37	0.33	1.37	1.44	1.48	0.58	0.96
P2O5	0.31	0.11	0.08	0.51	0.84	0.49	0.13	0.47
Rb	5.5	7.3	5.8	44.1	48.0	42.1	49.0	28.0
Sr	387	233	466	634	698	590	319	557
Y	16.6	14.9	15.4	19.9	20.7	18.2	10.0	18.2
Zr	67	64	53	192	221	196	86	20
Nb	12.5	6.6	3.1	87.5	77.5	61.3	14.4	47.2
Cs	0.12	0.09	0.04	0.32	0.29	0.23	0.40	0.24
Ba	194	81	94	460	367	360	97	325
La	12.2	5.4	3.8	49.7	47.7	34.8	9.0	28.4
Ce	27.7	12.3	9.1	92.0	97.8	69.0	20.5	60.8
Pr	3.7	1.7	1.3	10.3	11.5	8.2	2.8	7.5
Nd	16.5	7.9	6.4	39.3	44.7	32.5	12.9	30.5
Sm	3.7	2.2	1.9	7.1	8.3	6.3	3.2	6.2
Eu	1.4	0.8	0.7	2.2	2.5	2.0	1.1	2.0
Gd	3.8	2.6	2.4	5.9	6.8	5.5	3.1	5.5
Tb	0.59	0.45	0.42	0.82	0.90	0.74	0.43	0.76
Dy	3.6	2.8	2.8	4.4	4.7	4.1	2.4	4.1
Ho	0.69	0.60	0.60	0.82	0.83	0.73	0.40	0.74
Er	1.87	1.75	1.80	2.09	2.13	1.91	1.00	1.81
Tm	0.26	0.25	0.25	0.27	0.27	0.25	0.12	0.23
Yb	1.59	1.67	1.71	1.64	1.56	1.48	0.70	1.28
Lu	0.23	0.25	0.26	0.24	0.24	0.22	0.10	0.17
Hf	1.81	1.68	1.36	4.46	5.16	4.45	2.48	0.82
Ta	1.94	0.79	0.48	7.39	6.59	5.04	1.74	3.64
Pb	0.72	1.35	1.47	3.24	2.76	2.58	1.84	1.31
Th	0.57	0.64	0.29	6.03	4.64	3.95	0.87	2.70
U	0.14	0.20	0.09	1.38	1.55	1.01	0.24	0.55
MG#	73.0	73.0	73.0	73.0	72.9	73.1	73.1	73.1
Pressure estimates (H								
sample								
Al2O3								
CaO								
FeO								
MgO								
Na2O								

Group									
Location		Meidob Hills (MH)				Jebel Marra area (JM)			
coordinates N/E		15°18'; 26°30'				12°50'; 24°20'			
sample No	DF-6j	Me-3 e	Me-3 g	Me-5	GU-3	DM-10	D-2	DF-1B	GK-2a
SiO2	42.1	46.9	47.9	45.6	46.6	43.9	42.3	46.3	42.3
TiO2	4.1	2.5	2.6	3.1	2.4	2.8	3.9	2.8	3.3
Al2O3	13.3	16.4	16.3	14.6	13.5	14.7	13.6	12.0	12.8
Fe2O3	16.2	11.3	12.0	12.7	11.9	11.8	13.4	11.7	12.5
MnO	0.16	0.14	0.15	0.14	0.13	0.14	0.14	0.13	0.13
MgO	7.6	6.0	6.3	7.3	9.1	8.7	9.0	10.4	11.9
CaO	12.5	8.5	8.9	10.9	8.9	11.6	11.2	11.9	10.9
Na2O	2.6	3.6	4.2	3.3	2.8	3.2	3.0	2.6	2.6
K2O	0.5	2.2	2.2	2.1	1.7	1.3	1.2	0.8	1.8
P2O5	0.50	0.66	0.71	0.81	0.56	0.61	0.54	0.49	0.48
LOI	0.5	0.2	0.2	0.1	1.0	1.0	1.6	0.9	1.0
Total	99.9	98.4	101.5	100.6	98.7	99.7	99.9	99.9	99.8
Mg#	48.15	51.08	51.02	53.14	60.11	59.40	57.01	63.66	65.35
CIPW norm									
Plagioclase	33.23	44.96	37.89	30.16	42.06	30.31	28.73	35.89	18.6
Orthoclase	3.19	13.3	13.18	12.41	10.22	7.98	7.03	4.73	11.05
Nepheline	6.86	4.9	8.86	9.24	1.44	10.63	9.91	3.18	12.05
Leucite	0	0	0	0	0	0	0	0	0
Diopside	29.63	13.17	16.93	24.37	17.92	26.58	26.57	30.66	27.26
Hypersthene	0	0	0	0	0	0	0	0	0
Olivine	15.52	15.46	14.87	14.23	20.5	15.81	16.79	17.31	21.71
Ilmenite	8	4.94	4.9	5.83	4.73	5.49	7.69	5.36	6.32
Magnetite	2.39	1.68	1.74	1.86	1.8	1.75	2	1.74	1.86
Apatite	1.18	1.58	1.62	1.9	1.34	1.44	1.27	1.14	1.14
Ba	234	579	582	593	429	457	476	281	427
Rb	8	44	45	51	42	26	36	29	38
Sr	692	790	790	896	667	771	746	782	629
Cs	0.37	0.38	0.40	0.48	0.40	0.52	0.33	0.31	0.27
Ta	3.9	7.4	6.8	8.0	6.1	3.7	6.6	4.3	4.7
Nb	35.2	90.3	89.8	92.4	80.6	45.4	64.2	46.5	49.1
Hf	5.1	5.4	5.5	6.8	5.7	4.8	7.1	5.3	4.8
Zr	186	258	257	339	271	205	301	232	202
Y	23.4	24.1	24.1	24.9	22.3	22.2	22.6	22.4	19.8
Th	1.6	7.1	7.0	7.7	6.5	3.6	4.2	3.3	3.4
U	0.36	1.83	1.80	2.05	1.73	0.87	1.19	0.91	0.94
Pb	5.4	3.4	3.5	4.5	3.0	5.8	4.6	3.3	3.3
La	28.6	56.9	56.4	57.4	46.5	30.3	38.0	30.5	31.7
Ce	65.1	107.7	108.2	111.6	87.0	62.1	79.6	65.0	65.2
Pr	8.5	12.3	12.3	12.9	9.8	7.8	9.8	8.2	8.0
Nd	36.1	45.7	45.6	49.3	37.6	31.8	39.3	34.8	32.8
Sm	7.9	8.2	8.2	9.4	7.2	6.7	8.0	7.4	6.7
Eu	2.6	2.7	2.7	3.0	2.3	2.2	2.5	2.4	2.1
Gd	7.0	7.0	6.9	7.9	6.4	6.1	7.0	6.9	5.8
Tb	0.98	0.95	0.96	1.09	0.89	0.84	0.97	0.96	0.83
Dy	5.4	5.3	5.2	5.7	4.9	4.8	5.1	5.2	4.3
Ho	0.92	0.98	0.98	0.98	0.89	0.91	0.92	0.89	0.79
Er	2.32	2.52	2.48	2.43	2.28	2.36	2.28	2.29	2.02
Tm	0.30	0.33	0.33	0.30	0.29	0.31	0.29	0.28	0.25
Yb	1.67	2.04	1.98	1.75	1.76	1.93	1.72	1.64	1.53
Lu	0.24	0.28	0.30	0.25	0.24	0.29	0.25	0.24	0.22
age Ma	25.5	0.3	0.21	6.8	3.3	23.1	23.1	22.9	23.1
2σ error	0.7	0.1	0.1	0.2	0.3	0.7	0.7	0.7	0.7
87/86 Sr	0.703229	0.703411	0.703391	0.703585	0.703228	0.703449	0.703169	0.703086	0.703185
±2σ(m) error*	0.000008	0.000007	0.000010	0.000008	0.000008	0.000008	0.000011	0.000017	0.000008
87Rb/86Sr	0.0340	0.1614	0.1636	0.1652	0.1835	0.0957	0.1406	0.1051	0.1739
87/86Sr i	0.703217	0.703410	0.703390	0.703569	0.703219	0.703418	0.703123	0.703052	0.703128
2σ error*	0.000008	0.000007	0.000010	0.000009	0.000008	0.000009	0.000012	0.000017	0.000009
143/144Nd	0.512863	0.512811	0.512785	0.512814	0.512865	0.512834	0.512828	0.512902	0.512870
±2σ(m) error*	0.000007	0.000005	0.000005	0.000005	0.000004	0.000004	0.000005	0.000005	0.000006
147Sm/144Nd	0.1325	0.1092	0.1090	0.1153	0.1156	0.1267	0.1231	0.1293	0.1233

Group									
Location		Meidob Hills (MH)				Jebel Marra area (JM)			
coordinates N/E		15°18'; 26°30'				12°50'; 24°20'			
sample No	DF-6j	Me-3 e	Me-3 g	Me-5	GU-3	DM-10	D-2	DF-1B	GK-2a
143/144 Nd i	0.512841	0.512811	0.512785	0.512809	0.512863	0.512815	0.512809	0.512883	0.512851
2σ error*	0.000007	0.000005	0.000005	0.000005	0.000004	0.000004	0.000005	0.000005	0.000006
e-Nd_0	4.4	3.4	2.9	3.4	4.4	3.8	3.7	5.1	4.5
e_Nd_t	4.6	3.4	2.9	3.5	4.5	4.0	3.9	5.4	4.8
μ	4	35	33	30	37	10	17	18	19
ω	20	140	134	114	146	42	62	69	70
206Pb/204Pb	19.68	19.62	19.61	19.46	19.98	19.74	20.16	20.08	19.99
206Pb/204Pbi	19.66	19.62	19.60	19.43	19.96	19.70	20.10	20.02	19.92
2σ error*	0.02	0.02	0.02	0.02	0.02	0.02	0.02	0.02	0.02
207Pb/204Pb	15.72	15.67	15.67	15.68	15.70	15.69	15.71	15.70	15.71
207Pb/204Pbi	15.72	15.67	15.67	15.68	15.70	15.69	15.71	15.70	15.71
2σ error*	0.02	0.02	0.02	0.02	0.02	0.02	0.02	0.02	0.02
208Pb/204Pb	39.82	39.68	39.69	39.42	39.72	39.76	40.03	39.72	39.90
208Pb/204Pbi	39.79	39.68	39.69	39.38	39.70	39.71	39.95	39.64	39.82
2σ error*	0.04	0.05	0.05	0.05	0.05	0.04	0.04	0.04	0.04
Correction for crystal fı									
olivine added	47	32.5	33.5	32.5	23	23.5	29.5	17.5	15.5
SiO2	41.2	45.5	45.1	43.8	46.1	43.4	42.2	45.6	42.4
TiO2	2.6	1.9	1.8	2.2	1.9	2.3	3.0	2.3	2.8
Al2O3	8.3	12.0	11.4	10.5	11.0	11.7	10.3	10.2	11.1
Fe2O3	16.0	12.5	12.8	13.2	12.5	12.3	13.8	12.0	12.7
MnO	0.10	0.10	0.11	0.10	0.10	0.11	0.11	0.11	0.11
MgO	21.8	17.1	17.5	18.0	17.1	16.8	18.7	16.4	17.2
CaO	7.8	6.2	6.3	7.8	7.2	9.3	8.4	10.1	9.4
Na2O	1.6	2.6	2.9	2.4	2.3	2.6	2.3	2.2	2.3
K2O	0.33	1.60	1.57	1.50	1.36	1.05	0.87	0.66	1.58
P2O5	0.31	0.48	0.50	0.58	0.45	0.48	0.41	0.41	0.42
Rb	7.4	44.0	44.5	51.0	42.3	25.5	36.2	28.4	37.8
Sr	430	569	563	645	529	608	553	655	537
Y	14.5	17.3	17.2	17.9	17.7	17.5	16.8	18.8	16.9
Zr	115	186	183	244	215	162	224	194	172
Nb	21.9	65.0	64.0	66.5	63.9	35.8	47.6	39.0	42.0
Cs	0.23	0.27	0.28	0.34	0.32	0.41	0.24	0.26	0.23
Ba	146	417	415	426	340	361	353	236	365
La	17.7	40.9	40.2	41.3	36.8	23.9	28.2	25.5	27.1
Ce	40.4	77.5	77.1	80.3	68.9	48.9	59.0	54.5	55.8
Pr	5.3	8.8	8.8	9.3	7.7	6.1	7.3	6.9	6.8
Nd	22.4	32.8	32.4	35.5	29.8	25.1	29.1	29.1	28.0
Sm	4.9	5.9	5.8	6.8	5.7	5.3	5.9	6.2	5.7
Eu	1.6	2.0	1.9	2.1	1.8	1.7	1.9	2.0	1.8
Gd	4.3	5.0	4.9	5.7	5.0	4.8	5.2	5.8	5.0
Tb	0.61	0.69	0.68	0.78	0.71	0.67	0.72	0.80	0.71
Dy	3.3	3.8	3.7	4.1	3.9	3.8	3.8	4.3	3.7
Ho	0.57	0.71	0.70	0.70	0.70	0.72	0.68	0.74	0.68
Er	1.44	1.81	1.76	1.75	1.81	1.86	1.69	1.92	1.73
Tm	0.19	0.24	0.23	0.22	0.23	0.24	0.22	0.24	0.22
Yb	1.04	1.47	1.41	1.26	1.39	1.52	1.28	1.37	1.31
Lu	0.15	0.20	0.21	0.18	0.19	0.23	0.19	0.20	0.19
Hf	3.16	3.92	3.95	4.87	4.51	3.78	5.27	4.47	4.13
Ta	2.43	5.30	4.83	5.73	4.81	2.90	4.87	3.61	4.05
Pb	3.33	2.48	2.52	3.27	2.41	4.60	3.39	2.73	2.83
Th	0.96	5.09	5.00	5.53	5.17	2.81	3.09	2.77	2.90
U	0.23	1.31	1.28	1.48	1.37	0.69	0.89	0.77	0.80
MG#	73.0	73.0	73.0	72.9	73.0	73.0	72.9	73.1	72.9
Pressure estimates (H									
sample								DF-1B	GK-2a
Al2O3								3.8	3.5
CaO								3.5	3.9
FeO								3.4	3.7
MgO								3.7	3.9
Na2O								7.6	7.3

Group								
Location	**Kas granite/south of Jebel Marra area**							
coordinates N/E								
sample No	ZA-467	KAS 417	KAS 414	KAS 414	KAS 449	KAS 449	KAS 451	KAS 451
	some Pb data are on HF-HNO3-leached K-feldspar							
SiO2								
TiO2								
Al2O3								
Fe2O3								
MnO								
MgO								
CaO								
Na2O								
K2O								
P2O5								
LOI								
Total								
Mg#								
CIPW norm								
Plagioclase								
Orthoclase								
Nepheline								
Leucite								
Diopside								
Hypersthene								
Olivine								
Ilmenite								
Magnetite								
Apatite								
Ba	1852		2262		2680			
Rb	76		64		68			
Sr	602		765		969			
Cs								
Ta	2.3		2.5		3.4			
Nb	10.4		6.5		9.8			
Hf	3.2		1.6		1.6			
Zr	120		60		58			
Y	5.7		5.4		7.9			
Th	11.1		6.1		6.9			
U	5.6		0.9		1.3			
Pb	24.5		24.5		26.5			
La	52.1		38.2		46.6			
Ce	90.2		65.7		80.8			
Pr	9.4		6.9		8.5			
Nd	31.5		23.8		29.2			
Sm	4.4		3.5		4.5			
Eu	1.32		1.13		1.46			
Gd	2.64		2.01		2.85			
Tb	0.30		0.26		0.36			
Dy	1.34		1.19		1.75			
Ho	0.22		0.20		0.30			
Er	0.52		0.52		0.81			
Tm	0.07		0.07		0.11			
Yb	0.43		0.48		0.68			
Lu	0.07		0.08		0.11			
age Ma	560		560		560			
2σ error								
87/86 Sr	0.710430		0.708868		0.708638			
±2σ(m) error*	0.000009		0.000007		0.000009			
87Rb/86Sr	0.1269		0.0836		0.0702			
87/86Sr i	0.70750743		0.706943		0.707021486			
2σ error*								
143/144Nd	0.511153		0.511201		0.511252			
±2σ(m) error*	0.000006		0.000006		0.000005			
147Sm/144Nd	0.0848		0.088966679		0.092563			

Group								
Location	**Kas granite/south of Jebel Marra area**							
coordinates N/E								
sample No	ZA-467	KAS 417	KAS 414	KAS 414	KAS 449	KAS 449	KAS 451	KAS 451
143/144 Nd i			0.51084179		0.510875		0.510912	
2σ error*								
e-Nd_0			-29.0		-28.0		-27.0	
e_Nd_t			-21.0		-20.3		-19.6	
μ			14		2		3	
ω			29		16		17	
206Pb/204Pb	K-feldspar	K-feldspar	17.06	K-feldspar	16.86	K-feldspar	17.03	K-feldspar
206Pb/204Pbi	16.81	16.73	15.77	16.60	16.65	16.60	16.76	16.66
2σ error*								
207Pb/204Pb			15.64		15.65		15.63	
207Pb/204Pbi	15.62	15.65	15.56	15.66	15.64	15.64	15.61	15.66
2σ error*								
208Pb/204Pb			37.92		37.79		37.66	
208Pb/204Pbi	37.35	37.42	37.10	37.29	37.34	37.34	37.19	37.58
2σ error*								
Correction for crystal fı								
olivine added								
SiO2								
TiO2								
Al2O3								
Fe2O3								
MnO								
MgO								
CaO								
Na2O								
K2O								
P2O5								
Rb								
Sr								
Y								
Zr								
Nb								
Cs								
Ba								
La								
Ce								
Pr								
Nd								
Sm								
Eu								
Gd								
Tb								
Dy								
Ho								
Er								
Tm								
Yb								
Lu								
Hf								
Ta								
Pb								
Th								
U								
MG#								
Pressure estimates (H								
sample								
Al2O3								
CaO								
FeO								
MgO								
Na2O								

Standards run with the samples

	PCC-1		GSR-3		BHVO-1		JB-3	recom.
		recom. values		*recom. values*		*recom. values*		values
SiO2	42.44	*41.71*	44.72	*44.64*	49.28	*49.94*	51.28	*51.04*
TiO2	<0.10	*0.01*	2.51	*2.36*	2.89	*2.71*	1.52	*1.45*
Al2O3	0.66	*0.67*	13.87	*13.83*	13.39	*13.80*	17.11	*16.89*
Fe2O3	8.94	*8.25*	13.68	*13.40*	12.52	*12.23*	12.18	*11.88*
MnO	0.12	*0.12*	0.18	*0.17*	0.18	*0.17*	0.19	*0.16*
MgO	44.26	*43.43*	7.95	*7.77*	7.48	*7.23*	5.64	*5.20*
CaO	0.57	*0.52*	9.44	*8.81*	11.35	*11.40*	9.94	*9.86*
Na2O	<0.10	*0.03*	3.55	*3.38*	2.38	*2.26*	2.83	*2.82*
K2O	<0.05	*0.01*	2.23	*2.32*	0.54	*0.56*	0.72	*0.78*
P2O5	<0.05	*0.002*	1.01	*0.95*	0.27	*0.27*	0.29	*0.29*
LOI	4.82	*4.82*	2.78	*2.78*	0.21	*0.21*	0.23	*0.23*
Total	101.81	*99.57*	101.92	*100.41*	100.49	*100.78*	101.93	*100.60*

Element	BHVO-1	*recom. valu*	AGV-1a	*recom. valu*	BIR-1	*recom. values*
	136.08	*139.00*	1183.70	*1226.00*	6.92	*7.00*
Rb	10.22	*11.00*	67.06	*67.30*	0.37	*0.25*
Sr	426.45	*403.00*	664.25	*662.00*	112.19	*108.00*
Cs	0.11		1.28	*1.28*	0.01	*0.01*
Ta	1.15	*1.23*	0.81	*0.90*	0.04	*0.04*
Nb	18.78	*19.00*	13.58	*15.00*	0.67	*0.60*
Hf	4.86	*4.38*	5.29	*5.10*	0.62	*0.60*
Zr	187.64	*179.00*	234.20	*227.00*	15.64	*15.50*
Y	26.26	*27.60*	17.89	*20.00*	15.02	*16.00*
Th	1.35	*1.08*	6.66	*6.50*	0.03	*0.03*
U	0.48	*0.42*	2.03	*1.92*	0.01	*0.01*
Pb	2.46	*2.60*	37.67	*36.00*	3.49	*3.00*
La	16.72	*15.90*	39.17	*38.00*	0.68	*0.62*
Ce	41.21	*39.00*	69.81	*67.00*	1.94	*1.95*
Pr	5.81	*5.70*	8.55	*7.60*	0.41	*0.38*
Nd	26.82	*25.20*	32.59	*33.00*	2.49	*2.50*
Sm	6.60	*6.20*	5.89	*5.90*	1.12	*1.10*
Eu	2.24	*2.06*	1.64	*1.64*	0.54	*0.54*
Gd	6.55	*6.40*	4.61	*5.00*	1.96	*1.85*
Tb	0.98	*0.96*	0.64	*0.70*	0.37	*0.36*
Dy	5.72	*5.20*	3.69	*3.60*	2.73	*2.50*
Ho	1.10	*0.99*	0.71	*0.67*	0.61	*0.57*
Er	2.79	*2.40*	1.83	*1.70*	1.79	*1.70*
Tm	0.35	*0.33*	0.25	*0.34*	0.28	*0.26*
Yb	2.20	*2.02*	1.69	*1.72*	1.72	*1.65*
Lu	0.30	*0.29*	0.26	*0.27*	0.27	*0.26*
Y/Ho	23.80	*27.88*	25.19	*29.85*	24.82	*28.07*
Zr/Hf	38.62	*40.87*	44.29	*44.51*	25.02	*25.83*
Nb/Ta	16.35	*15.45*	16.72	*16.67*	17.40	*15.00*
U/Pb	0.36	*0.39*	0.31	*0.30*	0.41	*0.33*

PCC-1, GSR-3, BHVO-1, AGV-1a, BIR-1 (Govindaraju, 1994); JB-3 (Imai et al. 1995)

	XRF calibration >> calibration range <<<		No. of	absolute	upper limits
	min.	max.	standards	stand.dev. "+/-"	based on standard control
SiO2	0.10	76.00	36	0.47 w.%	91 wt%
TiO2	0.10	3.00	24	0.02 w.%	
Al2O3	0.20	30.00	30	0.20 w.%	60 wt%
Fe2O3	0.10	13.50	30	0.05 w.%	55 wt%
MnO	0.03	0.30	26	0.003 w.%	
MgO	0.25	50.00	25	0.19 w.%	
CaO	0.30	65.00	34	0.11 w.%	
Na2O	0.10	6.50	26	0.07 w.%	
K2O	0.05	10.00	27	0.07 w.%	13 wt%
P2O5	0.05	1.00	20	0.01 w.%	

(4) Sample preparation, analytical methods, and data quality

*Sample preparation, analytical methods, and data quality***.** Samples were first crushed using a hammer and, after removing of parts with visible alteration by weathering or with xenoliths, passed through a jaw crusher. The crushed samples were cleaned in distilled water in order to remove the dust fraction. Approximately 100 g of fragments (~10 – 5 mm) free of xenoliths were selected under the binocular microscope. Samples were ground in a tungsten-carbide chatterbox for 5 minutes. The loss on ignition was determined on ca. 2 grams of dry (110°C) powdered sample at 1000°C. Whole rock samples were analyzed for major elements by XRF (PHILIPS PW 1404) at Technical University Berlin on fused glass disks using Oxiquant and X-40 Philips software. Reproducibility of the in-house standard is (n = 90; wt% ±1sd): SiO_2: 60.1±0.75; Al_2O_3: 19.0±0.27; Fe_2O_3: 5.8±0.11; MnO: 0.13±0.004; MgO: 1.1±0.13; CaO: 5.1±0.06; Na_2O: 4.6±0.23; K_2O: 2.2±0.04; TiO_2: 0.56±0.012; P_2O_5: 0.20±0.008. Values for internationals standards are in Table 1.

Powdered samples of silicate rocks (younger than 20 Ma) were treated in hot 6M hydrochloric acid and washed several times in ultra-clean water, samples older 20 Ma were treated with acetic acid and ultra-clean water. The dried samples were weighed into Savillex® screw top beakers. Samples were dissolved in 52% HF on the hot plate at 180°C for at least 36 h. After drying, the samples were redissolved in 6N HCl and split into two fractions, one for Pb isotope determination and one for Sr and Nd isotope analysis. Pb was separated using standard HBr – HCl chemistry; Sr and the rare earth element (REE) fractions were separated in a first step from the same solution and Nd was isolated in a second step from the other REE using HDEHP-coated Teflon® powder. Laboratory procedures at GFZ Potsdam are described in Romer et al. (2005). REE, U, Th, Pb, Rb, and Sr contents were determined by ICP-MS at GFZ Potsdam (experimental procedure at GFZ Potsdam and accuracy from international reference material see Dulski (2001); international standards run with our samples are in Table 1).

All isotope ratios were determined using TIMS. Nd and Sr isotope ratios were measured using dynamic multi-collection on a MAT 262 mass spectrometer and on a VG 54 Sector mass spectrometer at the GFZ-Potsdam, respectively. Nd isotopic ratios were normalized to $^{146}Nd/^{144}Nd = 0.7219$, Sr isotopic ratios to $^{86}Sr/^{88}Sr = 0.1194$. During the analytical work at GFZ-Potsdam the NBS 987 Sr standard yielded $^{87}Sr/^{86}Sr = 0.710265 \pm 28$ (2 σ; n = 47) and the La Jolla Nd standard yielded $^{143}Nd/^{144}Nd = 0.511850 \pm 8$ (2 σ, *n* = 46). Pb isotope ratios were measured at GFZ-Potsdam using static multi-collection on a MAT 262 mass spectrometer at controlled temperatures between 1220 - 1250°C. The 2 σ reproducibility of all Pb isotope ratios of the NBS SRM 981 standard ($^{206}Pb/^{204}Pb = 16.902 \pm 0.015$, n = 58) is better than 0.1% and a 2 σ error of 0.1% is assumed for the measured samples considering the uncertainty of correction for mass fractionation. Instrumental mass-fractionation has been corrected using 0.1% per a.m.u. (atomic mass unit) on the base of the NBS SRM 981values. Procedural blanks were < 30 pg for Pb, <50 pg Nd and < 100 pg for Sr. No blank corrections have been applied to the measured ratios because blank contribution was insignificant in comparison to the amount of the respective elements in the sample.

K-Ar dating Small fragments of matrix material avoiding visible xeno- and phenocrystal were selected under the binocular microscope. Potassium was determined in duplicate by flame photometry using an Eppendorf Elex 63/61. The samples were dissolved in a mixture of HF and HNO3 according to the technique of Heinrichs and Herrmann (1990). CsCl and LiCl were added as an ionization buffer and internal standard, respectively. The argon isotopic composition was measured in a Pyrex Glass extraction and purification line couple to a VG 1200 C noble gas mass spectrometer operating in static mode. The amount of radiogenic ^{40}Ar was determined by isotope dilution method using a highly enriched 38Ar spike (Schuhmacher, 1975). The spike is calibrated against the biotite standard HD-B1 (Fuhrmann et al. 1987). The age calculations are based on the constants recommended by the IUGS

quoted in Steiger and Jäger (1977). The stated analytical error for the K/Ar age calculations is given at the 95% confidence level (eTable 2). Details of argon and potassium analyses for the laboratory at Göttingen University are given in Wemmer and Ahrendt (1991).

(5) eFigures 1-6

eFigure 1

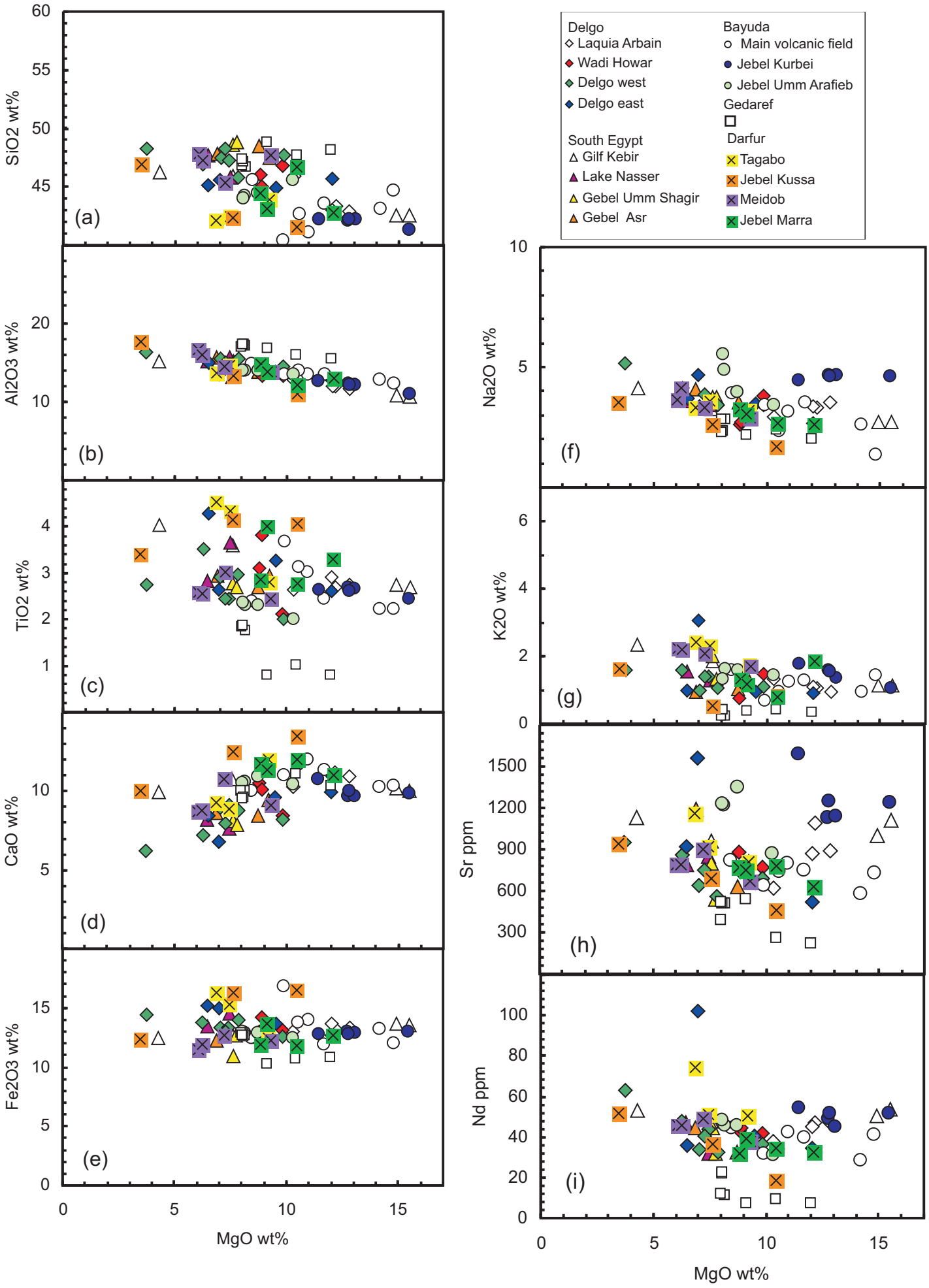
Delgo
Laquia Arbain
Wadi Howar
Delgo west
Delgo east
South Egypt
Gilf Kebir
Lake Nasser
Gebel Umm Shagir
Gebel Asr
Bayuda
Main volcanic field
Jebel Kurbei
Jebel Umm Arafieb
Gedaref
Darfur
Tagabo
Jebel Kussa
Meidob
Jebel Marra
SiO2 wt%
Al2O3 wt%
TiO2 wt%
CaO wt%
Fe2O3 wt%
Na2O wt%
K2O wt%
Sr ppm
Nd ppm
MgO wt%
(a)
(b)
(c)
(d)
(e)
(f)
(g)
(h)
(i)

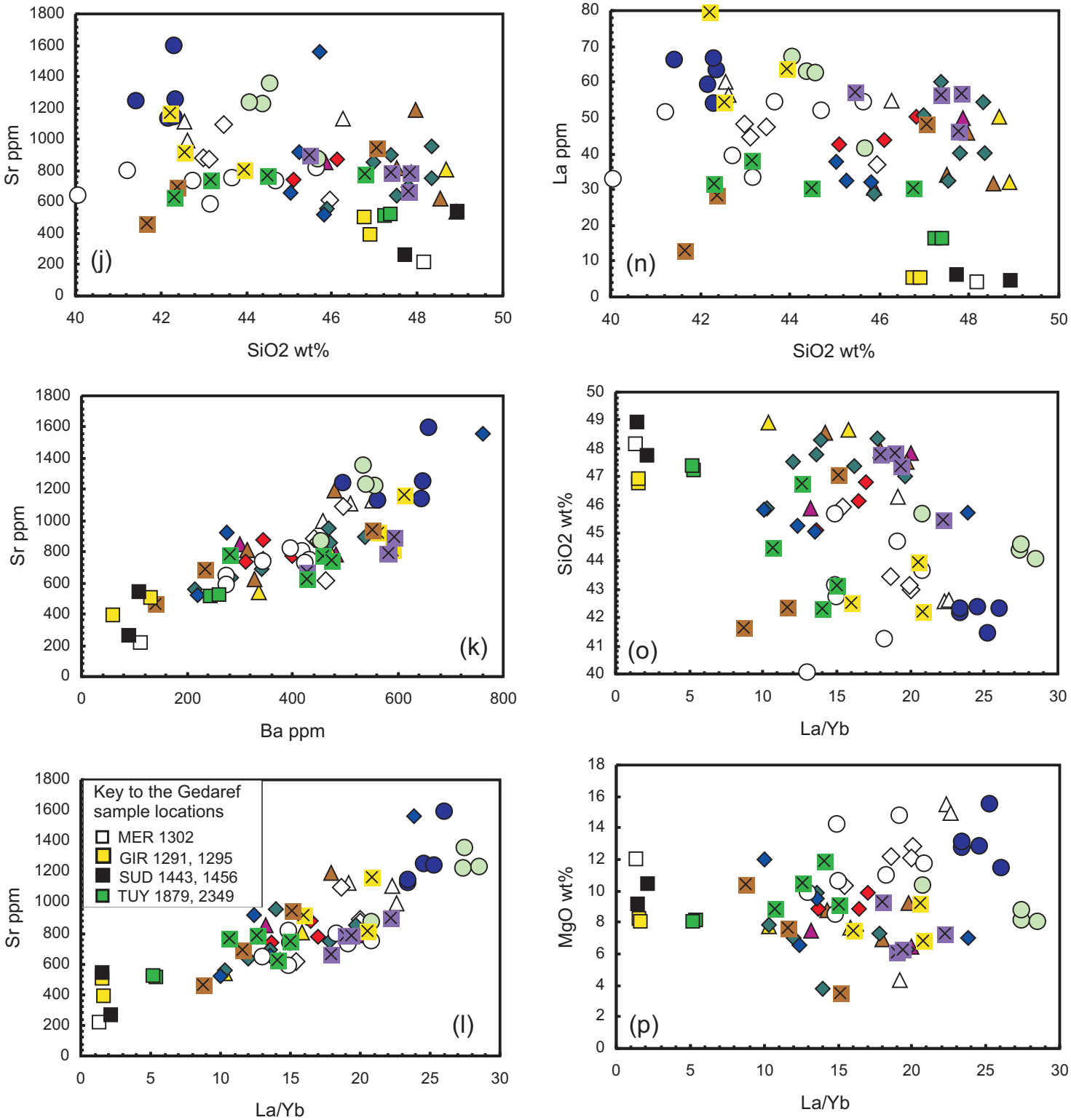

eFigure 1 (a-i) Major and selected trace elements plotted against MgO as an indicator of magmatic fractionation. **(j, n)** Incompatible trace elements plotted against SiO2 as possible indicator of magmatic fractionation or crustal contamination and **(k,l,m,o)** variations between incompatible trace elements.There is no consistent correlation between MgO and La/Yb **(p)**.

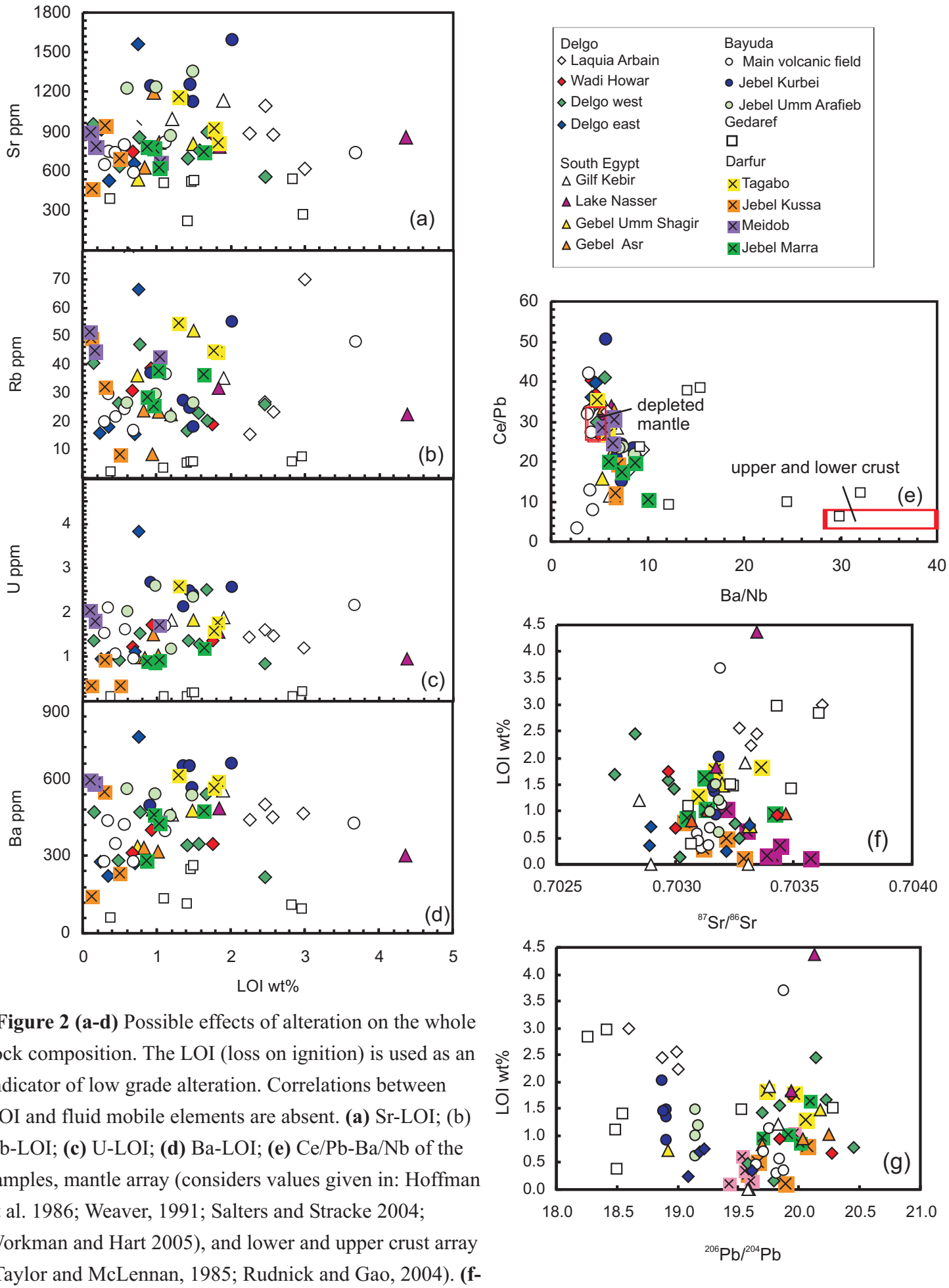

eFigure 2 (a-d) Possible effects of alteration on the whole rock composition. The LOI (loss on ignition) is used as an indicator of low grade alteration. Correlations between LOI and fluid mobile elements are absent. **(a)** Sr-LOI; (b) Rb-LOI; **(c)** U-LOI; **(d)** Ba-LOI; **(e)** Ce/Pb-Ba/Nb of the samples, mantle array (considers values given in: Hoffman et al. 1986; Weaver, 1991; Salters and Stracke 2004; Workman and Hart 2005), and lower and upper crust array (Taylor and McLennan, 1985; Rudnick and Gao, 2004). **(f-g)** There is no systematic correlation between LOI and initial Sr and Pb isotope ratios, which can be both redistributed during low grade alteration. Mind, that, e.g., the Gedaref area comprises several distant localities.

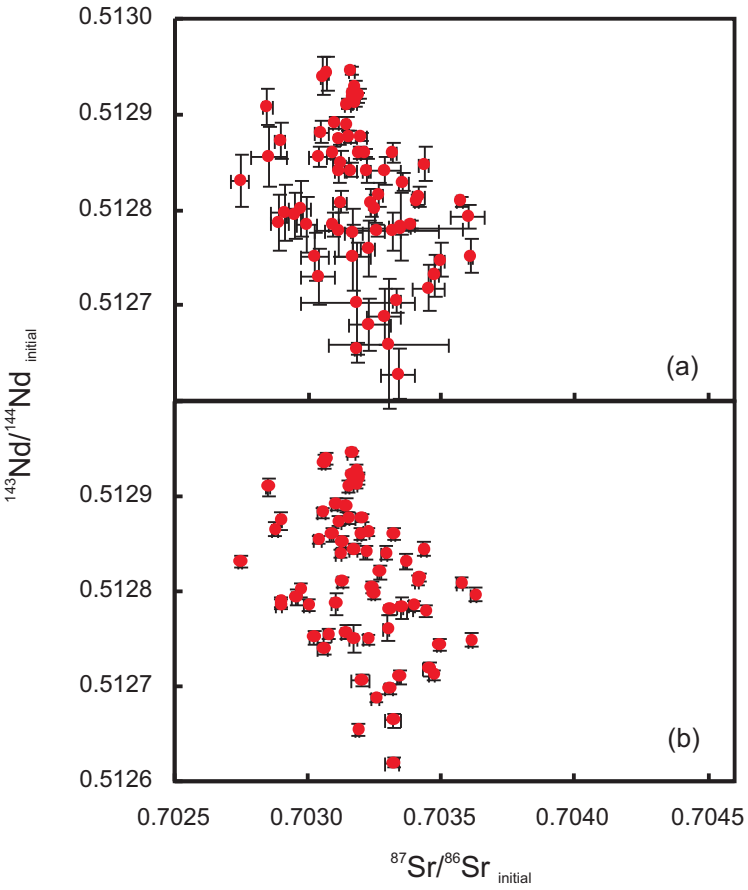

eFigure 3 a, b, c, d Propagated errors for the initial **(a, b)** Nd, Sr, and **(c, d)** Pb isotope ratios from Figures 5a and 6a. Errors are calculated including the analytical precision of the isotope ratios, an assumed uncertainty of 1% on the parent element ratio, and **(a, c)** an arbitrary uncertainty of 50% the crystallization ages and **(b, d)** the uncertainty reported for the crystallization ages (eTable 1). Even assuming a 50% error on the crystallization ages(a,c), the data are still distinguished in the regional compositional framework. Errors calculated using the reported uncertainty of the K-Ar age determinations (eTable 1) result in error bars on initial **(b)** Nd, Sr isotope ratios and **(d)** $^{206}Pb/^{204}Pb$ ratios which are mostly within the size of the symbols used in Figures 6, 7. The error on **(d)** the $^{207}Pb/^{204}Pb$ ratios is dominated by the assumed uncertainty of 0.1% on the Pb isotope ratios due to near-exhaustion of the ^{235}U parent isotope.

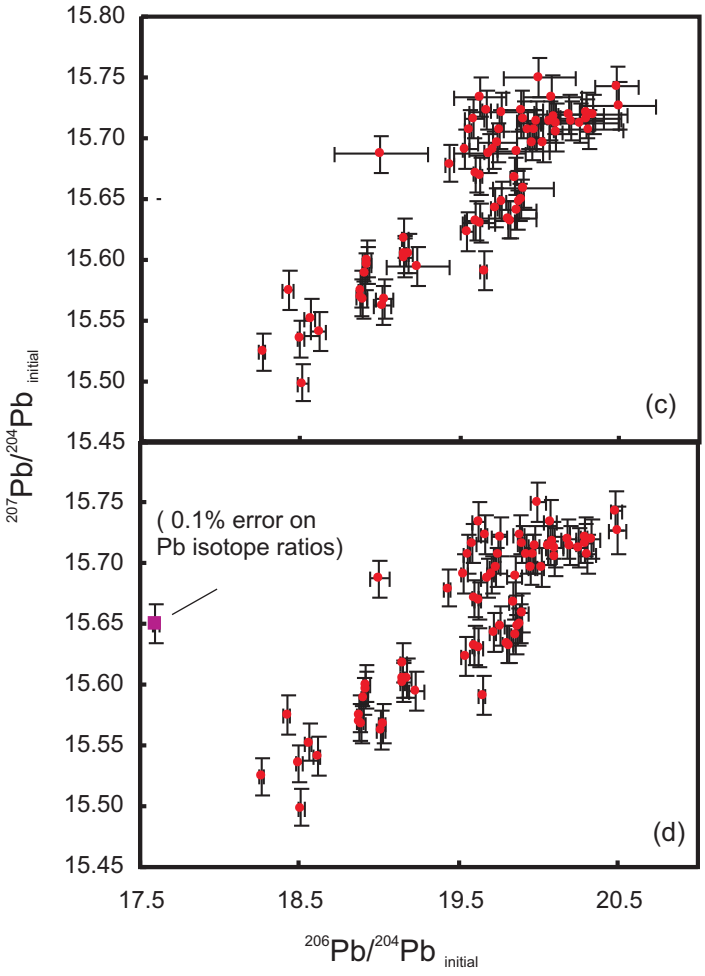

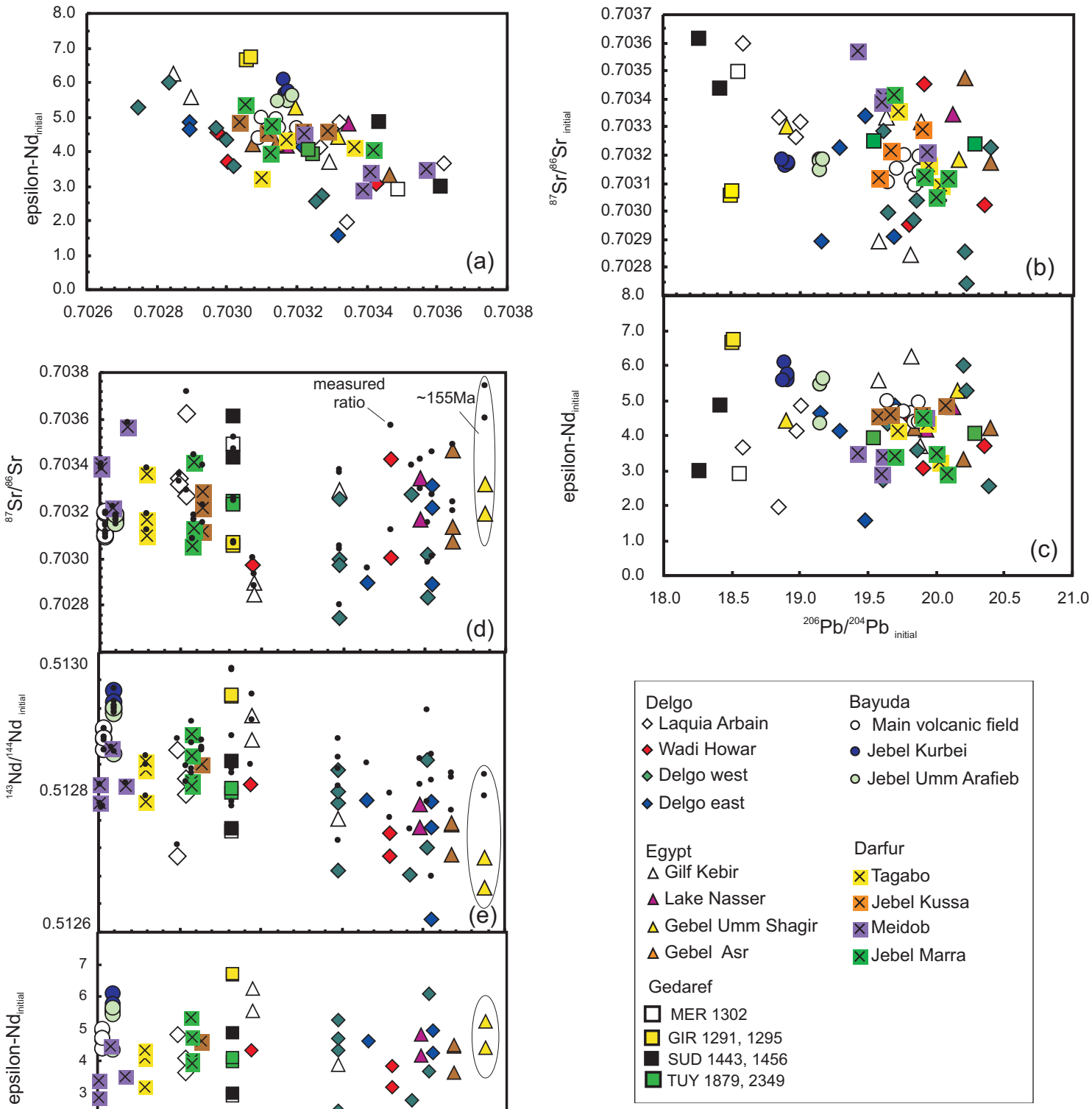

eFigure 4 a-c (a) Correlations between initial Sr and Nd isotope compositions are absent or cloudy at the individual sample localities (Gedaref and Delgo groups comprise several localities; rocks from the different localities are not co-genetic and hence the interpretation of correlations are necessarily speculative). Variable initial **(b)** Sr isotope ratios and **(c)** Nd isotope compositions are not correlated with the variable $^{206}Pb/^{204}Pb$ ratios of the selected intra-plate magmatic rocks, except in the Bayuda main volcanic field. Correlations between isotope ratios and **(d,e,f,g)** and age of crystallization are absent, but all samples with unradiogenic $^{206}Pb/^{204}Pb$ ratios are < ~33 Ma.

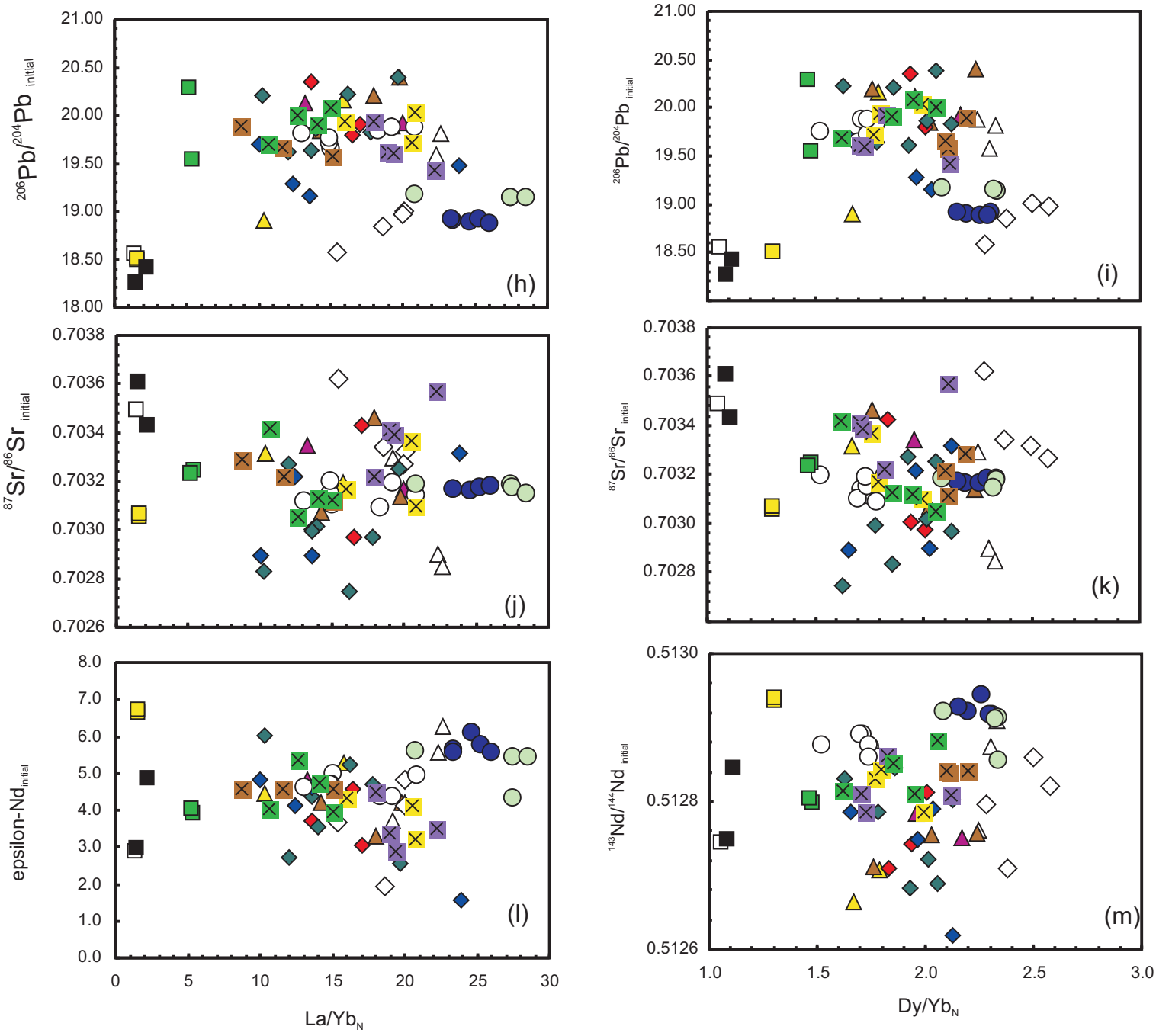

eFigure 4 h-m Correlations between isotope composition and La/Yb and Dy/Yb as possible indicators of variable depth of melting are absent.

eFigure 5

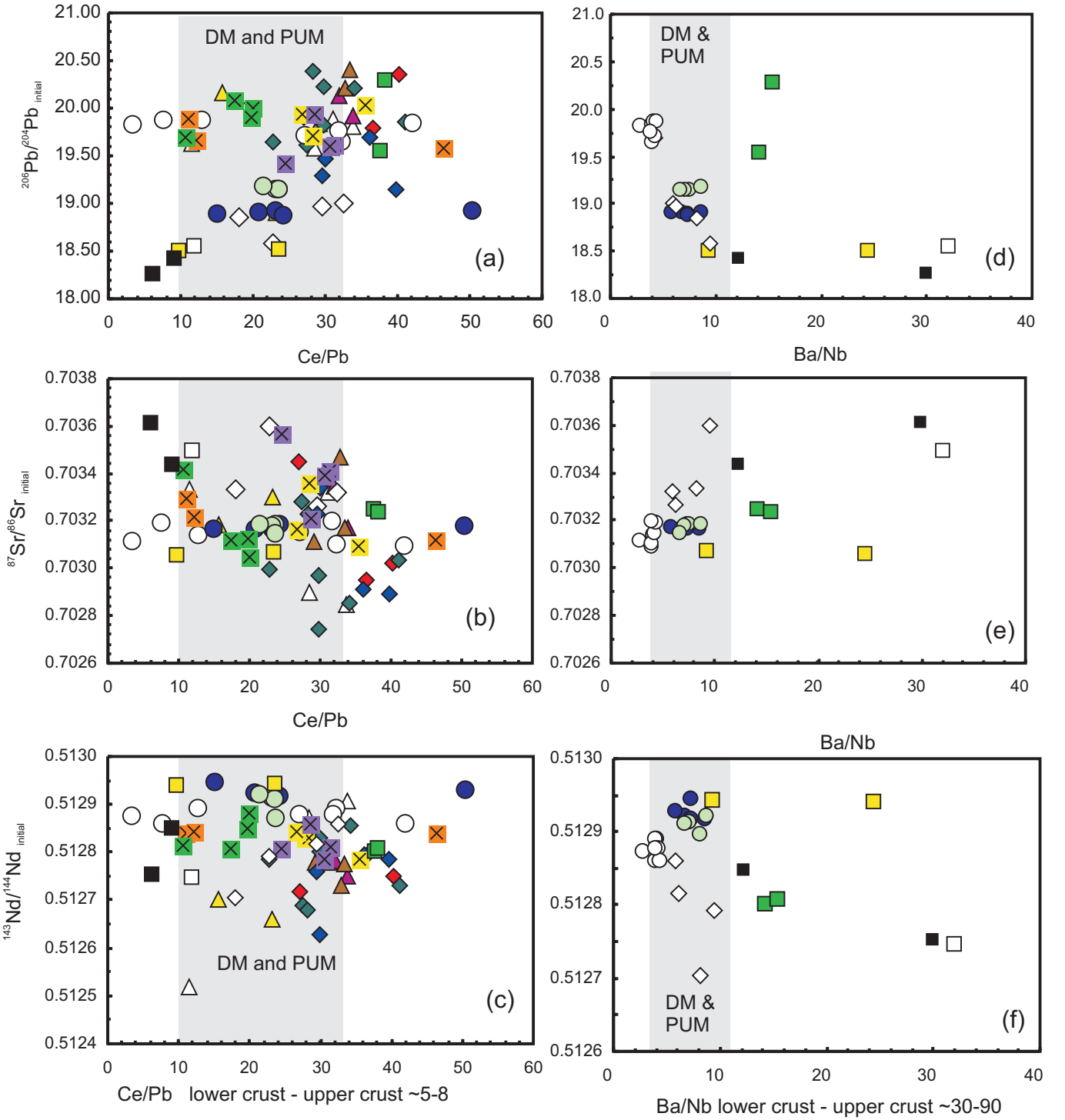

eFigure 5 a-f (a) $^{206}Pb/^{204}Pb$, **(b)** $^{87}Sr/^{86}Sr$, and **(c)** $^{143}Nd/^{144}Nd$ initial ratios plotted against the Ce/Pb ratios; **(d, e, f)** the same isotope ratios of selected samples with unradiogenic Pb isotope ratios (including the radiogenic Bayuda main volcanic field for comparison) plotted against Ba/Nb ratios. The Gedaref sample localities are distinguished by different markers. $^{206}Pb/^{204}Pb$, $^{87}Sr/^{86}Sr$, and $^{143}Nd/^{144}Nd$ ratios versus **(g,h,i)** Th/Nb and **(j,k,l)** La/Nb. Both element ratios, especially the La/Nb ratio, are considered to be more refractive during low grade alteration. Most samples plot in the array of mantel compositions or below (which is common in OIB type rocks from enriched mantle sources). The compositional range of lower and upper crust is also indicated. Correlations between isotope composition and Nb/U are absent **(m,n,o)**. Influence of crustal compositions is not distinguished except in some Gedaref samples. References see the text.

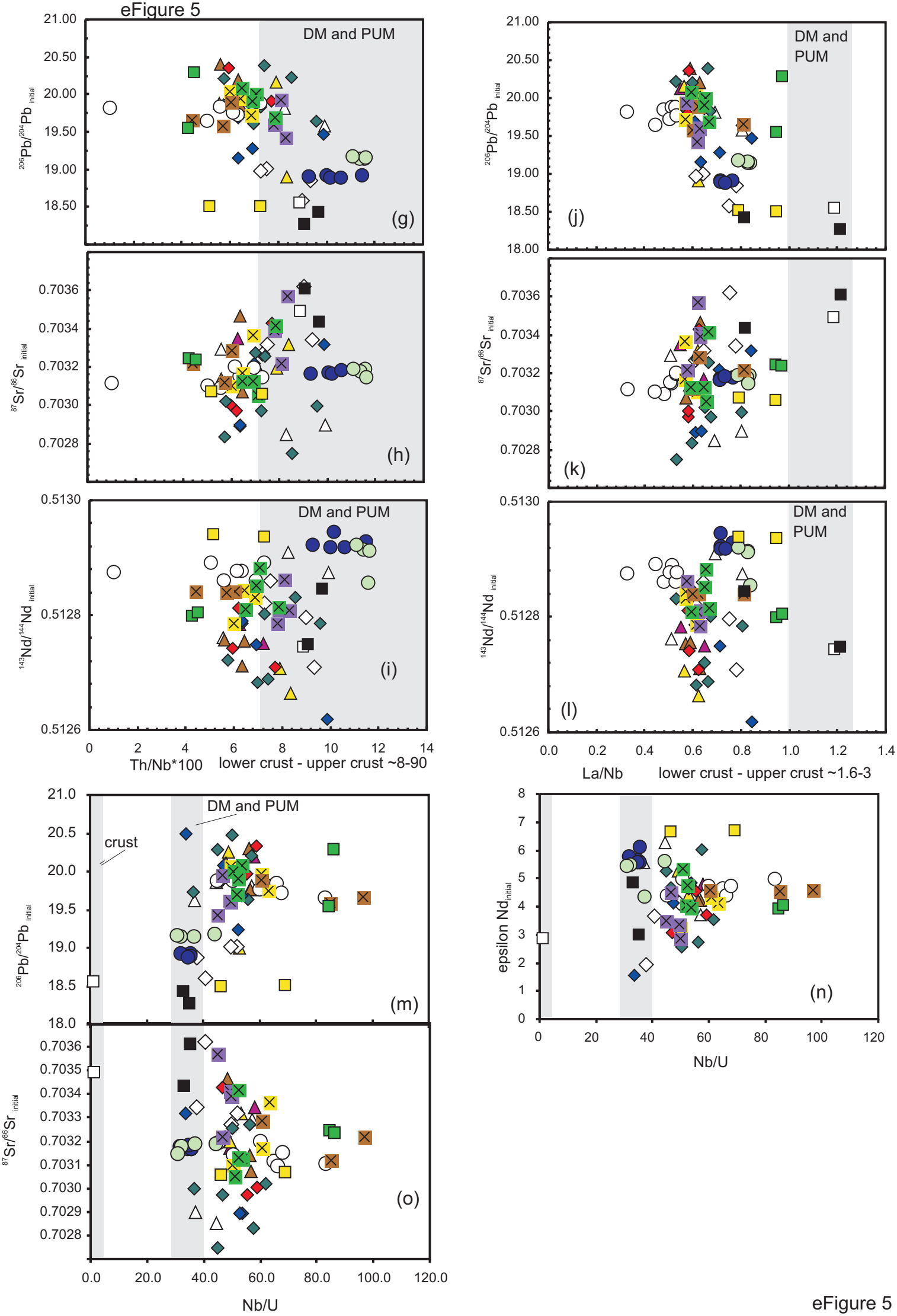
DM and PUM
(g)
(h)
(i)
(j)
(k)
(l)
(m)
(n)
(o)
crust
$^{206}Pb/^{204}Pb_{initial}$
$^{87}Sr/^{86}Sr_{initial}$
$^{143}Nd/^{144}Nd_{initial}$
epsilon $Nd_{initial}$
Th/Nb*100
lower crust - upper crust ~8-90
La/Nb
lower crust - upper crust ~1.6-3
Nb/U

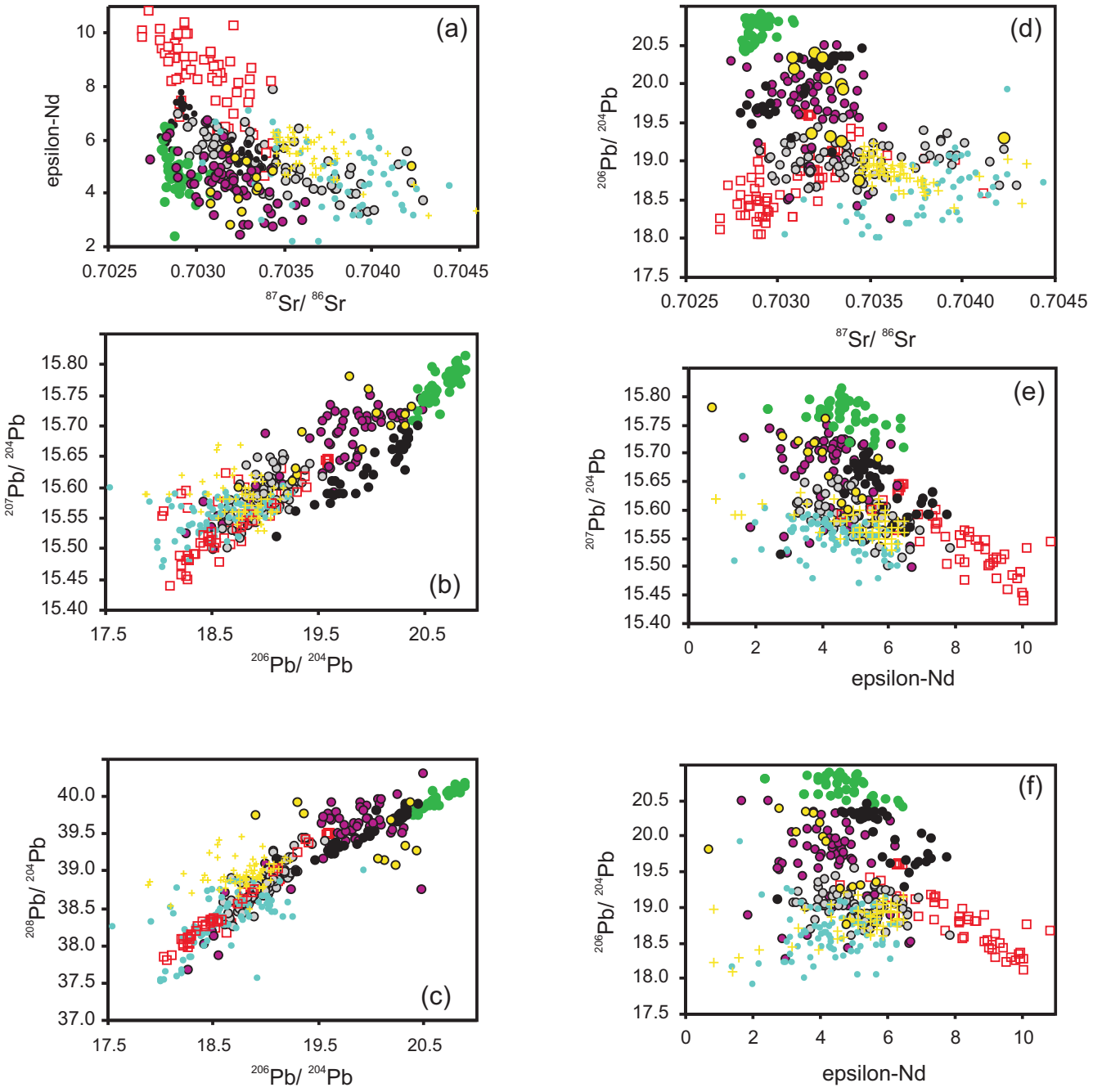

eFigure 6 (a-f) Relations between the isotopic compositions of the NE-African intra-plate magmatic rocks and regional mantle derived rocks: Red Sea & Gulf of Aden spreading center, Afar (~30Ma; plateau basalts) and younger Djibouti basalts representing the plume, Arabian intra-plate magmatism and high-μ sources of OIBs (St Helena, FOZO sensu Stracke et al., 2005). This is the data base of compositional fields shown in Figure 8 of the main text. References see the text.

(6) References

Barth H, Meinhold KD (1979) Mineral prospecting in the Bayuda Desert. Bundesanstalt Geowiss. Rohstoffe, Hannover (unpublished report)

Bernau R, Darbyshire DPF, Franz G, Harms U, Huth A, Mansour N, Pasteels P, Schandelmeier H (1987) Petrology, geochemistry and structural development of the Bir Safsat-Aswan Uplift/Southern Egypt. Journal of African Earth Science 6: 79-90

Cahen L, Snelling NJ, Delhal J, Vail JR, (1984) The Geochronology and evolution of Africa. Oxford Clarendon Press, 512p

Dulski P (2001) Reference materials for geochemical studies: New analytical data by ICP-MS and critical discussion of reference values. Geostandards Newsletters 25: 87-125

Franz G, Puchelt H, Pasteels P (1987) Petrology, geochemistry and age relations of Triassic and Tertiary volcanic rocks from SW Egypt and NW Sudan. Journal of African Earth Sciences 6: 335-352

Franz G, Pudlo D, Urlacher G, Haußmann U, Boven A, Wemmer K (1994) The Darfur Dome, western Sudan: the product of a subcontinental mantle plume. Geologische Rundschau 83: 614-623

Fuhrmann U, Lippolt HJ, Hess JC (1987) Examination of some proposed K±Ar standards:40Ar/39Ar analyses and conventional K-Ar data. Chemical Geology (Isotope Section) 66: 41-51

Govindaraju K (1994) 1994 compilation of working values and sample description for 383 geostandards. Geostandards Newsletter 18 (Special Issue): 158p

Heinrichs H, Herrmann AG (1990) Praktikum der Analytischen Geochemie. Springer, Berlin, 669 p

Hofmann AW, Jochum KP, Seufert M, White WM (1986) Nb and Pb in oceanic basalts: New constraints on mantle evolution. Earth and Planetary Science Letters 79: 33-45

Imai N, Terashima S, Itho S, Ando A (1995) 1995 compilation of analytical data for minor and trace elements in seventeen GSI geochemical reference samples 'Igneous Rock Series'. Geostandards Newsletter 19: 135-213

Meneisy MY, Kreuzer H (1974) Potassium-argon ages of Egyptian basaltic rocks. Geologisches Jahrbuch 9: 21-31

Romer RL, Heinrich W, Schröder-Smeibidl B, Meixner A, Fischer CO, Schulz C (2005) Elemental dispersion and stable isotope fractionation during reactive fluid-flow and fluid immiscibility in the Bufa del Diente aureole, NE-Mexico: Evidence from radiographies and Li, B, Sr, Nd, and Pb isotope systematics. Contributions to Mineralogy and Petrology 149: 400-429

Rudnick RL, and Gao S (2004) Composition of the continental crust. In: Treatise on Geochemistry volume 3, The Crust, Rudnick RL (editor) Elsevier, New York, 1–64

Salters VJM, Stracke A (2004) Composition of the depleted mantle. Geochemistry Geophysics Geosystems 5: doi:10.1029/2003GC000597.

Schuhmacher E (1975) Herstellung von 99.9997% 38Ar für die 40K/40Ar Geochronologie. Chimia 24: 441-442

Steiger RH, Jäger E (1977) Subcommission on geochronology: convention on the use of decay constants in geo- and cosmochronology. Earth and Planetary Science Letters 36: 359-362

Stracke A, Hofmann AW, Hart SR (2005) FOZO, HIMU, and the rest of the mantle zoo, Geochemistry Geophysics Geosystems 6: doi:10.1029/2004GC000824

Taylor SR, McLennan SM (1985) The Continental Crust: Its Composition and Evolution. Blackwell Publisher, Oxford

Weaver BL (1991) The origin of ocean island basalt end-member compositions: trace element and isotopic constraints. Earth and Planetary Science Letters 104: 381-397

Wemmer K, Ahrendt H (1991) Comparative K–Ar and Rb–Sr age determinations of retrograde processes on rocks from the KTB deep drilling project. Geologische Rundschau 86 (supplement): S272-S285

Wipki M (1995) Eigenschaften, Verbreitung und Entstehung von Kaolinlagerstätten im Nordsudan. PhD thesis, Technische Universität Berlin, Verlag Dr. Köster, Berlin, 213 p

Workman RK, Hart SR (2005) Major and trace element composition of the depleted MORB mantle (DMM). Earth and Planetary Science Letters 231: 53-72